Title
A Novel Multi-Faceted Strategy to Identify the In Vivo Dynamics of Spinal Locomotor Networks

Author
pham, bau

Publication Date
2019

Peer reviewed|Thesis/dissertation

UNIVERSITY OF CALIFORNIA

Los Angeles

A Novel Multi-Faceted Strategy to Identify the *In Vivo* Dynamics of Spinal Locomotor Networks

A dissertation submitted in partial satisfaction

of the requirements for the degree

Doctor of Philosophy in Bioengineering

by

Bau Ngoc Pham

2019

ABSTRACT OF THE DISSERTATION

A Novel Multi-Faceted Strategy to Identify the *In Vivo* Dynamics of Spinal Locomotor Networks

by

Bau Ngoc Pham

Doctor of Philosophy in Bioengineering

University of California, Los Angeles, 2019

Professor Victor R. Edgerton, Chair

Recovering motor function remains a paramount goal of spinal cord injury (SCI) injury research. Solutions to this problem has been approached in many ways, but epidural stimulation (ES) of the lumbosacral spinal cord in combination with physical training has shown the most promise by facilitating voluntary leg movements in SCI patients and has even enabled independent stepping in one case. Improving our understanding of the anatomy of spinal locomotor networks, how they physiologically interact with proprioception to execute locomotion *in vivo*, and how ES combined with physical training mechanistically reorganizes spinal networks will provide crucial information in how to use ES optimally to improve clinical outcomes along with inspiring future design of epidural electrodes and training programs. This thesis aims to adapt an engineering and big data workflow to answer these pressing biological problems, namely finding a way to generate large sets of data from current immunohistochemistry (IHC) techniques known to generate very little and to find a way to

analyze this large amount of data in a time efficient manner when the current gold standard has been manual analysis.

Though IHC has the potential to uncover properties like neural activation over a whole network (i.e. the spinal cord), current IHC methods are limited to two dimensions through the use of thin sectioning and staining. This methodology cannot reliably answer questions that pertain to a broad three dimensional network. Developments like tissue clearing, make neural tissue optically transparent so that light microscopy can scan through a whole tissue volume similar to MRI, and thus recreate a 3D reconstruction. This study aims to adapt the passive CLARITY technique (PACT) to not only clear mouse spinal cord tissue, but to combine PACT with retrograde neural tracing and IHC staining. Muscle-specific neural tracing with pseudorabies virus (PRV), cholera toxin subunit b (CTB), and dextran amine have worked with PACT clearing to create 3D reconstructions of these muscle-specific neural networks. Furthermore, PACT clearing can be combined with IHC techniques to label thick tissue sections for c-fos, a neural activity marker, and chx10, a marker for V2a spinal interneurons. The quality of the IHC labeling of PACT-cleared tissue prove to be just as robust and effective as IHC labeling of thin tissue sections. The combination of PACT with IHC labeling of c-fos gives a niche technique that can capture system and neural network wide activity during *in vivo* locomotion that also has cellular resolution while also having the flexibility for further molecularly phenotyping. There is no current methodology that can accomplish this in a mammalian system.

To take full advantage of the ability to gather large three dimensional IHC data sets, an equally powerful animal model should be paired with it. Though, c-fos is widely used to identify

system wide neural activation with cellular resolution *in vivo*, it has its limitations in that it can only capture neural activation of one event. This limits its ability to compare different activation patterns due to a lack of direct neuronal comparison between different animals. For example, c-fos labeling alone cannot answer the aforementioned question of how ES and physical mechanistically changes spinal networks without a built-in control that allows for direct neuronal comparison that can't be done between two different c-fos patterns from two different animals. Targeted recombination in active populations (TRAP) allows researchers to capture two different c-fos activation patterns in the same animal. TRAP animals have only been used to research brain circuits. In this study we perform a pilot study to optimize TRAP for use in the spinal cord by investigating spinal circuit activation during resting, stepping, and incline stepping. The results show that c-fos and tdTomato, expressed via TRAP, measure neural activity differently. However they both encode activity spatially in a similar manner. TRAP reveals that spinal locomotor circuits use spatial encoding to execute different locomotor tasks. Furthermore, TRAP reveals redundancies in spinal networks while also suggesting that their activation for repeating the same motor task is highly probabilistic in nature. The use of TRAP animals can give multiple views and insights of network activation during locomotor events. Additionally, this technique can be combined with PACT tissue clearing to reveal the connectivity of activated spinal networks since the tdTomato expression from TRAP is not limited to the nucleus like c-fos.

Estimation of cell nuclei in images stained for the c-fos protein using immunohistochemistry (IHC) is infeasible in large image sets. Use of multiple human raters to increase throughput often creates variance in the data analysis. Machine learning techniques for biomedical image analysis have been explored for cell-counting in pathology, but their performance on IHC staining, especially to label activated cells in the spinal cord is unknown. In this study, we evaluate

different machine learning techniques to segment and count spinal cord neurons that have been active during stepping. We present a qualitative as well as quantitative comparison of algorithmic performance versus two human raters. Quantitative ratings are presented with cell-count statistics and Dice (DSI) scores. We also show the degree of variability between multiple human raters' segmentations and observe that there is a higher degree of variability in segmentations produced by classic machine learning techniques (SVM and Random forest) as compared to the newer deep learning techniques. The work presented here, represents the first steps towards addressing the analysis time bottleneck of large image data sets generated by c-fos IHC staining techniques, a task that would be impossible to do manually.

The ability to generate large IHC data sets combined with a powerful animal model in which the analysis can be automated provides a powerful workflow and foundation to answer critical biological questions that can further the efficacy of ES and physical training to treat SCI patients. Future experiments can answer how neural network activation changes before and after an acute or chronic spinal cord injury along with how do chronically injured spinal cord activation change with ES and physical training. Answering these basic questions can potentially allow us to better understand how to optimally apply ES and physical training and can also show us how we should design future ES devices to optimally facilitate spinal reorganization to achieve functional motor outcomes.

The dissertation of Bau Ngoc Pham is approved.

Stephanie Kristin Seidlits

Alan Garfinkel

Allan MacKenzie-Grahm

Victor R. Edgerton, Committee Chair

University of California, Los Angeles

2019

DEDICATION

In loving memory of my mother Chi Vu Pham. Your sacrifice and dedication has enabled me to push myself this far and shaped the person I am today.

In loving memory of my sisters Nina and Christine Pham. Your presence in my life planted my desire to shed light on how the central nervous system works.

In loving memory of Matthew Ian Triscott and Thomas Brandon Rolfes. Your friendship has made my life all the better and your support and constant belief in my abilities have enabled me to finish my Ph.D. when I did not think I could overcome the obstacles of coping with my mother's death and subsequent failure of my first try at my preliminary exams.

TABLE OF CONTENTS

I. Chapter I: Background and Significance 1
A. Overview and impact of spinal cord injury (SCI) 1
B. Automaticity of the spinal cord 2
C. Epidural Stimulation (ES) Targets Spinal Automaticity to SCI 4
D. Mapping out and uncovering spinal circuits 7
E. Workflow big data 15
II. Chapter 2: Uncovering spinal circuits in 3d using tissue-clearing 17
A. INTRODUCTION 18
B. METHODS 21
1) Animals 21
2) Experimental protocol 22
3) Tracer injections 22
4) Clearing methodologies 25
5) Microscopy 32
6) Software and 3D reconstruction 33
C. RESULTS 34
1) SeeDB 34
2) PACT protocol 35
D. DISCUSSION 40
III. Chapter 3: Genetic Tagging of Active Neurons Uncovers Encoding Properties of Spinal Networks Executing Two Repeated or Different Locomotor Tasks 46
Abstract 46
A. INTRODUCTION 47
B. MATERIALS AND METHODS: 50
1) Animals: 50
2) Experimental Design: 51
3) Tissue preparation: 53
4) Immunohistochemistry: 53
5) Quantification and data analyses: 54

6) Statistical analyses: 55
C. RESULTS: 56
1) 4-OHT injection (75 mg/kg) of FosTRAP mice immediately after the end of locomotor activity produced robust tdTomato labelling of active neurons 56
2) “TRAPed” neurons express tdTomato that labels the soma and processes. 59
3) Different locomotor events show differential expression profiles in number and spatial distribution when captured by either c-fos or tdTomato. 60
4) FosTRAP mice show more colabeling (positive for tdTomato and c-fos) when repeating the same task compared to performing different tasks. 62
5) Expression of Tdtomato and c-fos differs in spatial distribution and spatial counts when both are activated by the same locomotor task 65
D. DISCUSSION 66
1) Interpretations of network activity of different locomotor events based on c-fos, tdtomato, or both 70
2) Colabeling in FosTRAP animals reveal insights into the physiology of spinal networks 71
3) Locomotor neural network activities are measured differently with Tdtomato and c-fos 74
4) Limitations 75
E. CONCLUSION 76
IV. Application of Machine learning to Immunohistological images 78
A. INTRODUCTION 79
B. METHODS 81
1) Dataset 81
2) Classic Machine Learning Techniques 81
3) U-nets 82
4) D. Multi-scale network 82
C. RESULTS 84
D. DISCUSSION AND FUTURE WORK 85
V. Conclusion and future directions 89
A. CONCLUSIONS 89
B. FUTURE DIRECTIONS 91

1) Learning how spinal networks differentially activate to execute different types of movement 91
2) Understanding the effects of acute and chronic spinal cord injury 92
3) How do spinal networks change with ES, physical training, and pharmacological intervention 93
4) Shedding light on modeling spinal epidural stimulation and recordings 94
5) Towards reverse engineering activated neural networks and creating bio-inspired architectures for artificial intelligence or artificial general intelligence 96
REFERENCES 98

LIST OF FIGURES AND TABLES

Table 2-1: Recipe for fructose solutions in SeeDB protocol. 24

Figure 2-1: General outline of CLARITY and PACT protocol...**Error! Bookmark not defined.**6

Figure 2-2: Results of SeeDB. 33

Figure 2-3 Imaging PRV tracing after clearing with SeeDB. .....**Error! Bookmark not defined.**3

Figure 2-4: Mouse spinal cord tissue before and after undergoing PACT protocol. ..... **Error! Bookmark not defined.**4

Figure 2-5: 3D reconstruction of PRV tracing with PACT. 35

Figure 2-6: 3D reconstruction of CTB tracing with PACT. 35

Figure 2-7: 3D reconstruction of dextran amine tracing with PACT. 36

Figure 2-8: 3D reconstruction of c-fos staining with PACT..... 37

Figure 2-9: 3D reconstruction of the activatoin of a traced neural circuit... **Error! Bookmark not defined.**

Figure 3-1: Outline of FosTRAP experimental design and visualization. 50

Figure 3-2: Optimization results of FosTRAP use in the spinal cord 55

Figure 3- 3: Tissue clearing and IHC reveal the 3D morphology and processes of activated neurons. .....**Error! Bookmark not defined.**

Figure 3-4: Spatial distribution and counts of c-fos activated by resting or stepping ..... **Error! Bookmark not defined.**8

Figure 3-5: Spatial distribution and counts of tdTomato activated by different locomotor activities. 60

Figure 3-6: Counts and distribution of colabeling. 61

Figure 3-7: Gross counts of tdTomato, c-fos, and colabeling for experimental groups and locomotor activities. 62

Figure 3-8: Differences in spatial distribution and counts of c-fos and tdTomato activated by stepping. 64

Figure 3-9: Differences in spatial distribution and counts of c-fos and tdTomato activated by resting. 65

Figure 4-1: Performance of different segmented techniques compared to human raters. 78

Table 4-1: Precision and recall for machine learning techniques when compared to human raters. 79

Figure 4-2: Qualitative results of machine learning techniques and human raters.……...**Error! Bookmark not defined.**

ACKNOWLEDGEMENTS

I would like to thank my parents, Bau and Chi Pham, for raising me and constantly sacrificing in order to invest in my education. I would especially like to thank my late mom for her love and support throughout my life, her pushing me to the best of my abilities, and instilling the values that I have today. I would like to think my late sisters, Nina and Christine Pham, for giving me the inspiration to study the nervous system. I would also like to thank my aunts, uncles, and cousins for providing me with a network of support when I first moved to Los Angeles and throughout my studies at UCLA. I would also like to thank the Gammel family for being my "second" family and for all of their love and support throughout my life and during my time at UCLA.

I would like to thank my Committee Chair and thesis advisor, Dr. V. Reggie Edgerton for your guidance, professional development, and support during my time in your lab. You have allowed, encouraged, and challenged me to use my creativity to come up with my own project. Furthermore, you have allowed me to be myself throughout this whole period and have been patient with me through my ups and downs. I would like to thank Dr. Niranjala Tillakaratne for your unwavering support and belief in me. You have been there to talk me through my lows and have always reasserted your unwavering belief in me and my talents even when I did not see them in myself. You have taken care of me like a mom by bringing me food, providing a couch to nap on, encouraging me to take care of myself, and always looking out for my best interest. I would like to thank the rest of my committee, Dr. Allan MacKenzie, Dr. Alan Garfinkel, and Dr. Stephanie Seidlits for being active members of my committee by giving me advice and encouragement throughout the process. Dr. Mackenzie, you and Dustin Roberts introduced me to the CLARITY tissue clearing technique that became my first chapter. Dr. Garfinkel, you showed

me how to use resampling techniques and spatial statistics. Dr. Stephanie Seidlits, you have taken a keen interest in my project and my career development. Before you became a member of my committee you took time to talk with me and my friends about what it was like to begin your academic career and how you've approached it. Thank you all for believing in me and embracing my outlandish and overly ambitious ideas.

I would like to thank all my lab mates and friends; Dr. Yury Gerasimenko, Dr. Parag Gad, Dr. Michael Selvan Joseph, Dr. Roland R. Roy, Dr. Hui Zhong, Dr. Monzural Alam, Dr. Neil Rath, Ray Chia, Paul Duru, Mei Si Xiao, Aubrey Hornak, Michael Thornton, Steve Guzman, Victoria Lee, Kyleigh De Petro, Alexa Tierno, Nelly Kokikian, Kathleen Huynh, Nina Juan-Sing, Dr. Griselda Yvone, Dr. Katie Ingraham, Dr. Rana Khankan, Dr. Jaehoon Choe, Sharon Zdunowski, Mandy Turner, Benita Jin, Mihiri and Lokubanda Tillakaratne for all their help, love, friendship and emotional support in the process of completing my studies. I also thank Jiangyuan "Jerome" Luo, Harnadar Anand, Pia Salcedo, Olivia Kola, Connie Nguyen, Qing Dai, and Sarah Gaunt, the undergraduates who helped me throughout my Ph.D. and without their contributions none of this would be possible.

VITA

Education

2011	B.S. Biomedical Engineering and Neuroscience Tulane University New Orleans, Louisiana
2014	M.S. Bioengineering University of California Los Angeles Los Angeles, California

Positions

2015-2018	Teaching Assistant NS 102, 101L, 101C, M170 Dept. of Neuroscience University of California, Los Angeles
2017-present	Tech Fellow UCLA Technology Development Group University of California, Los Angeles

Honors and Awards

2015	UCLA Brain Research Institute Core Voucher (Edgerton/Pham)
2014, 2015, 2017	NIH UL1TR000125 UCLA CTSI Core Voucher (Edgerton /Pham)
2017	NIH S10 Shared Instrument Grant - $1,000,000 for a new multi-photon microscope **(**Bentolila et al.)

Publications

Monzurul Alam, Willyam Rodrigues, Bau Ngoc Pham, Nitish V. Thakor, "Brain-machine interface facilitated neurorehabilitation via spinal stimulation after spinal cord injury: Recent progress and future perspectives", Brain Research, Volume 1646, 2016, Pages 25-33, PMID: 27216571

Pham B, Gaonkar B, Whitehead W, Moran S, Dai Q, Macyszyn L, Edgerton VR, "Cell Counting and Segmentation of Immunohistochemical Images in the Spinal Cord: Comparing Deep Learning and Traditional Approaches," *2018 40th Annual International Conference of the IEEE*

Engineering in Medicine and Biology Society (EMBC), Honolulu, HI, 2018, pp. 842-845. PMID: 30440523

Kobayakawa, K., DePetro, K. A., Zhong, H., Pham, B., Hara, M., Harada, A., Nogami, J, Ohkawa, Y, Edgerton, V. R. (2019). Locomotor Training Increases Synaptic Structure With High NGL-2 Expression After Spinal Cord Hemisection. *Neurorehabilitation and Neural Repair*, *33*(3), 225–231. PMID 30782076

Abstracts

Pham Jr, B.N., Gad, P., Choe, J., Nandra, M., Gerasimenko, Y., Tai, Y.C., Zhong, H., Roy, R.R., and Edgerton, V.R. Relationship between Epidurally Evoked Motor Potentials under Non-Weight-Bearing or Weight-Bearing Conditions and Stepping Patterns in Spinal Rats. Abstract for poster presentation, Soc. for Neurosci. San Diego, CA, 2013.

Pham, B.N., Jr, Zhong H, Roy RR, Tillakaratne N, Edgerton VR. Use of Clarity to Visualize Activated Sensory-Motor Circuits in Mouse Spinal Cords. 9th Annual Dynamics of Microcircuits Symposium, UCLA, 2015.

Pham, B.N. Jr., Zhong, H., Roy, R.R., Tillakaratne, N., and Edgerton, V.R. Use of Peripheral Nerve Stimulation To Locate Interneurons Associated with Group I and Group II Afferents in Intact Mouse Spinal Cords. Abstract for poster presentation, Soc. for Neurosci, Chicago, IL, 2015.

Pham, B.N. Jr., Zhong, H., Tillakaratne, N., and Edgerton, V.R. PACT clearing technique to identify and trace activated neurons in the spinal network during locomotor behavior. Abstract for poster presentation, Soc. for Neurosci, San Diego, CA, 2016.

DePetro, K.A., Zdunowski, S., Tillakaratne, N.J.K., Pham, B., Zhong, H, Edgerton, V.R. Possible mechanisms underlying conversion of nonfunctional to functional states among spinal networks after spinal cord injury. Abstract for poster presentation, Soc. for Neurosci, San Diego, CA, 2016.

Pham, B.N., Anand, H., Luo, J., Kola, O., Zhong, H., Tillakaratne, N., Edgerton, V.R. Use of FosTRAP mice to analyze and compare spinal motor circuit activation during two different locomotor behaviors. Abstract for poster presentation, Soc. For Neurosci, Washington, D.C., 2017

Pham, B.N., Goankar, B., Tillakaratne, N., Zhong, H., Edgerton, V.R. Automatic segmentation techniques to facilitate quantitative analyses of spinal locomotor networks reconstructed in 3D using tissue clearing. Abstract for poster presentation, Soc. For Neurosci, San Diego, CA, 2018

Luo, J., Anand, H., Pham, B.N., Edgerton, V.R. Using FosTRAP model to compare mice lumbar spinal cord neuronal activations when stepping with and without incline. Abstract for poster presentation, Soc. For Neurosci, San Diego, CA, 2018

I. CHAPTER I: BACKGROUND AND SIGNIFICANCE

ABBREVIATIONS USED:

SCI: spinal cord injury; CPG: central pattern generator; EMG: electromyography; ES: epidural stimulation; BCI: brain computer interface; TS: transcutaneous stimulation; IN: interneurons; NMDA: N-methyl-D-aspartic acid; IHC: immunohistochemistry; IEG: immediate early gene

A. Overview and impact of spinal cord injury (SCI)

In the United States, approximately 276,000 people suffer from spinal cord injury (SCI) (DeVivo and Chen 2011) with roughly 12,500 new cases per year (Selvarajah, Hammond et al. 2014). The causes of SCI mostly occurr from physically traumatic events like vehicular accidents (38%), falls (30%), gun violence (14%), and sports-related injuries (9%) (Oteir, Smith et al. 2014). The prevalence of SCI worldwide is estimated to be 50-906 people per million (Furlan, Sakakibara et al. 2013) but this estimate has not been confirmed by a global study. Worldwide, approximately 250,000-500,000 new people sustain an SCI every year (Maitan, Frigerio et al. 2018). This number is predicted to increase with further worldwide economic development and increasing use of automobiles (Jazayeri, Beygi et al. 2015).

SCI costs an estimated $9.7 billion dollars annually (Berkowitz 1998). The lifetime cost of SCI varies with the severity of injury and the age of onset. The first year of treatment can cost anywhere from $386,562 (AIS D) to $1,129,302 (high tetraplegia) with recurring costs ranging from $44,766 (AIS D) to $196,107 (high tetraplegia) annually. However, the cost and impact of SCI outreaches just the medical costs. Some of these costs include lost wages, lowered earning potential, decreased mental health, lower quality of life, and the physical and mental tolls of the

caregivers that tend to SCI patients. SCI mainly affects caregivers in domains related to time management, physical condition of caregivers, and their sense of personal failure (Maitan, Frigerio et al. 2018). The effects and burdens of SCI show a need to develop treatments for patients with SCI to improve their quality of life while also lowering the burden to their caregivers and immediate family. In a survey of patients with SCI, clear patterns emerged in what they prioritized for future treatments. Their priorities consisted of regaining motor, bowel, bladder, and sexual function. Finding a solution that allows SCI individuals to regain functional motor movement remains the holy grail of spinal cord injury research. However, this solution currently appears to be at the interface of biology, physiology, and engineering. Developing further biological and physiological knowledge of the spinal cord and the neural circuits that comprise it can direct the design and engineering of future tools to exploit this knowledge. However, the vice versa situation can happen in which new engineered techniques can help provide new insights in the physiology of the spinal cord. The bidirectional and symbiotic relationship of these two disciplines is imperative in finding a solution to spinal cord injury.

B. Automaticity of the spinal cord

Although locomotion looks simple, the neurophysiology behind it requires complex integration of sensory information along with supraspinal input from the brain and involves many different ascending and descending tracts that include: reticulospinal, vestibulospinal, rubrospinal, corticospinal, and propriospinal tracts. From a humanistic point of view, although not exclusive to humans, some of our locomotion appears to be “automatic”, especially in a situation without any obstacles. Humans do not actively think of engaging every flexor and extensor during movement nor do they think of their coordination. To some extent, this seems “automatic” for us, leaving us to think of higher priority problems even during locomotion.

Previous research has shown that cyclical motion like stepping is indeed "automatic" and that this automaticity is located within the spinal cord.

Central pattern generators (CPG) seem to underlie the automaticity of motor control in the spinal cord. CPG's are neural networks that can effect oscillatory and highly coordinated activation of motor pools in the absence of sensory input. Previous studies have demonstrated the existence of CPG's in lower invertebrates like lampreys (Williams, Sigvardt et al. 1990). Seminal studies done in the cat have also shown the existence of CPG's in the mammalian spinal cord (Grillner and Zangger 1979). This study isolated the cat spinal cord by completely transecting it at the T12-T13 level along with a second transection that varied between the L3-L7 levels and dissecting out the dorsal roots to prevent any peripheral afferent activity. Administration of L-DOPA and Nialamide, a monamine oxidase inhibitor allowed for locomotor-like activity to be seen in the alternating EMG pattern of flexors and extensors in the foot, ankle, and knee. This study also showed that the hindlimb CPG network in the cat spanned from L6-S1. Furthermore, it was shown that spinal interneurons within these segments drive the action of these CPG's through their rhythmic activity during fictive locomotion (Edgerton, Grillner et al. 1976). Later studies would also demonstrate the existence of CPG's in other animals like rodents (Bertrand and Cazalets 2002). Though these CPG's can generate a wide range of cyclical locomotor-like behavior, they cannot respond to the environment without the input of sensory information. Navigation of even the simplest of environments requires some sensory feedback and without it, CPG's alone cannot sustain posture or locomotion under these basic conditions (Gerasimenko, Sayenko et al. 2017).

Not only can CPG's generate motor like patterns in the absence of sensory information, an underappreciated property of CPG's is their ability to receive complex patterns of sensory

information and then integrate it in a way to activate populations of neurons in sequence to sustain successful stepping in real time that is highly adaptable even in the absence of input from the brain (Gerasimenko, Sayenko et al. 2017). Many studies have shown that CPG's alone cannot control movement, and that sensory information, especially proprioception, can serve as the primary controller (Shik and Orlovsky 1976). Some examples include studies in which spinalized cats and rats have the ability to step on a moving treadmill despite suffering a complete mid-thoracic spinal transection (Andersson, Forssberg et al. 1981, Gerasimenko, Ichiyama et al. 2007, Lavrov, Courtine et al. 2008). Furthermore, the spinalized stepping patterns adapted to changing speeds of a treadmill by using the proprioceptive information generated from the interface of the hindlimb and the moving treadmill. The same preparation failed to generate any significant locomotor-like movement when the animal was lifted so that the hind paws did not make contact with the moving belt, thus further demonstrating the importance of sensory information in controlling movement (Ichiyama, Courtine et al. 2008, Courtine, Gerasimenko et al. 2009). Kinematic and electromyographic (EMG) changes that correlated with treadmill speed and load bearing provided additional evidence on top of what was already seen observationally. This phenomenon of automaticity in the spinal cord presents an intriguing target in re-enabling locomotion after spinal cord injury.

C. Epidural Stimulation (ES) Targets Spinal Automaticity to SCI

Many different ideas and techniques have tried to regain movement in animals and humans after SCI ranging from cellular approaches like stem cell therapy to brain-computer interface (BCI) to various electrical stimulation techniques. Various stem cell therapies have allowed for functional recovery in various animal models and modest functional improvement in clinical

trials. However, stem cell therapy still faces ethical and safety obstacles (Gazdic, Volarevic et al. 2018, Csobonyeiova, Polak et al. 2019, Jin, Medress et al. 2019). BCI's aim to decode motor intent using various neural and EMG recordings and then translate this decoded intent into a functional output through different means that range from robotic prostheses to electrical neural and muscular stimulation. These types of techniques have achieved a range of success in improving the quality of life of SCI patients (Alam, Rodrigues et al. 2016). However, these BCI and subsequent stimulation techniques have their limitations. Movement has many degrees of freedom with complex interactions and coordination with the rest of the body. Even simple motor events like arm movement has an actionable state space that is large enough to push the boundaries of what current neural recordings can handle along with their decoding algorithms, especially when wanting to execute movement in real-time. Second, some of these BCI technologies aim to stimulate muscles or other parts of the nervous system to achieve functional movement which requires complex flexor and extensor coordination even in a stable environment, let alone a dynamic one. Current stimulation techniques are not sophisticated enough to produce smooth movement through artificial coordination, and they also stimulate muscles and peripheral nerves in an unnatural way that leads to fatigue after a short time. Approaches that take advantage of the natural automaticity of the spinal cord have already shown great promise in restoring functional movement in animals and humans with SCI.

Recent studies have shown the efficacies of subthreshold epidural stimulation (ES) combined with physical training and pharmacological intervention to facilitate movement after SCI. Previous studies highlight how repetitive physical training can allow animals to learn motor tasks like standing and stepping that are robust to perturbations (Lovely, Gregor et al. 1986, Barbeau and Rossignol 1987, Lovely, Gregor et al. 1990, Barbeau and Rossignol 1994, de Leon,

Hodgson et al. 1998, Fong, Cai et al. 2005, Liu 2007, Courtine, Song et al. 2008, Ichiyama, Broman et al. 2011, Zhong, Roy et al. 2012). Combinations of ES with physical training and pharmacological agents like strychnine (glycinergic antagonist) and quipazine (serotonergic agonist) have facilitated stepping on a moving treadmill with body-weight support in rats with a complete mid-thoracic spinal transection (Ichiyama, Gerasimenko et al. 2005, Gerasimenko, Lavrov et al. 2006, Gerasimenko, Ichiyama et al. 2007, Edgerton, Courtine et al. 2008). Furthermore, the advantages of targeting spinal automaticity with ES can be seen in experiments in which spinal rats can perform forward and sideward bipedal stepping on a moving treadmill when their body orientation is gradually shifted from a forward facing position to a sideways facing one (Shah, Garcia-Alias et al. 2013). Achieving this type of outcome would be too complex to acomplish via BCI along with coordinated muscle and/or peripheral nerve stimulation. ES and physical training have translated to humans as improvements in standing with and without a standing cage and in bladder function along with enabling voluntary leg movements (Harkema, Gerasimenko et al. 2011, Roy, Harkema et al. 2012, Rejc, Angeli et al. 2015). Combining ES with more dynamic, task-specific physical training for an extended amount of time over 43 weeks has enabled a spinal cord injured subject to step independently on a treadmill without trainer assistance or body weight support (Gill, Grahn et al. 2018). Transcutaneous stimulation (TS) has adapted the same strategy as ES plus physical training, except in a non-invasive way. TS has enabled spinal cord injured subjects to stand with self-assistance (Sayenko, Rath et al. 2019) and to step over-ground with the assistance of an exoskeleton (Gad, Gerasimenko et al. 2017). Although ES and TS can improve motor ability in SCI patients, the mechanism of plasticity or the underlying circuitry is poorly understood. Understanding spinal circuitry, how they execute different locomotor tasks, and how they

undergo reorganization after spinal cord injury and subsequent rehabilitation can further improve clinical outcomes for SCI patients. For example, understanding how spinal circuits execute locomotor tasks can give insight into improving stimulation parameters that best facilitate plasticity for that specific task. This knowledge can also be used to design future ES electrode arrays, dictating how many contacts are needed and how fine or coarse these contacts need to be.

D. Mapping out and uncovering spinal circuits

Despite the success of ES and TS stimulation of the lumbar spinal cord in helping SCI patients regain functional movement, relatively little is known about the anatomy and physiology of spinal locomotor networks, and even more so when it comes to their physiology under *in vivo* conditions, especially when it comes to the effects of ES and physical training on their reorganization post spinal cord injury. Understanding how these networks execute different locomotor tasks can provide insight of where and how to stimulate the spinal cord to best facilitate these particular movements. Even understanding how these networks execute the same task can provide insight into creating paradigms that allow for robust execution of a given task outside of a controlled rehabilitative setting. In short, expanded knowledge of how spinal locomotor networks function will provide clues in how we should be using electrode arrays to facilitate functional gains in SCI patients, especially as they become more sophisticated in their capabilities.

Spinal circuitry research has focused on unraveling the neural networks behind central pattern generation (CPG). The first efforts in unveiling the identity of CPG's started with research on lower vertebrates like the lamprey and Xenopus tadpole. These efforts have yielded detailed network structures of the CPG's responsible for swimming, their mechanisms, and how they are

modulated (Roberts, Soffe et al. 1998, McLean, Merrywest et al. 2000, Grillner 2003, Kiehn 2006). However, identifying CPG's in these animals do not necessarily correlate with the identity and function of mammalian CPG's. Ironically, knowledge of mammalian CPG's pales in comparison to lower vertebrates despite the discovery of walking mammalian CPG's over 100 years ago (Brown 1911). More recent research has focused on uncovering the identity of the mammalian CPG along with their functionality.

The advantages of uncovering CPG circuits in lower vertebrates lie in the lower complexity of their nervous system compared to mammals. In order to replicate this in mammals, researchers used reduced *in vitro* preparations of mammalian spinal cords to probe CPG circuits. These experiments ranged from anesthetized preparations to isolated spinal cord preparations.

Single-cell electrophysiological recordings using an anesthetized cat preparation were first used to probe the function of spinal interneurons (Edgley and Jankowska 1987, Jankowska 2008). Under this preparation, stimulating hook electrodes were placed on dissected peripheral nerves from specific muscles while intracellular or extracellular electrodes were placed on target spinal interneurons and target motorneurons. The hook electrodes stimulated peripheral nerves at varying multiples of the minimum activation threshold to activate Group I, II, III muscle afferent fibers and subsequent recordings from interneurons determined which of these afferent types provided input to it. Anti-dromic stimulation of motorneurons with interneuron recordings determined which muscle the interneuron projected to. In some experiments the recorded interneuron was filled in order to demarcate it for later histological analysis. One study took this setup a step further and was able to identify that interneurons activated by group II afferent input had rhythmic activity during the flexor phase of locomotion induced through brainstem stimulation (Shefchyk, McCrea et al. 1990). A summary of the types and functions of

interneurons found through this methodology can be summarized in a review by Jankowska (Jankowska 2008). This experimental design in probing spinal interneurons and CPG networks has severe limitations. Though these types of experiments elucidated where and what type of sensory input certain spinal interneurons received along with their projections, they do not reveal what role they play in actual locomotion. Furthermore, the sheer number of mammalian spinal interneurons and the many different types they come in make it intractable to piece together the puzzle of CPG networks using only single-cell recordings (Kiehn 2006). Advancements in *in vitro* experimental setups and breakthroughs in genetics opened the door for more extensive probing of spinal locomotor circuits.

Isolated spinal cord preparations in neonatal and postnatal rodents have allowed researchers to investigate the role of spinal interneurons (IN's) in so-called "fictive" locomotion. The isolated spinal cord preparation was initially used to study spinal reflex pathways (Otsuka and Konishi 1974). However, it was discovered that application of N-methyl-D-aspartic acid (NMDA) receptor agonist caused rhythmic alternating activity in leg activity that could be recorded from the ventral roots (Kudo and Yamada 1987, Smith and Feldman 1987). Further studies would show that application of 5-HT, dopamine, and 5-HT combined with NMDA produced rhythmic motor activation that most resembled walking that had coordinated flexor-extensor activity along with left-right alternation (Cowley and Schmidt 1994, Kjaerulff and Kiehn 1996, Iizuka, Nishimaru et al. 1998). Furthermore, advancements in finding unique genetic markers have grouped spinal IN's into four distinct classes (V0, V1, V2, and V3) based upon their developmental origin and transcription factor expression (Briscoe, Sussel et al. 1999). The neuronal cell types in each of these classes have common features including cell body location and axonal projection. The combination of fictive locomotion in isolated spinal cord preps

combined with genetic manipulation or ablation have led to the discovery of different roles these IN's may play in central pattern generation of movement. V0 IN's express Evx1 transcription factor and emerge from Dbx1 progenitor cells. This group of IN's are only commissural that initially extend their axons rostrally on the contralateral side of the spinal cord and ablation of these IN's prevented left-right alternation in isolated spinal cords (Moran-Rivard, Kagawa et al. 2001, Pierani, Moran-Rivard et al. 2001, Lanuza, Gosgnach et al. 2004). V1 IN's project axons ipsilaterally and ablation of V1 IN's prevented "fictive" locomotion at higher speeds (Gosgnach, Lanuza et al. 2006). Interrupting neurotransmission of V1 and V2b IN's showed disruption of flexor-extensor alternation in isolated spinal cord prep (Zhang, Lanuza et al. 2014). Additional experiments in this study used an anesthetized *in* vitro prep similar to Jankowska and colleagues showed an abolished reciprocal inhibitory reflex with the silencing of V1 and V2b IN's. V2 IN's project intersegmentally on the ipsilateral side. Despite their ipsilateral projections, ablation of V2a IN's led to a disruption in left-right alteration in isolated spinal cord prep (Crone, Quinlan et al. 2008). It was shown that V2a IN's make excitatory contact with commissural V0 IN's which have been previously implicated in left-right alternation. Isolated spinal cord preps have shown that V2a IN's remain active over a wide range of locomotor frequencies, but show preferential firing at higher frequencies (Dougherty and Kiehn 2010, Zhong, Droho et al. 2010, Zhong, Sharma et al. 2011). V3 IN's project contralaterally to motorneurons and IN's and have two different subpopulations (Borowska, Jones et al. 2013). Ventral V3 populations located in lamina VII have few branching processes and can generate rapid, tonic firing of spikes. Dorsal V3 IN's show more complex morphology along with relatively slow average spike frequency. They have strong adaptation along with large post-inhibitory rebound potentials. These studies have made great progress in uncovering distinct genetic lineages of spinal interneurons and what role in the

CPG of movement they play. However these studies only uncover their role *in vitro*. Fictive locomotion differs from true *in vivo* locomotion since it presents a dynamic environment. Subsequent studies of these distinct types of interneurons have further researched their roles *in vivo* using ablation studies.

Subsequent studies involving these spinal IN's explored their role during *in vivo* locomotion through the use ablation and silencing as opposed to the use of genetic knockouts. Knocking out genes related to certain spinal IN's led to reconfiguration and repurposing of other spinal interneurons, leading to misinterpreting their experimental results (Kullander, Butt et al. 2003). Subsequent transgenic models would selectively knockout certain spinal IN's through the use of toxins, like DTA, linked to the expression of transcription factors unique to certain IN's or provide a means of silencing their activity through the same genetic markers. Ablation of these V0 IN's lead to disruptions in left-right alternation at varying stepping speeds that lead to a hopping motion in adult mice (2-10 Hz) (Talpalar, Bouvier et al. 2013). Furthermore, selective ablation of inhibitory V0 IN's lead to disrupted left-right alternation at low speeds, whereas selective ablation of excitatory V0 IN's lead to disrupted left-right alternation at medium to high speeds. Animals with ablated V1 IN's showed lower capability of performing the rotarod test at higher speeds compared to wild type mice (Gosgnach, Lanuza et al. 2006). Mice pups in which function of V1 and V2b IN's were silenced showed abnormal behavior in response to tail pinch and in the righting response, which could be attributed to disrupted flexor-extensor coordination (Zhang, Lanuza et al. 2014). A subsequent study on these IN's done on juvenile mice showed that V1 IN's primarily inhibit flexors while V2B IN's primarily inhibit extensors (Britz, Zhang et al. 2015). Ablation of V2a IN's show disrupted left-right alternation at high speeds, but not at low speeds (Crone, Zhong et al. 2009). These types of experiments work under the assumption

that these genetic markers exclusively express in these particular IN's, whereas in reality, these markers are not completely specific to them and could express in other types of IN's, albeit in a small number of them (Kiehn 2006). As shown, in previous experiments, these V0, V1, V2, and V3 IN's have subdivisions within themselves and are not functionally homogenous. Therefore ablating an entire population of mixed functionality requires careful interpretation. Caution must be taken in interpreting these studies since the observed result of ablating an entire population of interneurons may emerge as the result of disrupting multiple downstream and indirect effects and thus obscuring their true function. Furthermore, these studies do not define the role of these spinal interneurons in executing different types of locomotion *in vivo* while intact nor do they capture how they interface with sensory and proprioceptive input that can modulate and coordinate their activity to execute different locomotor tasks *in vivo*. Additionally, chronic disruptions of these locomotor networks through ablation can lead to activity-dependent reorganization of these locomotor networks in adult preparations, and thus can obscure subsequent interpretations (Myers, Lewcock et al. 2005). These studies have provided tremendous insight into the composition, anatomy, and function of spinal IN's involved in locomotion. However, these studies do not define the role of these IN's during locomotion nor show their modulation in different types of locomotion. C-fos has shown the ability to label spinal interneuron activity during *in vivo* locomotion, and can be a means of delineating their role in specific locomotor tasks without the use of ablation. Immunohistochemistry (IHC) can label c-fos activity, while also leaving flexibility to molecularly phenotype these spinal neurons for other properties, like the genetic lineages mentioned earlier.

The use of immediate early genes (IEG) has revealed properties of how spinal networks execute *in vivo* locomotion in adult mammals. IEG's are classes of genes that activate transiently

and rapidly in response to cellular stimuli. Certain classes of IEG's, like c-fos, has been used as biomarkers for neural activity. Several studies have used c-fos as a marker to identify neurons active during locomotion in the brain (Ruigrok, van der Burg et al. 1996) and in the spinal cord of cats (Huang, Noga et al. 2000, Dai, Noga et al. 2005) and rodents (Ahn, Guu et al. 2006). Some studies use c-fos to identify locomotor-related neurons for subsequent electrophysiological characterization (Dai and Jordan 2010), whereas other studies combine c-fos with transgenic and immunohistochemical markers to identify certain spinal interneurons active during locomotion (Wilson, Blagovechtchenski et al. 2010). Studies exploring the role of V0-3 IN's have used c-fos to identify the activity of these neurons during fictive (Lanuza, Gosgnach et al. 2004, Griener, Zhang et al. 2015) and *in vivo* locomotion (Zhang, Narayan et al. 2008, Bretzner and Brownstone 2013). V0 IN's show differential c-fos activation in their subtypes during fictive locomotion with $V0_V$ IN's showing preferential activation over $V0_D$ (Griener, Zhang et al. 2015). Interestingly, this study found that $V0_D$ received input from primary afferents whose activation are noticeably absent during fictive locomotion compared to *in vivo* locomotion; thus supporting the notion of cautionary interpretation of experimental results from fictive locomotion. Dorsal and ventral V3 IN's showed differential c-fos activity after either swimming or running (Talpalar, Bouvier et al. 2013). Running caused an increase in c-fos activity of both dorsal and ventral V3 IN's, whereas swimming only caused an increase in c-fos activity of ventral V3 IN's. It is believed that ventral V3 IN's serve as premotor neurons and dorsal V3 IN's serve as relays mediating sensory input. Silencing or inhibiting V3 interneuronal activity led to increased variability in locomotor burst amplitude and period along with asymmetrical left-right activity. These c-fos studies support Edgerton and Kiehn's caution in interpreting ablation studies, particularly in regards to the heterogeneity of functions within the V0-3 interneuronal subtypes. Furthermore, it reasserts the

importance of studying *in vivo* locomotion and the role that sensory information plays in it despite its increased complexity over reduced preparations like isolated spinal cords.

Besides associating particular spinal neurons with locomotion, c-fos has also been used to probe how spinal networks function to execute tasks and to help investigate the role ES and step training has on these networks after spinal cord injury. C-fos labeling showed that spinal networks handle increased loading by increasing motorneuron excitability through increased activation of cholinergic interneurons around the central canal (Tillakaratne, Duru et al. 2014). In this experiment, rats were separated into groups based upon locomotor activity: a non-locomotion control, 30 minutes of stepping at a 0 degree incline, and 30 minutes of stepping on a 25 degree incline. Rats that stepped on an incline showed more c-fos activation of cholinergic interneurons around the central canal than both the 0 degree stepping condition and control groups. Furthermore, the use of muscle-specific neural tracing with cholera toxin subunit b demonstrated that this increased c-fos activation could stem from increased drive from proprioception and supraspinal input. The use of c-fos also demonstrated that these networks use different spatial activation patterns to execute different tasks. C-fos activation showed different spatial distributions when activated by forward stepping versus backward stepping in cats (Merkulyeva, Veshchitskii et al. 2018). Backward stepping showed a significant increase in c-fos activity of neurons in the L7 spinal segment, particularly in the intermediate area of the gray matter, compared to forward stepping. C-fos studies have shown that step training makes spinal networks more specific and efficient after step training (Ichiyama, Courtine et al. 2008, Duru, Tillakaratne et al. 2015, Chen, Marsh et al. 2017). Locomotor training combined with ES improved stepping ability after complete spinal transection in rats as seen from behavior observations along with EMG and kinematic analysis. In trained animals it was shown that there

was decreased c-fos activity throughout the lumbosacral spinal cord compared to untrained animals, thus showing a pruning effect that made spinal networks more efficient at generating locomotion (Ichiyama, Courtine et al. 2008). This finding was further supported in that step-trained rats had lower c-fos activation in cholinergic neurons surrounding the central canal than untrained rats after complete spinal transection and ES (Duru, Tillakaratne et al. 2015). Animals suffering from incomplete SCI showed lower c-fos activity in the lumbar activity in response to step training, compared with no step training, when given sequentially after treatment with anti-Nogo-A antibodies that ameliorated the suppression of fiber growth activity that Nogo has on the spinal cord (Chen, Marsh et al. 2017). These studies demonstrate the potential of c-fos as a tool to investigate the anatomy and physiology of spinal networks along with investigating how these networks change with SCI and SCI after treatment. However, c-fos has its limitations in the amount of data that it can generate which stems from the time and labor intensiveness of conducting studies that use IHC.

E. Workflow big data

Anatomical knowledge of spinal locomotor circuits along with physiological understanding of how they interact with sensory input to execute locomotor tasks *in vivo* are paramount questions that need to be answered in order optimize ES and physical training for treatment of SCI patients. IHC labeling of c-fos provides an advantageous means of answering how locomotor networks execute tasks *in vivo* compared to other modalities that capture neural network activation. Techniques like fMRI and EEG can capture system wide activation, but have very poor spatial resolution, whereas multi-electrode arrays and calcium imaging have fine spatial resolution but are limited in the total volume that they can record from which restricts their

ability to capture network wide activation. IHC and c-fos labeling occupies a unique niche in that it can potentially capture network wide activation with cellular resolution, which is powerful enough to answer the question of how spinal locomotor networks operate *in vivo*. However, current IHC techniques have limitations in its workflow that other neural activity recording techniques do not have. In order to answer the biological questions posed earlier, IHC and c-fos techniques must adapt a big data type of workflow. First, this requires a method that gathers large amounts of data similar to fMRI, EEG, and calcium imaging. Second, there needs to be an automated analysis that can parse through this data like the algorithms developed to analyze data of the aforementioned methods.

II. CHAPTER 2: UNCOVERING SPINAL CIRCUITS IN 3D USING TISSUE-CLEARING

ABBREVATIONS USED:

IHC: immunohistochemistry; IEG: immediate early gene; PRV: pseudorabies virus bartha; CTB: cholera toxin subunit B; SeeDB; see deep brain; TA: tibialis anterior; SOL: soleus; IBC: institutional biosafety committee; RT: room temperature; PACT: passive clarity technique; SDS: sodium dodecyl sulfate; RIMS: refractive index matching solution; NDS: normal donkey serum; A4P0: acrylamide 4% paraformaldehyde 0%; GFP: green fluorescent protein; ALMS: advanced light microscopy services; CNSI: California nanosystems institute

ABSTRACT

Though IHC has the potential to uncover properties like neural activation over a whole network (i.e. the spinal cord), current IHC methods are limited to two dimensions through the use of thin sectioning and staining. This methodology cannot reliably answer questions that pertain to a broad three dimensional network. Developments like tissue clearing, make neural tissue optically transparent so that light microscopy can scan through a whole tissue volume similar to MRI, and thus recreate a 3D reconstruction. This study aims to adapt the passive CLARITY technique (PACT) to not only clear mouse spinal cord tissue, but to combine PACT with retrograde neural tracing and IHC staining. Muscle-specific neural tracing with pseudorabies virus (PRV), cholera toxin subunit b (CTB), and dextran amine have worked with PACT clearing to create 3D reconstructions of these muscle-specific neural networks. Furthermore, PACT clearing can be combined with IHC techniques to label thick tissue sections for c-fos, a neural activity marker, and chx10, a marker for V2a spinal interneurons. The quality of the IHC labeling of PACT-cleared tissue prove to be just as robust and effective as IHC

labeling of thin tissue sections. The combination of PACT with IHC labeling of c-fos gives a niche technique that can capture system and neural network wide activity during *in vivo* locomotion that also has cellular resolution while also having the flexibility for further molecularly phenotyping. There is no current methodology that can accomplish this in a mammalian system.

A. INTRODUCTION

Neural networks have complex arrangements and connectivity, which can be probed in many different ways ranging from electrophysiology to histology. Despite the abundance of different methodologies to study neural networks, none of them can be considered perfect and all of them have their drawbacks when it comes to either spatial or temporal resolution. For example, electrophysiology can achieve fine temporal resolution that can resolve at the single-cell level, but has its limits when it comes to the number of neurons it can monitor or the volume that it can record from. A method like electrophysiology does not have the volumetric capacity to study an expansive neural network like the spinal locomotor network that covers the entire spinal cord. Furthermore, a method like fMRI has the volumetric capacity to monitor the entire spinal cord, but it cannot track neural activity at the single-cell level. To answer questions like, "What are the identities of the interneurons responsible for processing sensory information for certain locomotor tasks? Where are they located and where are they projecting this information to?" we need to turn to histological techniques that can provide network wide information at a single-cell resolution.

Histology, particularly immunohistochemistry (IHC), has been used to probe neural networks *in vivo*. At the center of this analysis has been the use of immediate early genes (IEG), like Arc

or c-fos, as a biomarker for neural activity. It does not have the fine temporal resolution of electrophysiology, but studies have shown that IEG's have the time resolution to delineate neurons active during a specific event. Previous studies have used c-fos as a neural activity marker to label neurons in the spinal cord that have been active during certain locomotor tasks before or after spinal cord injury (Ahn, Guu et al. 2006, Ichiyama, Courtine et al. 2008, Tillakaratne, Duru et al. 2014, Duru, Tillakaratne et al. 2015). Furthermore, IHC can uncover other information about active neurons like their morphology, phenotypic identity, and their projections that electrophysiological and other non-invasive methodologies cannot answer. IHC can uncover morphology using antibodies that label the soma, unveil phenotypic identities using antibodies for certain neurotransmitters, and reveal projections and connectivity using neural tracers like pseudorabies virus (PRV) and cholera toxin subunit B (CTB). Though histological techniques have the ability to provide system wide information of neural networks, to execute this practically remains inefficient with intensive time and large labor costs.

Typical histology and IHC requires thin sections, ranging from 5-50 μm, followed by antibody staining and subsequent imaging through microscopy. These techniques use thin sections due to dense and irregularly shaped lipid interfaces from the cell membrane and myelin sheath that can 1) prevent sufficient antibody penetration deep into tissue and 2) cause light scattering and diffraction that prevents optical imaging deep into tissue. However, mouse brain and spinal cord tissue can extend tens of millimeters in any dimension, making cutting and staining every tissue in a whole brain or spinal cord intractable without a large enough workforce. Furthermore, registration, alignment, and tissue-warping errors create problems when trying to stack manually cut and stained tissue sections and can cause inaccurate three dimensional recreations of neural networks. To mitigate the time and labor cost of sectioning and

staining tissue, researchers have employed a sampling technique with their tissue sections. However, even with a sampling rate of using every other tissue section, there is still a lot of missing information from the unused tissue sections let alone giving up the ability to recreating connectomes of neural networks. Over the past few decades, many innovations have been developed to solve some of these problems (Helmchen and Denk 2005, Tsai, Kaufhold et al. 2009, Kleinfeld, Bharioke et al. 2011). Automated methods for mechanically sectioning tissue prevent potential damage that comes with manual sectioning while also mitigating some of the time and labor costs. Serial block-face mechanical or optical ablation methods (Rauschning 1986, Toga, Ambach et al. 1994, Ewald, McBride et al. 2002, Li, Gong et al. 2010) can create detailed brain maps when used with imaging modalities like two-photon tomography, electron microscopy, or array tomography (Tsai, Friedman et al. 2003, Denk and Horstmann 2004, Micheva and Smith 2007, Ragan, Kadiri et al. 2012). However, these methods have its limits when it comes to volumes that they can handle, and furthermore, have limited potential to incorporate molecular or cellular labeling like IHC into the process (Livet, Weissman et al. 2007, Osten and Margrie 2013). These limitations have paved the way for optical clearing techniques to make its mark when analyzing neural networks.

Optical clearing techniques aim to make tissue transparent or "see-through" so that microscopy methods with an automatic stage can scan through the whole tissue volume (ex. A confocal microscope will take 500 images each spaced 2 μm apart for a 1 mm thick section of clarified tissue). Tissue appears opaque due to a couple of reasons: 1) Lipids from cells and myelin causes light refraction and scattering and 2) tissues have inhomogeneous refractive indices causing light to scatter non-uniformly and thus create a "distorted" image. Different optical clearing methods clear tissue by resolving either one or both of these reasons. Certain

optical clearing methods involve immersion of the specimen in a medium so that the refractive indices of the tissue and the medium become homogenous, thus reducing light scattering and increasing the depth and range of optical imaging. These methods include Scale and SeeDB (Ke, Fujimoto et al. 2013, Ke and Imai 2014, Vartak, Rahman et al. 2015). Though these techniques make the tissue transparent, they do not remove the lipids from the cell membrane or myelin, making the tissue unsuitable for molecular probing or phenotyping. Other techniques render tissue transparent by removing lipids, which include the CLARITY and PACT techniques (Chung and Deisseroth 2013, Yang, Treweek et al. 2014, Treweek, Chan et al. 2015). These protocols embed the tissue with hydrogel monomers which then polymerize and form covalent bonds with endogenous proteins. This allows for the removal of lipids with a strong detergent while also keeping proteins of interest in place. The removal of lipids while keeping proteins in place make the tissue suitable for molecular probing that can penetrate the whole tissue volume. The majority of studies that employ optical clearing methods do so to study brain circuits (Chung and Deisseroth 2013, Ye, Allen et al. 2016), but there are a couple of studies that clear the spinal cord (Soderblom, Lee et al. 2015). In the following study, we employ tissue-clearing techniques to the spinal cord to probe spinal network activity during locomotion and to trace muscle-specific spinal circuits.

B. METHODS

1) Animals

Adult C57BL/6 mice were used to troubleshoot both the SeeDB (n = 10) and the PACT protocol (n = 10). Mice were obtained through The Jackson Laboratory (Ellsworth, ME) and

through Charles River (Hollister, CA). All surgical and experimental procedures were conducted under strict guidance provided by UCLA Chancellor's Animal Research Committee.

2) Experimental protocol

All animals in these procedures were acclimated and trained to step on a treadmill for 30 minutes.

After three training sessions on the treadmill, mice would undergo surgery for intramuscular injections of either pseudorabies virus Bartha (PRV), cholera toxin subunit B (CTB, List Biologicals, CA), or dextran amine (MW: 3kDa, Invitrogen). Animals were split into two different injection groups: Group 1 had mice that received unilateral injections of PRV into their left tibialis anterior (TA) and Group 2 had mice that received bilateral injections of tracers that included PRV into the left TA, dextran amine into the right TA, and CTB into the left soleus (SOL). All animals were given 96 hours to recover from surgery, and after the recovery period all animals performed one last 30 minute bout of quadrupedal stepping on a treadmill. One hour after the completion of stepping, animals were euthanized with a mixture of sodium pentobarbital. All animals were transcardially perfused with cold 4% PFA and then post-fixed in 4% PFA at 4C for 24 hours. Each mouse's spinal cord was dissected and fixed in a gel of 2% agarose where their spinal cords would be sectioned into 1 mm segments using a vibratome. These segments would then undergo tissue clearing and subsequent IHC.

3) Tracer injections

All surgical procedures were conducted under aseptic conditions. Forty-five minutes prior to surgery the mice were put under anesthesia using isoflurane gas mixed with oxygen at 1.0%-

2.5% and delivered via facemask. The hindlegs were carefully shaved with clippers (#50 clipper blade). The surgical site was scrubbed with betadine scrub solution followed by an ethyl alcohol (70-90%) wipe which was repeated three times. Ophthalmic ointment was applied to both eyes immediately before surgery to prevent drying of eyes. A sterile drape was used to cover the majority of the mouse while exposing the surgical site. Following surgery prep, the animals were transferred to the surgical table where there was another facemask to deliver isoflurane gas mixed with oxygen at 1.0%-2.5%. During surgery, the animal's breathing was visually monitored (chest movement 1breath/1sec) and anesthesia was modified accordingly.

All surgeries were conducted in a BSL2 approved room on a water-circulating heating pad maintained at 37˚ degrees Celsius to help maintain body temperature. Under anesthesia, a skin incision in the upper leg compartment was made over the TA. The TA was then separated from the other leg muscles by breaking down fascia and connective tissue using probes. After muscle separation neural tracer injections were delivered using a 10 µL Hamilton Syringe with a 30 gauge needle (Hamilton, Reno, NV) at 5 different sites in the TA, 3 injections proximal to and 2 injections lateral to the tibial bone. The virus was injected slowly to minimize leakage and the area was flushed with warm sterile saline to clear the area of any virus that may have leaked out. After injection into the TA, the SOL was located and separated out from the other leg muscles in a similar manner as the TA. A 10 µL Hamilton Syringe with a 30 gauge needle delivered neural tracers at 3 different sites in the SOL. After TA and SOL injections, the incision was closed using Ethilon 6.0 sutures. This procedure was then repeated for the opposite leg. After surgery animals were given an analgesic (Buprenex, 0.05-0.1 mg/kg) subcutaneously to alleviate pain associated with the surgical procedure, which was also given twice a day for 3 days following the surgery. The mice were allowed to recover in an incubator maintained at 37◦C until they fully

awoke with the use of their fore- and hindlimbs. Upon recovery from anesthesia the mice were then given 2 ml of lactated Ringer's solution subcutaneously to minimize dehydration and then returned to their home cages. All of these surgical procedures and postsurgical animal care are performed routinely in our laboratory and have been described previously (Courtine, Gerasimenko et al. 2009, Tillakaratne, Duru et al. 2014, Duru, Tillakaratne et al. 2015). The volume and location of injection for different neural tracing options can be found below:

Pseudorabies virus

Pseudorabies Bartha virus (PRV) usage was approved by UCLA Institutional Biosafety Committee (IBC). PRV handling, injections, animal care and terminations were carried out under Bio Safety Level II in a negative air flow lab space inside fume hood according to the IBC approved standard operating procedure. PRV was kindly provided by Dr. Lynn Enquist at Princeton University, Center for neuroanatomy with Neurotropic Viruses (CNNV grant no. P40RR018604). PRV 152 (~15 µl of $1.24x10^9$ pfu/ml; total virus $1.9x\ 10^7$) was injected into the TA at a volume of 10 µl. The infection time of PRV was 96 hours.

Cholera toxin subunit B (CTB)

CTB came in two different color variants of 488 (green) and 647 (far red). Injectable CTB solution was made at 1% (w/v) in sterile saline solution. It was injected at a volume of 2 µL for both the TA and the SOL with an infection time lasting 96 hours.

Dextran amines

Dextran amine came in a green variant and was diluted to a 10% (w/v) in 2% DMSO in sterile saline. This solution was injected at a volume of 3 µL in only the SOL and was allowed 96 hours to traverse from the muscle to the motor neurons in the spinal cord.

4) Clearing methodologies

See Deep Brain (SeeDB):

Overview:

SeeDB is a clearing methodology that aims to create a homogenous refractive index throughout the tissue that matches the medium. It accomplishes this by serially immersing the tissue in solutions of increasing concentrations of fructose. This protocol was made to be a cheap alternative for tissue-clearing compared to CLARITY due to the relative affordability of the materials and reagents. The following protocol has been adapted from (https://bio-protocol.org/e1042#biaoti17549) (Ke, Fujimoto et al. 2013, Ke and Imai 2014, Vartak, Rahman et al. 2015).

Solutions:

The sucrose solutions and the final SeeDB solution requires dissolving D(-)-fructose (Sigma-Aldrich, catalog number: F0127) completely in 1x PBS in a 50 mL conical centrifuge tube. Dissolving higher concentrations of fructose requires higher temperatures. After dissolution of fructose and subsequent cooling of the solution to room temperature add α-thioglycerol (Sigma-Aldrich catalog number: M1753) to give a concentration of 0.5% to prevent the Maillard

reaction. The following table outlines the recipe to create the increasing concentration of fructose solutions to be used and the final SeeDB solution.

<table>
<tr><td rowspan="2"></td><td colspan="3">Composition</td></tr>
<tr><td>Fructose</td><td>Solvent</td><td>α-thioglycerol</td></tr>
<tr><td>20% w/v</td><td>4 g</td><td rowspan="5">add distilled water to make a total volume of 20 ml</td><td rowspan="7">100 µl</td></tr>
<tr><td>40% w/v</td><td>8 g</td></tr>
<tr><td>60% w/v</td><td>12 g</td></tr>
<tr><td>80% w/v</td><td>16 g</td></tr>
<tr><td>100% w/v</td><td>20 g</td></tr>
<tr><td>SeeDB</td><td>20.25 g</td><td rowspan="2">add 5 ml distilled water</td></tr>
<tr><td>SeeDB37</td><td>27 g</td></tr>
</table>

Table 2-1: Recipe for fructose solutions in SeeDB protocol

Experimental protocol:

Before starting the protocol, post-fix tissue in 4% PFA overnight at 4^0C. After post-fixing, wash sample 3 x 10 min in PBS. Also prepare all fructose and SeeDB solutions fresh.

1) Incubate tissue in 20 mL of 20% w/v fructose inside a 50 mL conical tube on a tube rotator for 4-8 hours at either room temperature (RT) or 37^0C
2) Incubate sample like in previous step, except in 40% w/v fructose for 4-8 hours
3) Incubate sample in 60% w/v fructose in a manner similar to previous steps for 4-8 hours
4) Incubate sample in 80% w/v fructose in a manner similar to previous steps for 12 hours. This incubation should be at 37^0C
5) Incubate sample in 100% w/v fructose in a manner similar to previous steps for 12 hours. This incubation should be at 37^0C
6) Incubate sample in SeeDB in a manner similar to previous steps for 24 hours at 37^0C.

7) If tissue is not clear after step 6, incubate in SeeDB for another 24 hours. If tissue sample still isn't clear exchange current SeeDB solution for a fresh batch and incubate until clear.
8) Successfully cleared sample should look amber under a light source.

Passive CLARITY Technique (PACT) protocol:

Overview:

The PACT protocol was developed as an alternative to the CLARITY technique. This procedure does not require electrophoresis to circulate the SDS clearing solution throughout the tissue, and it uses a cheap alternative to FocusClear as an index matching solution to mitigate the cost of CLARITY clearing. Furthermore, this technique uses a less stringent and robust acrylamide hydrogel matrix to embed the tissue in. This allows for quicker clearing and deeper penetration of molecular probes. However, this also makes the tissue more fragile to harsh conditions. Like CLARITY, the PACT protocol follows the same procedure outlined below in the figure (Chung and Deisseroth 2013, Yang, Treweek et al. 2014, Treweek, Chan et al. 2015).

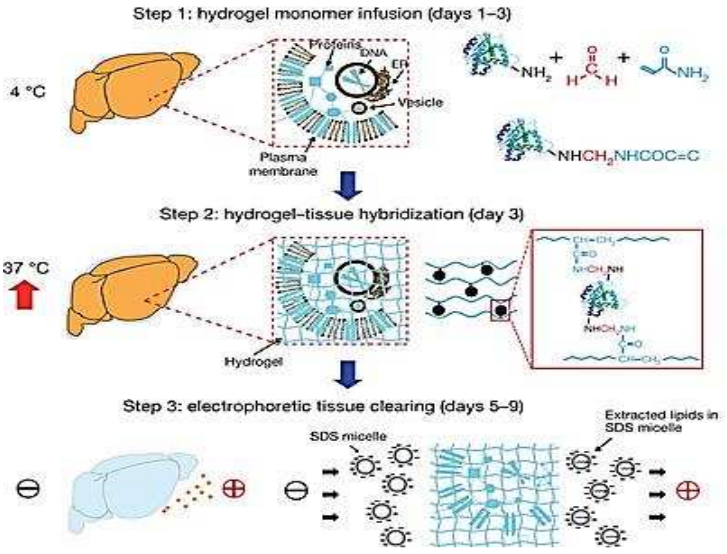

Figure 2-1: General outline of CLARITY and PACT protocol. This figure shows a high level overview of tissue clearing. The first step involves infusing the tissue with a hydrogel monomer so that it diffuses evenly throughout the tissue. The second step involves polymerizing the monomers to create a meshwork that will lock proteins into place. The third step involves removing lipids with a strong detergent like Sodium Dodecyl Sulfate (SDS). The SDS will envelop lipids in micelles which will then leave the tissue while the hydrogel meshwork keeps proteins locked into place.

Solutions:

4% Acrylamide monomer solution (A4P0):

A4P0 was made fresh for each round of PACT clearing. For 200 mL of A4P0 add 10 mL of 40% (w/v) acrylamide solution (Fisher Scientific catalog number: BP1402-1) to 100 mL of 2x PBS and 90 mL of ddH_2O. Mix this solution to dissolve 0.5 gram of VA-044 Initiator (Fisher Scientific catalog number:NC0632395).

8% Sodium dodecyl sulfate (SDS) solution:

This SDS solution is also known as the clearing solution and was made fresh for every round of PACT clearing. For 1 L of clearing solution, dissolve 80 g of SDS (Fisher Scientific catalog number: BP166-500) in 1x PBS. After the dissolution of SDS, volume up with 1x PBS to 1L, and then adjust pH to 8.5.

Refractive index matching solution (RIMS):

The purpose of RIMS is to make the refractive index of tissue homogenous so that light passes and bends in the same way when going through the tissue, and thus making it looks transparent. RIMS was made fresh for every round of PACT clearing. Add 40 g of Histodenz (Sigma-Aldrich #D2158) in 30 mL of 0.02M phosphate buffer with 0.01 sodium azide. Solution was dissolved in a 50 mL jar using a stir bar. The addition of histodenz was broken up 5 g at a time due to the low solubility of histodenz and its nature to clump. Once fully dissolved the pH of RIMS was adjusted to 7.5.

Protocol:

The protocol for CLARITY can be found online at http://clarityresourcecenter.org and the protocol for PACT has been published (Treweek, Chan et al. 2015). The following is presented as an overview of the PACT protocol and more details of the process and troubleshooting can be found in the publication by Treweek et al. 2015.

Embedding tissue into acrylamide hydrogel:

Place a 1 mm thick section of mouse spinal cord into 9 mL of A4P0 in a urinalysis tube (Fisher Scientific catalog number:14-375-138). Incubate for 3 days at 4^0C with gentle shaking to allow hydrogel monomer to evenly diffuse throughout the tissue. After incubation in A4P0 the tissue needs to be degassed to remove any dissolved oxygen that would hinder the polymerization of the hydrogel monomer. The first part of degassing involves removing dissolved oxygen by connecting the urinalysis tube to a vacuum line using a hypodermic needle and tubing. Turn on the vacuum line for 15 minutes while agitating the tissue and solution every 3 minutes. This can be done by hitting the urinalysis tube against a table. After successful vacuuming there should be very little amounts of bubbles the rise to the top after hitting the tube against the counter. After vacuuming, using the same hypodermic needle and tube connect the tube to a nitrogen gas line and bubble nitrogen gas through the solution for 5 minutes. This will dissolve inert nitrogen into the solution to prevent any subsequent dissolution of oxygen into the A4P0 solution. Once this is done transfer the urinalysis tube with the tissue into a 37^0C water bath for polymerization and leave for 3 hours. After the polymerization the A4P0 solution should become viscous like a syrup. After polymerization remove the tissue from A4P0 and place into costar wells, and wash in 1X PBS for 3 x 10 minutes.

Incubation in clearing solution:

After completing the PBS washes after polymerization is complete, place the tissue section in a 50 mL conical tube with 35 mL of 8% SDS and then seal the tube using parafilm. Place the tube on a heated a shaker at 50C under foil to prevent contamination with light. The temperature can be adjusted to speed up clearing. However, there is a tradeoff between decreasing clearing time and quenching endogenous fluorescent proteins due to the higher temperature. Incubation time can vary between 3-7 days. On average, 1 mm tissue sections were incubated in clearing solution for 7 days with exchanging of old clearing solution with new clearing solution every day. Everyday check the tissue for "clarity" or transparency, successfully cleared tissue should have homogenous levels of transparency throughout the tissue. After incubation in clearing solution wash out the residual SDS in the tissue by washing in 1X PBS for 48 hours and exchanging the PBS every 6 hours. Any residual SDS will manifest itself as a white cloudiness, especially after placed in 4^0C, that disappears when the tissue returns to room temperature and the SDS has dissolved back into solution. The residual SDS can hinder tissue transparency while also disrupting antibody attachment to its target due to the nature of SDS as a strong detergent. Once this step is done the tissue is either ready to undergo IHC or placed into RIMS for subsequent imaging.

Immunohistochemistry (Optional):

After PACT clearing, tissue underwent immunohistochemistry (IHC) to amplify a neural tracer and one other molecular biomarker. The IHC protocol had to be changed from the one used for typical free-floating 30 μm sections. One millimeter thick sections were blocked in 2% normal donkey serum (NDS) in 0.3% triton in 1X PBS for 24 hours at 4^0C. After blocking, tissue

was incubated in primary antibody solution, which consisted of primary antibody and 2% NDS in 0.3% in 1X PBS, for 7 days at 4^0C with gentle shaking. The 1 mm thick tissue section was incubated in a volume of 1.2 mL of primary antibody solution in a 12 well plate, and the solution would be exchanged for fresh primary solution every 2 days. Primary antibodies used to amplify neural tracers included chicken anti-GFP (1:400, Aves catalog number: GFP-1020) for PRV, goat anti-CTB (1:1000 List Biologicals #703) for CTB tracing, and goat anti-tdTomato (1:1000 LS Bio LS-C340696-600) for amplifying tdTomato expressed in TRAP mice. Biomolecular markers included rabbit anti-c-fos (1:1000, EMD Millipore ABE457) to label activated neurons and Chx10 (1:1000, Santa Cruz sc-365519) to label v2a interneurons. After incubation in primary solution, tissue sections were washed in 1X PBS for 24 hours with exchanges occurring every 4 hours. From here, tissue sections were incubated at 4^0C for 7 days with gentle shaking in secondary antibody solution, which included secondary antibody and 2% NDS in 0.3% in 1X PBS. Secondary antibodies used included FAB_2 fragments of donkey antibodies against chicken, goat, and rabbit (1:500 Jackson Immuno Research catalog number: 703-545-155, 705-586-147, and 711-586-152 respectively). PRV and c-fos were stained together with Alexa Fluor 488 (green) and Alexa Fluor 594 (red) respectively. CTB was stained with Alexa Fluor 647 (far red) and tdTomato was stained with Alexa Fluor 594 (red). Chx10 underwent TSA amplification where the secondary antibody used was FAB_2 fragments of donkey anti-rabbit conjugated with horseradish peroxidase (1:500 Jackson Immuno Research catalog number: 711-036-152). After incubation in secondary, tissue was washed with 1X PBS in a similar manner as after primary incubation. The tissue was then placed in RIMS after PBS wash. However, the Chx10 underwent a green TSA color reaction (1:500 Perkin Elmer catalog number: NEL745001KT) overnight after

PBS wash. The tissue was then washed for 12 hours with PBS exchanges every 2 hours after the TSA color reaction and then put into RIMS.

RIMS:

Once the tissue is ready to be imaged either after clearing or after IHC, place the tissue into 1.5 mL in a 5 mL tube or any volume sufficient enough to completely submerse the tissue in. Incubate the tissue until the tissue is transparent. The tissue will look opaque or translucent after the PBS wash following either the clearing process or IHC. Incubation in RIMS can last between 4 to 48 hours before sufficient transparency is achieved before imaging. The tissue can be stored in RIMS at 4^0C until it is able to be imaged. For longer term storage exchange the RIMS solution every week to prevent the growth of fungus.

5) Microscopy

Before imaging, cleared 1 mm sections of spinal had to be mounted in a hand-made imaging chamber. This involved taking one coverslip (.16-.19 mm thick 24 mm x 30 mm) and attaching one pre-made well (SunJin Labs catalog number: IS011) that was 0.5 mm thick onto it. These wells come with an adhesive side in which the covering could be peeled off and attached to any surface. To create a 1 mm deep well two of these pre-made wells were stacked on top of each other. After the well was created the cleared tissue section was transferred to the well via a transfer pipette and forceps were used to position the tissue so that the cross section of the gray matter was facing up. RIMS was then added to the well until it reached the top of the well and then a second coverslip was placed on top creating an imaging chamber sandwiched between two

coverslips. Kim wipes were used to absorb any RIMS that leaked out of the imaging chamber. Once the chamber was complete the tissue was ready to be imaged via a confocal microscope.

All tissue was imaged using a Leica SP5 confocal microscope at the Advanced Light Microscopy Services (ALMS) at the California NanoSystems Institute (CNSI) at UCLA. Images were acquired at a resolution of 1024 x 1024 using a 10x air objective (0.3NA). An image stack was acquired with an automatic stage that tiled images so that the merged imaged encompassed the entire spinal cord cross sections while also acquiring an image every 3 microns until the entire depth and volume has been imaged. The gain and power of the confocal lasers were automatically adjusted to compensate for decreasing brightness and intensity as the focus of the objective moved deeper into the tissue. For the 1 mm thick tissue section, quality images could only be acquired through a depth of 600 μm on average. To get images throughout the whole stack, the imaging chamber was flipped after the first round of imaging and then subsequently imaged. The resulting image stacks were exported as TIF files to an external hard drive for further processing and 3D reconstruction.

6) Software and 3D reconstruction

After the image stacks were exported as individual TIF files, different imaging software were used for image processing and subsequent 3D reconstruction. ImageJ (https://imagej.nih.gov/ij/) was used to enhance the brightness/contrast of all the images in the image stack along with performing cropping in the x or y directions. ImageJ was also used to convert images into 8 bit grayscale to be worked with by other software. Videos that played the sequence of 2D images in the image stack from rostral to caudal was also created using ImageJ.

The software, Vaa3D (https://alleninstitute.org/what-we-do/brain-science/research/products-tools/vaa3d/), created the three dimensional reconstructions of the processed image stacks from ImageJ. Vaa3D also performed three dimensional cropping in the x, y, and z directions. Cropping in the depth or z dimension was performed to eliminate the surface effect from obscuring the view of deeper images. The surface effect is a phenomena in which the outside of the tissue is significantly brighter than the deeper layers and thus obscures viewing deeper layers, especially when the viewing mode of the three dimensional reconstruction is maximum intensity projection. After proper cropping, Vaa3D created videos of the three dimensional reconstruction where the tissue is rotated along different axes.

C. RESULTS

1) SeeDB

The SeeDB protocol successfully cleared both 1 mm segments and entire lumbar segments of mouse spinal cords after 3-4 days of incubation in varying concentrations of fructose solution. The tissue appeared amber under ambient light (Figure 2-2), but the tissue was more translucent than “transparent”. Letters and markings were distinguishable when the cleared tissue specimen was placed over it, but it was not crystal clear like a window. To test whether SeeDB could clear

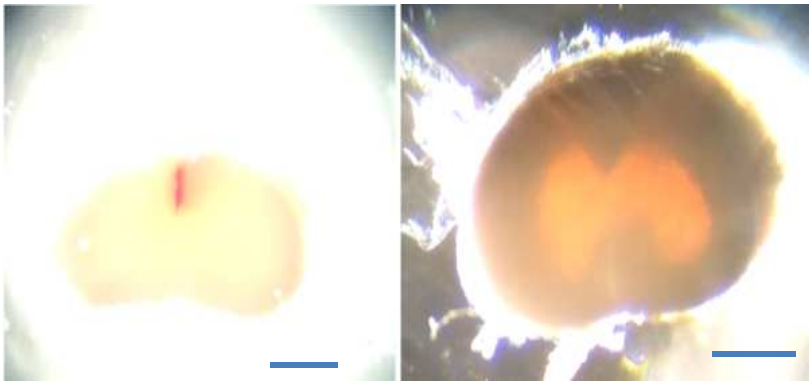

Figure 2-2: Results of SeeDB clearing. Both images are 1 mm sections of mouse spinal cord after the SeeDB process under a dissecting microscope. Notice the amber color under ambient light indicating successful completion of SeeDB. The tissue is also to transmit light through the thickness, but is not perfectly clear. Blue scale bars are 1 mm.

tissue in a manner needed for future experiments, spinal cord tissue from animals in which pseudorabies virus (PRV) was injected in the left tibialis anterior (TA) underwent this protocol. The lumbar segment was then imaged under a confocal microscope with an automatic stage. The resulting imaging could not resolve PRV+ neurons, and only showed autofluorescence on the outer surfaces of the lumbar enlargement (Figure 2-3). This autofluorescence appeared bilaterally for a

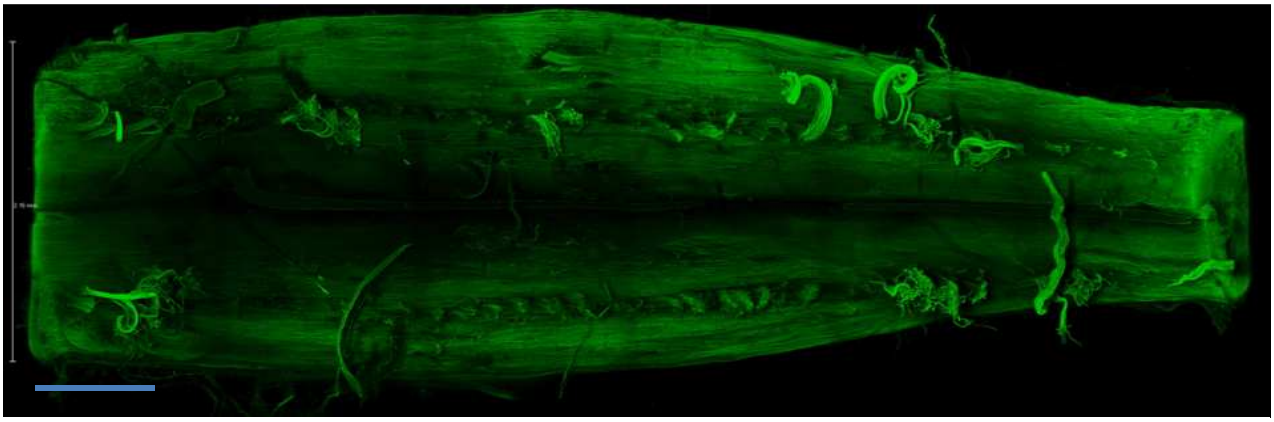

Figure 2-3: Imaging PRV tracing after clearing with SeeDB. This is the lumbar enlargement of a mouse spinal cord in which PRV was injected into the left tibialis anterior. The outside surface of the tissue shows heavy autofluorescence and does not show any PRV+ neurons. Blue scale bar represents 1 mm.

unilateral PRV injection. Furthermore, this technique was not compatible with IHC techniques. The cleared tissue returned to being opaque after removal from the SeeDB solution, and the viscosity of the SeeDB solution due to the high fructose concentration was not suitable for use with IHC. From these experimental results, the use of SeeDB was discontinued from further experiments.

2) PACT protocol

The PACT protocol cleared tissue better than the SeeDB protocol while also allowing tissue to undergo IHC. One millimeter thick tissue typically took 7 days to clear and looked transparent

after incubation in refractive index matching solution (RIMS) (Figure 2-4). PACT tissue-clearing

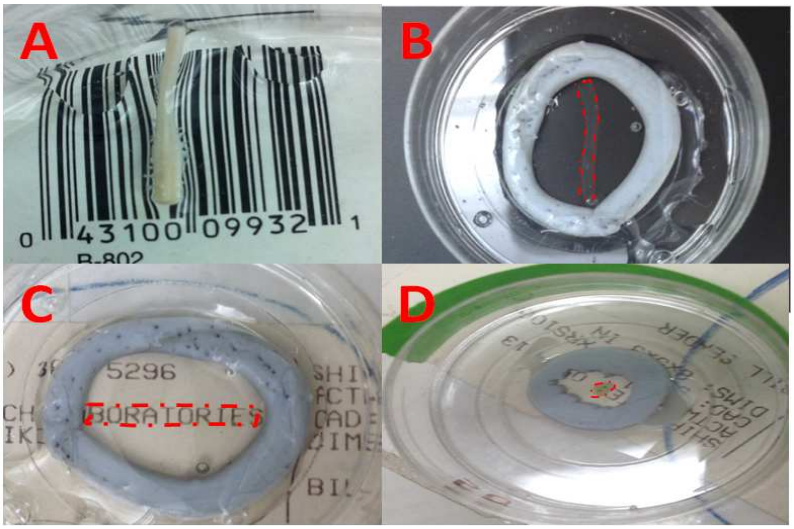

Figure 2-4: Mouse spinal cord tissue before and after undergoing the PACT protocol. A) Image of a mouse spinal cord after post-fix in 4% PFA. B) Spinal cord tissue after PACT. The red dotted line delineates the boundary of the cleared spinal cord. C) The same tissue in (B) except overlaid on top of letters. D) A 1 mm cross section of spinal cord outlined by the red dotted line over a semicolon.

successfully worked with various muscle-specific neural tracers like pseuduorabies virus (PRV) (Figure 2-5), cholera toxin subunit B (CTB) (Figure 2-6), and dextran amines (Figure 2-7). However, only CTB and dextran amines were able to be visualized without amplification with IHC. With IHC amplification, PACT-cleared tissue revealed the soma and extensive networks of processes of PRV+ neurons. Additionally, IHC amplification enhanced the visibility of CTB+ motorneurons while also revealing CTB+ axon terminals from muscle-specific afferents. Tissue

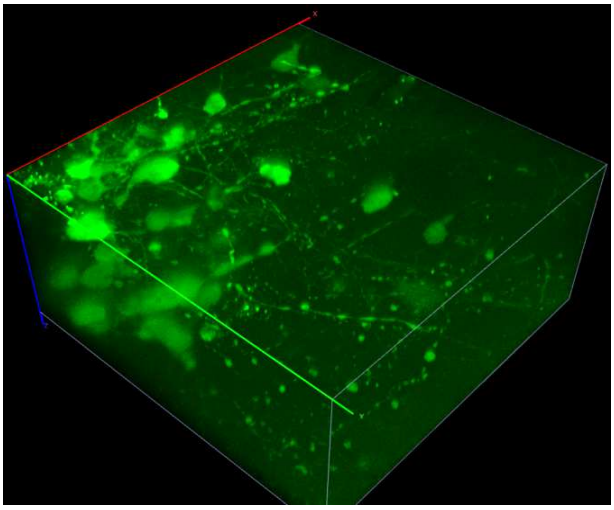

Figure 2-5: 3D reconstruction of PRV tracing with PACT. A 500 µm thick section of mouse spinal cord where PRV was injected into the left TA, taken around the central canal

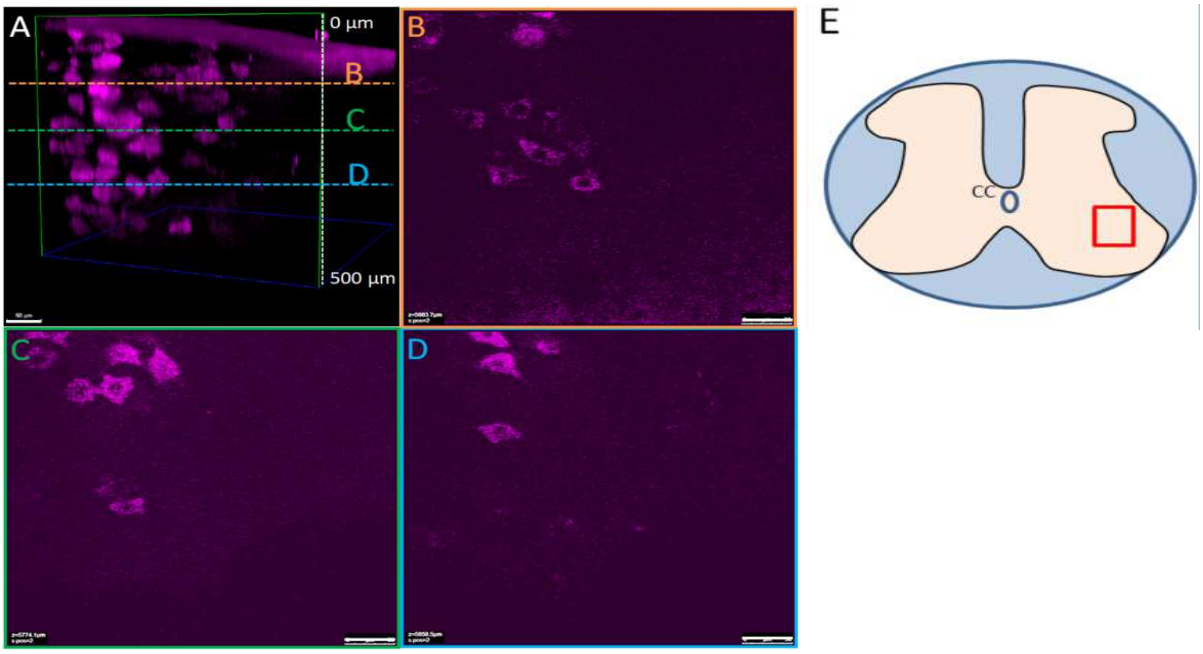

Figure 2-6: 3D reconstruction and 2D slices of CTB tracing with PACT. A) 3D reconstruction of CTB tracing in a 500 µm thick section. B) 2D image taken at a depth of 100 µm C) 2D image taken at a depth of 200 µm D) 2D image taken at a depth of 300 µm E) The red box indicates the location of CTB in the gray matter of the spinal cord

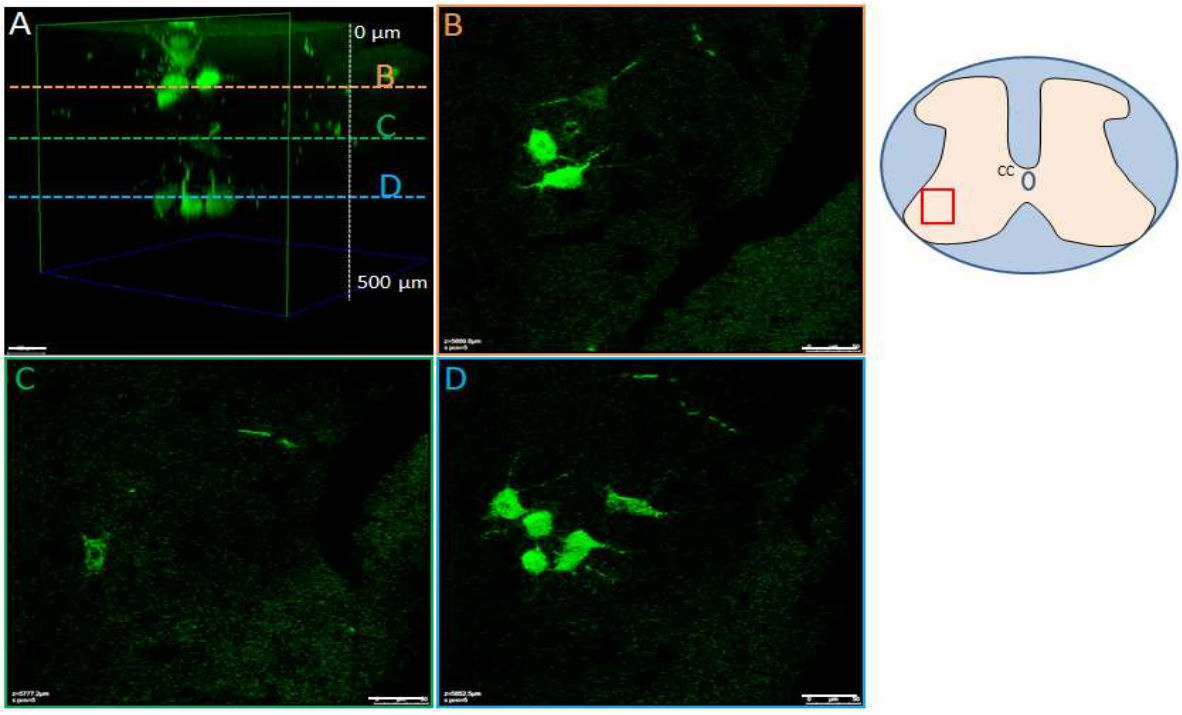

Figure 2-7: 3D reconstruction and 2D slices of dextran amine tracing with PACT. A) 3D reconstruction of dextran amine tracing in a 500 µm thick section. B) 2D image taken at a depth of 100 µm C) 2D image taken at a depth of 200 µm D) 2D image taken at a depth of 300 µm E) The red box indicates the location of dextran amine in the gray matter of the spinal cord

cleared with the PACT protocol was also able to be molecularly phenotyped for c-fos (Figure 2-8), an immediate early gene that labels active neurons, and chx10, a marker for v2a interneurons. Furthermore, IHC successfully labeled two different markers simultaneously in PACT-cleared tissue using GFP antibodies for PRV+ neuron labeling and c-fos to label neurons that have been active during a 30 minute bout of quadrupedal on a moving treadmill (Figure 2-9). The images acquired with the PACT protocol showed similar quality to standard sectioning and IHC techniques even when captured at a depth of 500 µm. However, the image quality with respect to brightness and the ability to resolve finer cellular structures decreased after this depth. Several adjustments were made to the imaging process to ensure that quality images were taken throughout the depth of the 1 mm tissue section. These adjustments

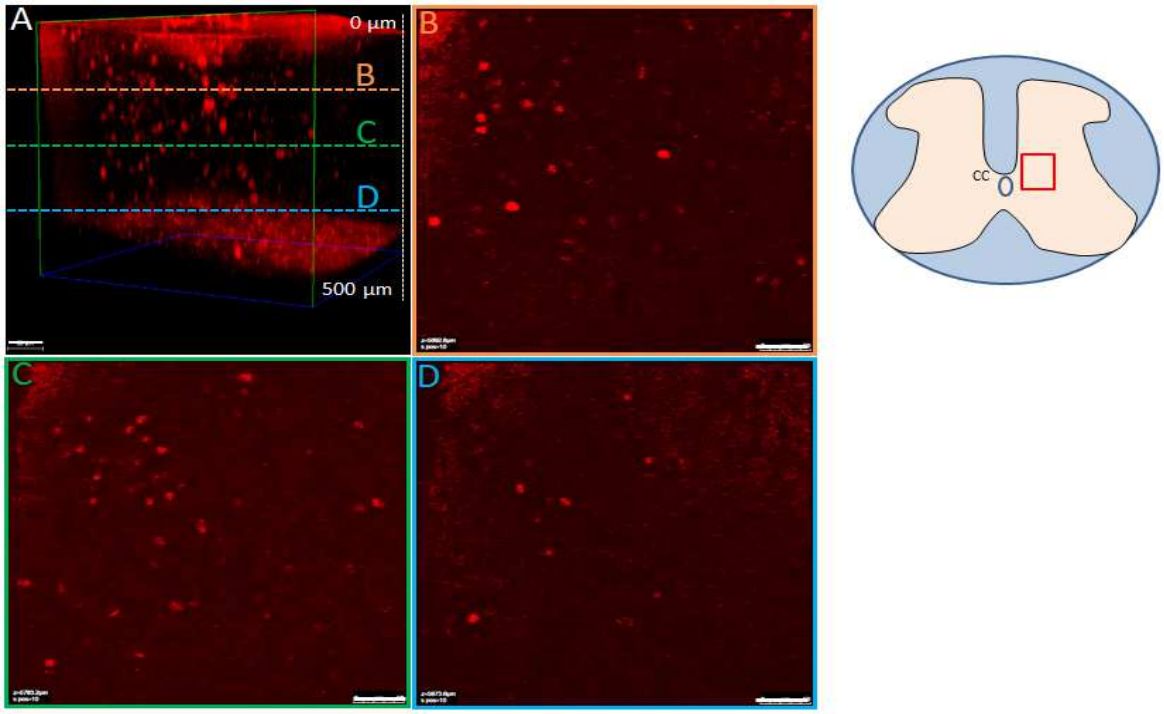

Figure 2-8: 3D reconstruction and 2D slices of c-fos with PACT. A) 3D reconstruction of c-fos staining in a 500 µm thick section. B) 2D image taken at a depth of 100 µm C) 2D image taken at a depth of 200 µm D) 2D image taken at a depth of 300 µm E) The red box indicates the location of c-fos in the gray matter of the spinal cord

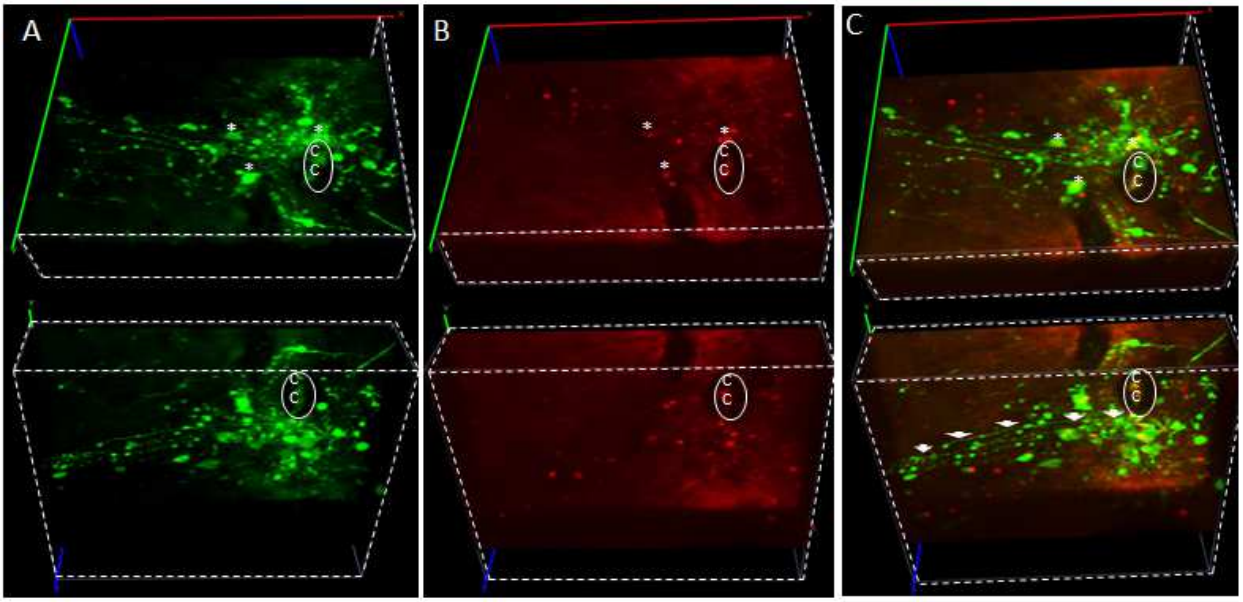

Figure 2-9: 3D reconstruction of the activation of a traced neural circuit. A) 3D reconstruction of PRV tracing in a 500 µm thick section. B) 3D reconstruction of c-fos activated by 30 minutes of stepping in the same section C) Overlay of A and B. Asterisks in the top row indicate neurons that are both PRV+ and c-fos+. CC demarcates the central canal. The white arrows in column C indicate the visualization of a process extending laterally from the central canal.

included automatically increasing laser power and gain to higher levels as the microscope went deeper into the tissue. In order to take quality pictures throughout the 1 mm depth despite imaging only up to 600 µm the tissue was then flipped an imaged from the other side at the same range in order to acquire images that spanned the whole thickness. The ability to apply the PACT protocol to mouse spinal cord tissue while also performing subsequent IHC provides a new means to collect large image datasets in a time efficient manner without losing any information due to sampling. It also provides a new means in which to visualize spinal locomotor network in three dimensions throughout its entirety.

D. DISCUSSION

The previous gold standard in collecting histological information involved cutting thin sections of tissue, performing immunohistochemistry (IHC), and then imaging using a light

microscope. Though effective at rendering tissue on a molecular and cellular resolution, traditional sectioning and IHC has limitations in its ability for generating data at a high throughput due to bottlenecks in time and labor intensiveness while also facing technical issues when registering and aligning manual tissue sections from free-floating IHC protocols. There have been automated sectioning techniques developed to alleviate these problems, as mentioned earlier, but they have their own drawbacks while also not being available in the lab. The development of optical tissue clearing techniques provides a means to efficiently visualize and molecularly phenotype large segments of neural tissue. Previously, these techniques were mostly applied to the brain with few studies pertaining to the spinal cord. This study explored the application of optical tissue clearing techniques to the spinal cord to identify muscle-specific circuits activated by 30 minutes of stepping on a moving treadmill.

This study employed two different optical tissue clearing techniques, SeeDB and PACT, on 1 mm thick sections of mouse lumbar spinal cord. Though both techniques successfully cleared the 1 mm thick sections, the PACT protocol outperformed the SeeDB protocol in making the tissue more transparent while also allowing the tissue to undergo IHC for various markers. The increased transparency allowed for PACT-cleared tissue that have undergone different neural tracer injections to be imaged via confocal microscope (Figure 2-5,6,7) compared to SeeDB-cleared tissue that yielded only autofluorescence (Figure 2-3). The ability to undergo IHC made neural tracer imaging more robust and crisp in PACT-cleared tissue due to the ability to amplify the tracers. These revealed fine neural structures such as processes and how they project and branch as they move rostrally or caudally. Additionally, the ability to undergo IHC with PACT cleared tissue gives more experimental flexibility when it comes to the choice of animal to be used and the questions that can be answered via screening for certain biomarkers with IHC for

future experiments. However, using IHC for cleared tissue restricts section thickness to be cleared to allow for proper penetration of antibodies. In subsequent experiments using IHC and PACT clearing tissue was sectioned in 1 mm sections as opposed to using the whole spinal cord or lumbar enlargement.

Despite the large tissue thickness, the PACT protocol allowed for deep penetration of antibodies during IHC and the resulting transparency of the tissue allowed for a confocal microscope to take images at a depth of up to 1 mm. However, 1 mm thick sections were imaged up to a depth of 500-600 μm on average. Images taken at deeper depths into the tissue showed less brightness intensity and less ability to resolve finer structures such as branching of processes. These issues arise due to antibodies not penetrating as well in deeper areas as compared to more superficial areas and also due to a lack of complete transparency. Even a little bit of "cloudiness" that leads to the tissue being more translucent can have significant effects to imaging depth. This cloudiness can arise due to many factors including fixation time, clearing time, and the composition of spinal cord tissue compared to brain tissue. Increased fixation time can lead to less transparency by making tissue harder to clear due to tighter and more stringent bonds created by PFA, but decreasing fixation time makes the tissue easier to clear at the risk of losing more proteins of interest due to less stringent fixation. Increasing the clearing time, can make tissue clearer at the expense of losing more proteins. Balancing the amount of clearness while also sufficiently preserving protein composition often requires that the tissue remain a little "cloudy" or translucent. Furthermore the tissue composition of the spinal cord makes it harder to clear compared to the brain. Though the brain has a greater volume, the spinal cord has a higher concentration of lipids due to its greater composition of white matter tracts per unit volume compared to the brain. The brain also has its gray matter in superficial layers and white matter in

deeper layers, whereas the spinal cord has white matter that surrounds and encapsulates the gray matter. This makes penetration with antibodies harder due to the layer of dense white matter that antibodies have to go through before reaching their targets in the gray matter. The gray to white matter composition also places limits on the imaging orientation of the spinal cord. Choosing an orientation to image the spinal cord depends on the experimental questions to be answered. This study and subsequent studies focus on the different types of neurons located in the gray matter and requires the tissue to be imaged in the rostral-caudal direction or "cross-sectionally". Imaging from the dorsal surface to the ventral surface would create lesser quality images due to having to image through the white matter surrounding the gray matter. Furthermore, this would increase imaging time by having to decrease the distance between each image taken in a series when going from dorsal to ventral as opposed to imaging cross-sectionally that will take the image of the entire gray matter before moving caudally to take another full image of the gray matter. Conversely, if a study's interest lies within tracing axons through the white matter then imaging dorsal to ventrally would provide a clearer image of the axons path as opposed to imaging "cross-sectionally" where you would have to decrease the distance between images to best capture the path of the axon. Furthermore imaging "cross-sectionally" would decrease image quality of the axon going deeper due to having to image through the whole thickness rostral-caudally which is much thicker than the thickness of the white matter going dorsal-ventrally. Along with dimness in deeper layers of the tissue, PACT-cleared tissue also suffered from over saturation or brightness on the outer superficial surfaces that extended up to 75 μm. This could have occurred due to saturation of either primary or secondary antibody to the outer surface due to the long incubation times in antibody solution. This effect is more likely due to the effects of secondary antibody for their higher tendency for non-specific binding. However, since

the conclusion of this study new IHC techniques have been developed to ameliorate this effect, called the SWITCH technique (Murray, Cho et al. 2015). The SWITCH technique uses a low concentration of SDS in the antibody solution to disrupt antibody-antigen binding until the antibody has homogenously diffused through the tissue and then subsequent incubation in PBS to remove the effects of SDS and restore antibody-antigen binding. For this study, the surface effect was ameliorated by adjusting laser and power settings of the microscope to lower the brightness of the outer surface while also employing cropping techniques to remove overly saturated sections of tissue. The possibilities of future experiments and analysis of PACT-cleared tissue far outweigh some of the limitations described previously.

The successful visualization of neural tracers and other biomolecular markers in the mouse spinal cord with optical tissue clearing opens up many future experiments and new analysis of previous experiments. Older neural tracing experiments with PRV or CTB can now undergo full 3D analysis. For example, the three dimensional distribution of muscle-specific CTB+ terminals can be characterized and uncover the extensiveness and influence that sensory information from one muscle has on the lumbar spinal circuits. Additionally, PRV studies can reveal the expansiveness of how neurons associated with a specific muscle can interconnect with the rest of the spinal cord through all spinal segments. These studies can be combined with activity biomarkers, like c-fos, to understand the location of muscle-specific interneurons activated by particular locomotor tasks. Understanding the three dimensional or network distribution of task-specific interneurons can further our understanding of stimulation parameters to use for certain tasks. Due to ability of PACT clearing to undergo multiple rounds of IHC, these muscle-specific tracing studies can be combined with neurotransmitter characterization to understand the compositional makeup of the types of interneurons needed to mediate muscle activity and to see

whether this compositional makeup differs for different muscle types. Future experiments with PACT clearing have the potential to uncover the connectome of the spinal cord. Combinations of retrograde tracers in the lumbar spinal cord with anterograde tracers in the cervical or thoracic spinal can reveal how different parts of the spinal cord communicate with each other and potentially reveal how the upper and lower trunk coordinate to produce smooth movement. Other combination of tracers that focus on either sensory or motor tracts can help further our understanding of proprioception's role in coordinating movement that spans multiple spinal segments. Understanding the spinal connectome and the connectivity patterns of different muscle groups can help create new physical training paradigms or techniques that can improve functional plasticity outcomes that have already been shown to improve behavioral outcomes in spinal cord injured animals and patients (Gerasimenko, Ichiyama et al. 2007, Ichiyama, Courtine et al. 2008, Lavrov, Courtine et al. 2008, Courtine, Gerasimenko et al. 2009, Harkema, Gerasimenko et al. 2011, Angeli, Edgerton et al. 2014, Duru, Tillakaratne et al. 2015, Gill, Grahn et al. 2018). Lastly, this technique can be used with different transgenic animals that have the power to unveil plastic changes in the spinal cord or to characterize multiple activation patterns in the same animal. These types of experiments can answer fundamental questions in the field of spinal cord injury such as how do spinal circuits change after injury, how do they reorganize with epidural stimulation and physical training, or even as simple of a question as how do spinal circuits encode different locomotor behaviors.

III. Chapter 3: Genetic Tagging of Active Neurons Uncovers Encoding Properties of Spinal Networks Executing Two Repeated or Different Locomotor Tasks

ABBREVIATIONS USED:

TRAP: targeted recombination in active populations; MLR: mesencephalic locomotor region; 4-OHT: 4-hydroxy tamoxifen; PFA: paraformaldehyde; S0 vs. S0: 0 degree stepping vs. 0 degree stepping; R vs. S0: resting vs. 0 degree stepping; S0 vs. R: 0 degree stepping vs. resting; S15 vs. S0: 15 degree stepping vs. 0 degree stepping; PBS: phosphate buffer solution; NDS: normal donkey serum; KDE: kernel density estimate

Abstract

C-fos is widely used to identify system wide neural activation with cellular resolution *in vivo*. However, c-fos can only capture neural activation of one event, limiting its ability to compare different activation patterns due to a lack of direct neuronal comparison between different animals. Targeted recombination in active populations (TRAP) allows researchers to capture two different c-fos activation patterns in the same animal. Previously, TRAP has only been used to research brain circuits. In this study we use TRAP to investigate spinal circuit activation during resting, stepping, and incline stepping. The use of TRAP animals can give multiple views and insights of network activation during locomotor events. The results show that c-fos and tdTomato, expressed via TRAP, measure neural activity differently. However, TRAP reveals spatial encoding of different locomotor tasks and redundancies in spinal networks while also suggesting that their activation for any one motor task is highly probabilistic in nature.

A. INTRODUCTION

Locomotion, while appearing simple, is actually a complex behavior that is modulated by a variety of factors that include, but are not limited to, the motor cortex, cerebellum, spinal cord, and all modalities of sensory input. The contributions from these and other networks that constantly receive sensory input ensure rhythmic alternation of flexors and extensors to produce coordinated gait patterns that is easily modified with changes in speed, surface, load, resistance, etc. as needed to execute the planned tasks. The identification of the central pattern generator in the spinal cord of cats (Jankowska, Jukes et al. 1967, Grillner and Zangger 1979, Grillner and Zangger 1984) showed that while a stereotypical locomotor pattern can be induced, sensory feedback is necessary for adapting to changing environmental conditions. This finding begets the question of how and which spinal interneurons underlie the dynamism of the spinal locomotor circuit to adapt to complex ensembles of sensory input under *in vivo* conditions.

Ventral root recordings in neonatal spinal cord preparations have made progress in identifying the interneurons primarily involved in "fictive" locomotion. This experimental approach has led to the characterization of four classes of interneurons (V0-V3) with distinct embryonic genetic lineages (Kiehn and Butt 2003, Whelan 2003, Clarac, Pearlstein et al. 2004, Kiehn 2006, Brownstone and Wilson 2008, Stepien and Arber 2008, Dougherty and Kiehn 2010, Dougherty and Kiehn 2010). V1 spinal neurons have been reported to determine the period length (speed) of the vertebrate locomotor output (Gosgnach, Lanuza et al. 2006), V2a interneurons have some influence on left-right coordination (Crone, Quinlan et al. 2008), and V3 interneurons have been associated with locomotor rhythm during walking (Zhang, Narayan et al. 2008). Although these studies have illustrated that the exclusion of one of these types of interneurons modulates the locomotor cycle, the role of these interneurons in *in vivo* systems using the sensory

system as a source of control during actual stepping (as opposed to fictive locomotion) remains largely unknown. More recent studies have focused on identifying these and other groups of neurons in the mature spinal cord in *in vivo* preparations. For example, using gene knock-ins and fluorescent reporters, V3 interneurons have been further classified into 2 subpopulations that inhabit distinct areas of the spinal cord with distinct electrophysiological properties (Borowska, Jones et al. 2013). Furthermore, using c-fos, these populations were probed in young adult mice *in* vivo and it was found that these two subpopulations played different roles during either swimming or running behaviors.

More recent approaches for identifying spinal neurons activated during *in vivo* locomotor activity include c-fos labeling in intact (Ahn, Guu et al. 2006) and spinal rats (Courtine, Song et al. 2008, Ichiyama, Courtine et al. 2008) and mice (Kim, Xiao et al. 2013, Dale, Ng et al. 2014), and in rats after mesencephalic locomotor region (MLR)-activated stepping (Huang, Noga et al. 2000). For example, the numbers of c-fos+ neurons in laminae I-V and VII increase when the duration of treadmill stepping is increased in intact rats (Ahn, Guu et al. 2006). We also observed that the number and type, e.g., inhibitory or excitatory, of interneurons activated during stepping is a function of the load, speed, duration, and resistance in both intact and spinal rats and that the types of neurons activated during locomotion was dependent on the step training status of the spinal rats (Tillakaratne, Duru et al. 2014, Duru, Tillakaratne et al. 2015).

Significant advances have been reported recently using a variety of genetic techniques to identify specific groups of neurons involved in different motor tasks (Azim, Jiang et al. 2014, Esposito, Capelli et al. 2014, Levine, Hinckley et al. 2014). Levine et al. (Levine, Hinckley et al. 2014) identified spinal neurons that receive both supraspinal and sensory input that also appeared to play a role in coordinating multiple motor pools. Azim et al. (Azim, Jiang et al. 2014)

identified interneurons with a similar function in regulating forelimb food retrieval, but identified a group of interneurons that seem to be mainly responsible for modulating a specific phase of food retrieval involved in reaching. Esposito et al. (Esposito, Capelli et al. 2014) using similar techniques were able to specifically label spinal interneurons receiving input from the nucleus medullary reticular formation that were crucial in the performance of the reaching task. While great strides have been made, a significant gap remains in methodologies aimed at determining a complete and thorough characterization and identification of spinal interneurons associated with locomotion *in vivo* and their spatial organization in a mature animal. None of these studies, however, demonstrate that a specific type of interneuron based on a specific genetic marker has a unique function in the execution of a specific motor task. Neither do any of these studies demonstrate the degree to which the same interneuron "type" participates in different tasks as has been shown in non-mammalian species (Buchanan 2001, Sillar, Combes et al. 2008, Roberts, Li et al. 2010).

The recent emergence of targeted recombination in active populations (TRAP) mice provides a potentially powerful genetic tool to dissect neural circuits. TRAP technique utilizes tamoxifen-dependent recombinase $CreER^{T2}$ that is expressed in an activity-dependent manner from the Fos promotor (Guenthner, Miyamichi et al. 2013, Cazzulino, Martinez et al. 2016). These mice also have an effector gene, i.e., tdTomato that is expressed in a Cre-dependent manner allowing for genetic access of neuronal activation during desired time frames. This allows for the comparison of two c-fos like activation patterns due to two different or even the same tasks in the same animal. However, the FosTRAP mouse model has only been used to study sensory networks in the brain. The proposed study aims to determine whether we can capitalize on TRAP to study the uniqueness or the level of sharing their function in the same or a different

motor task. The FosTRAP model has the potential to identify interneurons and their multi-functionality in executing different tasks as well as filling other gaps in knowledge related to the spatial anatomy and functionality of spinal locomotor networks.

B. MATERIALS AND METHODS:

1) Animals:

This experiment used adult FosTRAP developed at Stanford by the Luo Lab (Guenthner, Miyamichi et al. 2013). FosTRAP mice were obtained by creating a colony through Jackson Laboratories (JAX Mice & Services, Bar Harbor, ME). The Jackson Laboratory mated homozygous Ai14 females (JAX Mice & Services, stock 007914) with heterozygous Fos^{CreER} males (JAX Mice & Services, stock 021882). FosTRAP mice are the offspring that are heterozygous for both the R26-Ai14 gene and the Fos-CreER gene. The Ai14 mice have a tdTomato gene linked to the CAG that is floxed with a STOP cassette. Heterozygous Fos^{CreER} mice have a $CreER^{T2}$ gene knocked into one of the Fos promoters. FosTRAP utilizes tamoxifen-dependent recombinase, $CreER^{T2}$, expressed in an activity-dependent manner through the Fos promoter which then unlocks a STOP floxed tdTomato gene. The unlocked tdTomato gene will then continually express. This allows genetic access of neural activation during desired time frames which can then be compared to c-fos expressed during a later event. It must be noted that a new version of the FosTRAP mouse, named TRAP2, has since been developed after our experiments (JAX Mice & Services, stock 030323) (Allen, DeNardo et al. 2017, Girasole, Lum et al. 2018, DeNardo, Liu et al. 2019). All procedures were performed according to institutional and governmental regulations and in accordance with the guidelines delineated by the University

of California, Los Angeles (UCLA) Chancellor's Animal Research Committee concerning the ethical use of animals.

2) Experimental Design:

The first experiment optimized the injection timing of 4-hydroxytamoxofen (4-OHT, Sigma-Aldrich Corp, St. Louis, MO, catalog #H6278) that best captured neural activation from 30 minutes of stepping on a treadmill. Adult FosTRAP mice were divided among different injection time points relative to the beginning of stepping: 4 hours before stepping (-4Hr, n = 1), 2 hours before stepping (-2Hr, n = 2), 1 hour before stepping (-1Hr, n = 2), immediately before stepping (0Hr, n = 6), immediately after the completion of stepping (+0.5Hr, n = 7), and 1 hour after the completion of stepping (+1.5Hr, n = 3). There was also a group of FosTRAP which received a sham injection (vehicle w/o 4-OHT, n = 2). All groups received 4-OHT injections at a dosage of 75 mg/kg. The 4-OHT solution was made by dissolving 4-OHT in 100% ethanol, suspended in castor oil, stored in -20^{o}C, and then thawed and mixed with injectable saline for experimental use (Chevalier, Nicolas et al. 2014). All mice were acclimated to stepping on a treadmill for thirty minutes on 5 different occasions before stepping and receiving a 4-OHT injection. After stepping for 30 minutes on a treadmill (two 15 min sessions with a 5 minute break in between sessions), the mice were returned to their cages. FosTRAP mice remained in their cages for 14 days to allow for tdTomato production and subsequent diffusion. After 14 days, mice stepped for another 30 minutes on a treadmill under the same conditions as before. One hour after the completion of stepping, mice were transcardially perfused with 4% paraformaldehyde (PFA, Sigma catalog# 158127) in phosphate buffer.

The second experiment optimized the dosage of 4-OHT that best captured neural activation from 30 minutes of stepping on a treadmill. Adult FosTRAP mice were divided among different injection dosages: 0 mg/kg (sham, n = 2), 25 mg/kg (n = 1), 50 mg/kg (n = 2), and 75 mg/kg (n = 3). The dosage was capped at 75 mg/kg due to a previous finding in which 100 mg/kg was lethal (Guenthner, Miyamichi et al. 2013). All animals received their 4-OHT injection immediately after stepping, the optimal injection time found in the previous experiment. Mice stepped on the treadmill for 30 minutes, under the same conditions as the previous experiment, and were put back in their cages for 14 days. After 14 days mice stepped on a treadmill for 30 minutes and transcardially perfused with 4% PFA one hour after the completion of stepping.

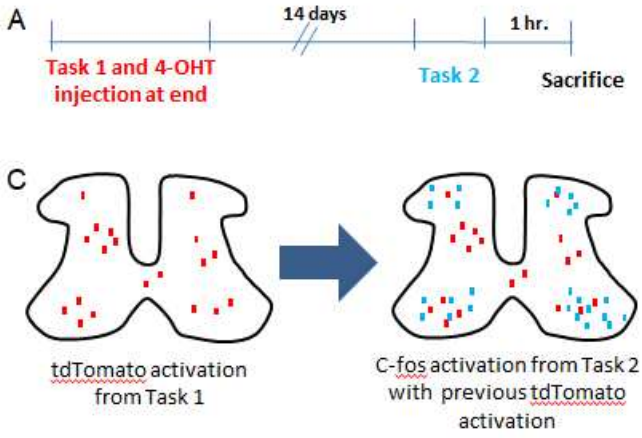

B

Group	Task 1 neurons (tdTomato)	Task 2 neurons (c-fos)
S0 vs. S0	30 min. of stepping	30 min. of stepping
S0 vs. R	30 min. of stepping	Resting
R vs. S0	Resting	30 min. of stepping
S15 vs. S0	30 min. of incline stepping	30 min. of stepping

Figure 3-1: Outline of FosTRAP experimental design and visualization. A) Experimental timeline. B) Table of experimental groups C) Visualization of immunostained c-fos after Task 1 and 2.

The third experiment compared and contrasted c-fos and tdTomato activation for the same locomotor task or for different locomotor tasks. These tasks include: resting, stepping at a 0 degree incline, and stepping at a 15 degree incline. The experimental outline can be seen in Figure 3-1, where at Day 0 the animal will perform 1 of the 3 locomotor tasks for Task 1 and then receive a 4-OHT injection (75 mg/kg) upon completion. After 14 days, the mice will perform 1 of the 3 locomotor tasks for Task 2 and then are transcardially perfused with 4% PFA

1 hour after completion of Task 2. Before Task 1 all animals were acclimated to the treadmill as in previous experiments. Neural activation due to Task 1 is labeled with tdTomato and neural activation due to Task 2 is labeled with c-fos. The 4 experimental groups can be seen in Figure 1. The first group compares tdTomato and c-fos activation due to stepping at a 0 degree incline for 30 minutes on a treadmill (S0 vs. S0). The second group compares resting (R, marked with tdTomato) and stepping at a 0 degree incline (S0, marked with c-fos) and denoted as R vs. S0. The third group compares stepping at a 0 degree incline (S0, marked with tdTomato) and resting (R, marked with c-fos) and denoted as S0 vs. R. The fourth group compares stepping at a 15 degree incline (S15, marked with tdTomato) and stepping at a 0 degree incline (S0, marked with c-fos) and denoted as S15 vs. S0.

3) Tissue preparation:

After perfusion with 4% PFA, the spinal cords were dissected and post-fixed overnight in 4% PFA at 4^0C. Spinal cords were then put in 30% sucrose for 5 days at 4^0C and divided into a segment spanning the L1-L6 spinal levels which was then frozen with Neg 50 (Thermo Scientific, Hudson, NH). These blocks were then stored in -80^0C until they were ready to be cut into 30 μm sections. Tissue sections were stored in 96 well plates with 1X phosphate-buffered saline (PBS) and 0.02% sodium azide at 4^0C.

4) Immunohistochemistry:

Sections from spinal level, L4, were examined for this study. L4 sections were identified based upon the morphology of the gray and white matter using an atlas (Charles Watson 2009). Twelve to fifteen sections, sampled at every 4^{th} section, underwent immunohistochemical analysis. The sections sampled spanned rostral, middle, and caudal sections of L4. Goat anti-tdtomato antibody (1:4000, LS Bio, Seattle, WA, catalog #LS-C340696) amplified tdTomato

produced during Task 1 and rabbit anti-c-fos (1:2000, EMD Millipore, Burlington, MA, catalog# ABE457) identified active neurons during Task 2. Neurons double-labeled with both tdTomato and c-fos indicated neurons activated by both Task 1 and Task 2 and were called, colabels. The chosen sections underwent immunohistochemistry as free floating sections, similar to previous studies (Niranjala, Ahn 2006). Briefly, sections were transferred into Costar netwells (15 mm membrane diameter, 74-mm mesh), rinsed for 30 min in 1x PBS, transferred to 96-well plates containing 180 µl/well of a mixture of c-fos and tdTomato antibody in 1x PBS containing 0.3% Triton X-100 and 5% normal donkey serum (NDS), and incubated for 3 days at 4^{o} C on an orbital shaker. Afterwards, sections were washed in 1x PBS as follows: two quick rinses, 2 x 5 min rinses, and 2 x 10 min rinses. Sections were incubated in a mixture (180 µl/well, 96-well plate) of secondary antibodies (Donkey anti-rabbit 488 at 1:500 and donkey anti-goat 594 at 1:500 from Jackson Immunoresearch, West Grove, PA, Code: 711-545-152 and 705-585-147 respectively) in 0.3% Triton X-100 and 5% NDS for 1 hour at room temperature on an orbital shaker. After secondary incubation, sections were washed as described above, mounted on Fisher Superfrost slides (Fisher Scientific, Pittsburg, PA), and coverslipped with Vectashield mounting media containing DAPI (Vector, Burlingame, CA).

5) Quantification and data analyses:

Spinal cord sections processed for fluorescent immunohistochemistry were examined under a Zeiss Axiophot microscope with appropriate fluorescent filter sets. Digital images of neurons labeled with c-fos, DAPI, and tdTomato were acquired with a Spot RT CCD Slider color camera (Diagnostics Instruments, Sterling Heights, MI) and using extended field of depth imaging in Image Pro Plus 7 (Media Cybernetics, Rockville, MD). Composite images of c-fos,

DAPI, and tdTomato were created with the color composite feature of Image Pro Plus 7. Neurons that expressed c-fos, tdTomato, or both were tagged using the manual tag analytical feature of Image Pro Plus 7. The manual tags were then exported to excel as x,y coordinates. Sections from the same animal had their points shifted and aligned with the central canal. These points were then uploaded using the Tableau Software (Tableau Software, Seattle, WA) and the laminae borders (as seen in the atlas) were overlaid onto the manual tag points. Tableau was then able to count the number of c-fos, tdTomato, or colabeled neurons in each lamina. Total c-fos activation was the sum of the number of c-fos positive neurons and the number of colabeled neurons. Similarly, total tdTomato activation was the sum of the number of tdTomato positive neurons and the number of colabeled neurons. Colabeling percentage was calculated by dividing the number of colabels by the total tdTomato activation and subsequent multiplication by 100. To visualize the spatial distribution of c-fos and tdTomato, a heat map of the x,y coordinates was generated using a kernel density estimate (KDE), which was done using the R software package. All quantification was performed blindly by assigning a code letter to each animal and deciphering this code only after all data analyses were complete.

6) Statistical analyses:

Mean comparisons of the numbers and percentages of c-fos, tdTomato, and colabels for all experiments were carried out using a factorial one-way analysis of variance model. The statistical analysis on the distribution of c-fos, tdTomato, and colabels from the third experiment used resampling techniques (Miller, Hilliard et al. 2010). X,Y coordinates, registered and aligned to the central canal, for a particular activity marker (c-fos or tdTomato) activated by a certain locomotor condition (resting, stepping, incline stepping) from all sections and animals was

compiled into a single list. This list would then be resampled with replacement 1000 times to create a 95% confidence interval, and the generated confidence interval would be compared to another group (activity marker + locomotor condition). Spatial locations of the compared group that were outside this confidence interval were considered significant. For this study two different comparisons were made: spatial distribution and spatial counts. Spatial distribution compared whether two conditions (ex. stepping c-fos vs. stepping tdTomato, stepping c-fos vs. resting c-fos, etc.) came from the same spatial distribution. In this analysis, resampling was done so that the number of x,y coordinates in the compared groups was the same. For example, there were more c-fos+ neurons than tdTomato+ neurons for stepping. The x,y coordinate list for tdTomato was upsampled with replacement to match the number of x,y coordinates for c-fos, and this was done 1000 times to create the confidence interval. Since the numbers of coordinates in the compared groups were the same, this analysis revealed proportionality differences between the two groups. In contrast, spatial counts analysis determined whether the absolute counts of neurons at a particular location were the same for the compared groups. In this case, the number of x,y coordinates in the resampled list matched that of the original list. Using the same example as earlier, the tdTomato coordinate list was not upsampled with replacement to match the length of the c-fos coordinate list but resampled to the same length of the original tdTomato list, and this was done 1000 times to create the confidence interval. Resampling was carried out using the R programming language.

C. RESULTS:

1) 4-OHT injection (75 mg/kg) of FosTRAP mice immediately after the end of locomotor activity produced robust tdTomato labelling of active neurons

Preliminary studies were done to optimize the dosage and timing of 4-OHT to study locomotion. Injection of 4-OHT at dosages of 0 mg/kg (sham), 25 mg/kg, 50 mg/kg, and 75 mg/kg were administered to mice immediately after the completion of stepping on a treadmill for 30 minutes. All dosages of 4-OHT resulted in significantly higher tdTomato expression than the sham injection, with 75 mg/kg having the highest amount of tdTomato expression (Figure 3-2). The sham group expressed very little and sparse tdTomato, thus showing that the FosTRAP model is tightly modulated with 4-OHT and shows little leakiness. The timing optimization experiment included four time points before the onset of treadmill stepping (4 hours, 2 hours, 1 hour, and immediately before stepping) and two time points after stepping (immediately after

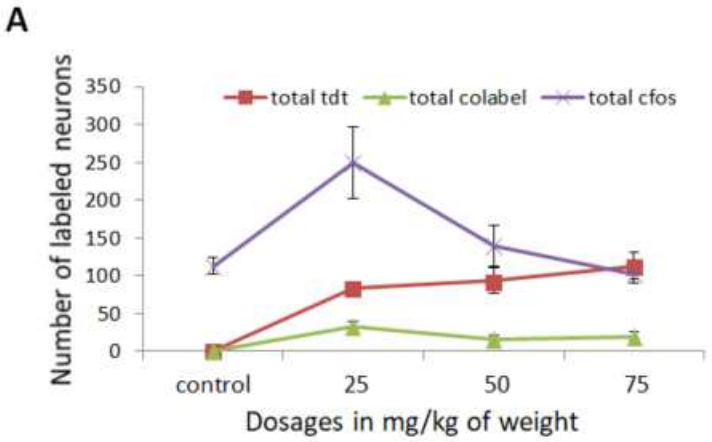

B

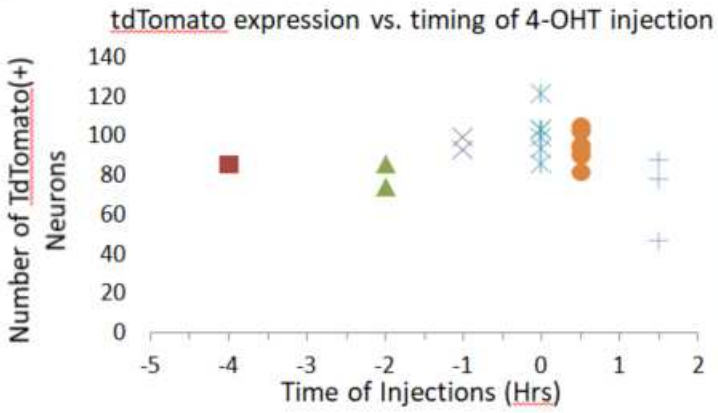

	Finished Experiment	Number of Animals Attempted
Sham	2	2
-4	1	4
-2	2	6
-1	2	2
0	6	10
0.5	7	7
1.5	3	3

Figure 3-2: Optimization results of FosTRAP use in the spinal cord. A) Comparing the number of c-fos (purple line), tdTomato (red line), and colabels (green line) with the dosage of 4-OHT (mg/kg). The dosage is measured on the x-axis (mg/kg) and the number of neurons labeled is on the y-axis. Control animals were given a sham injection of isotonic saline solution. B) Comparing expression of tdTomato with the timing of 4-OHT injection. The x-axis shows the time of 4-OHT injection in hours relative to the beginning of stepping, marked at 0. The table on the left shows the number of animals that were able to complete the task of stepping for 30 minutes compared to the number of animals tested

stepping and 1 hour after stepping). All injection time points resulted in similar amounts of tdTomato expression, suggesting that the exact timing of 4-OHT does not matter as long as it is before the end of stepping (Figure 3-2). However, the 4-OHT injection noticeably hinders the animals' ability to complete locomotor tasks, resulting in high attrition rates when injected before the onset of locomotion. These animals displayed characteristics like sluggishness and social isolation in the time leading up to the experiment, and often times completely stop

stepping on a treadmill. These abnormalities subside once the 4-OHT has cleared their systems. For subsequent experiments we injected 4-OHT at 75 mg/kg immediately after the end of the locomotor task. These parameters show robust tdTomato labeling while also minimizing attrition rate.

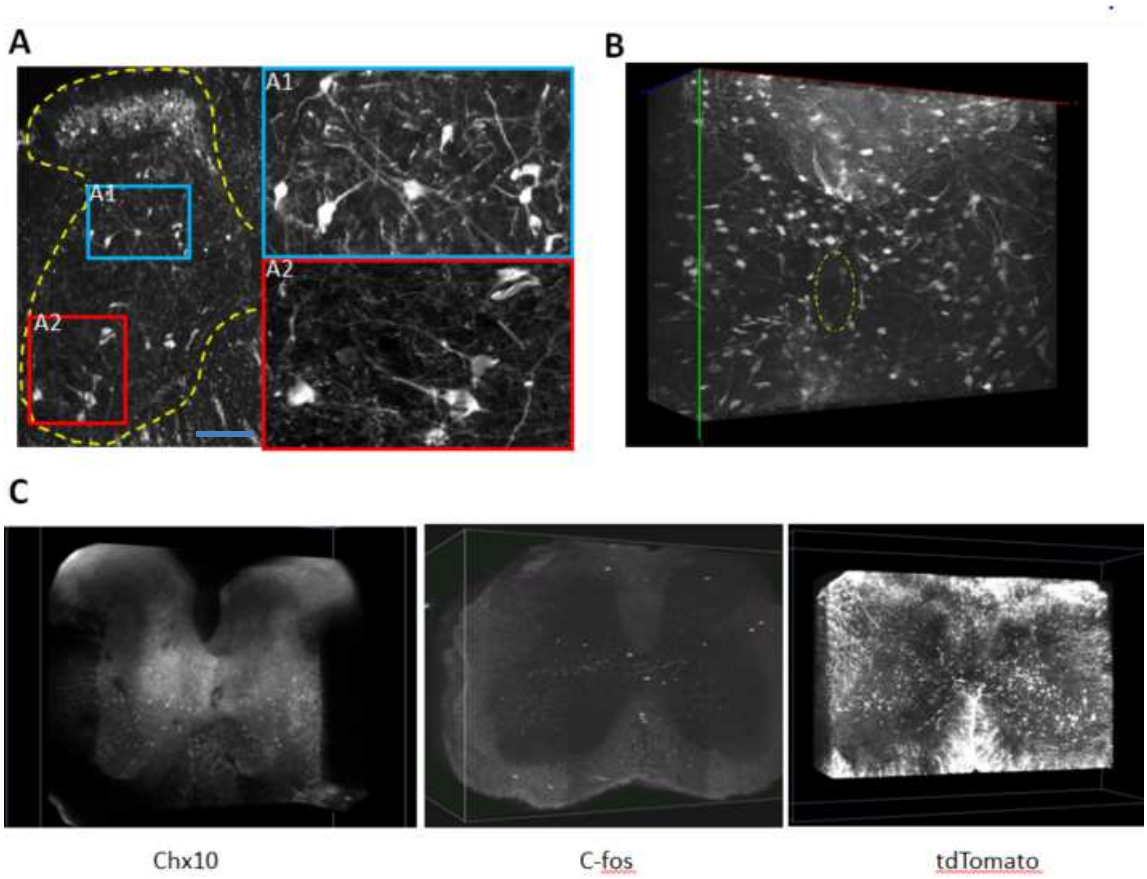

Figure 3-3: Tissue clearing and immunostaining reveal the 3D morphology and processes of activated neurons. A) Amplification of tdTomato through immunostaining. Blue scale bar is 200 µm. B) 3D reconstruction of TRAPed neurons in the gray matter surrounding the central canal, demarcated with the yellow line. C) 3D reconstruction videos of cleared tissue marking Chx10, a V2a interneuron marker, c-fos, and tdTomato.

2) "TRAPed" neurons express tdTomato that labels the soma and processes.

"TRAPed" neurons first express tdTomato in the nucleus, and if given enough time it can accumulate and spread to the soma and processes. This is especially noticeable after amplifying tdTomato with immunostaining (Figure 3-3). TRAP also labels what appear to be

oligodendrocytes in the white matter, which have been shown to produce c-fos (Muir and Compston 1996, Groves, Kihara et al. 2018). Tissue-clearing techniques, like CLARITY, maximize FosTRAP's ability to reveal processes of activated neurons and have the potential to reveal connectivity of activated spinal networks that a nuclear c-fos stain cannot show. Furthermore, this can be combined with biomarkers for genetic lineages, like Chx10, to uncover system wide activation and connectivity of genetically distinct interneurons.

3) Different locomotor events show differential expression profiles in number and spatial distribution when captured by either c-fos or tdTomato.

C-fos activated during resting and stepping show different spatial distributions and spatial counts with stepping condition having increased c-fos activation in all laminae. Kernel density estimates (KDE) were used to visualize the distribution and counts of activated neurons and give the probability of finding c-fos or tdtomato at each spatial location. The KDE's for stepping c-fos show prominent activation levels in the medial dorsal horn and intermediate laminae, whereas the KDE's for resting c-fos show the most prominent activation in the medial intermediate laminae and the central canal (Figure 3-4). Each KDE was normalized with respect to itself (i.e. the probabilities are with respect to sections found in that particular animal), and thus shows proportionate spatial activation between different animals and groups. Resting shows more proportionate activation around the central canal and medial laminae V-VII, whereas stepping shows more proportionate activation in the lateral dorsal horn. However, stepping shows higher spatial counts throughout all of the gray matter, with the greatest discrepancy found in the medial dorsal horn and laminae IV, V, and VII.

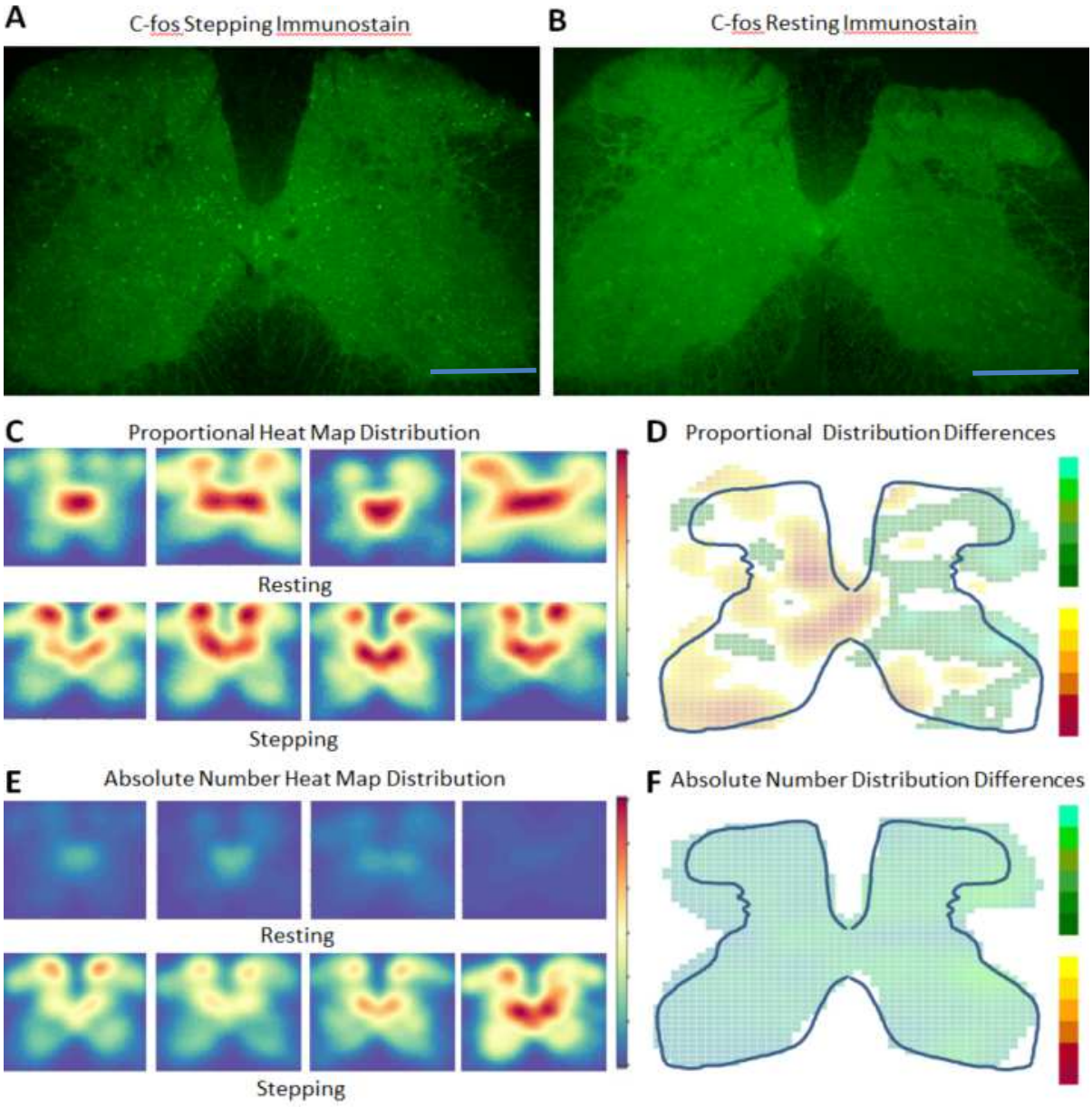

Figure 3-4: Spatial distribution and counts of c-fos activated by resting or stepping. A) Representative image of c-fos stepping immunostain. Blue scale bar is 500 µm. B) Representative image of c-fos resting immunostain. C) Each panel is a kernel density estimates (KDE) of either c-fos activated by resting or stepping from a single animal. Each animal's KDE is normalized with respect to itself showing proportionately the location of activated neurons. KDE's of all animals tested can be found in Figure S3. D) Map of the differences in proportional distribution between c-fos resting and stepping calculated from KDE's seen in Figure S3. The green end of the color bar represents areas where c-fos stepping is proportionately higher than resting and vice versa for the yellow/red end of the color bar. E) The same KDE's from (C) except all panels are normalized to the average KDE of c-fos stepping. This allows for a more direct comparison of location counts across animals and groups. KDE's of all animals tested can be found in Figure S4. F) Map of the differences in spatial counts between c-fos resting and stepping calculated from KDE's seen in Figure S4. The green end of the color bar represents areas where c-fos stepping outnumber resting and vice versa for the yellow/red end of the color bar.

Tdtomato activated during resting, stepping, and incline stepping showed what appears to be similar spatial distribution, but their spatial counts differed between locomotor tasks. Though the spatial distributions of all three locomotor tasks look similar, there are significant differences between stepping versus resting and incline stepping (Figure 3-5). Resting has proportionately more activation than stepping in the central canal and the intermediate laminae immediately surrounding it, and stepping has more proportionate activation in the dorsal horn and lateral intermediate laminae. Incline stepping has more proportionate activation than stepping in the ventral horn and in parts of medial laminae IV and V, whereas stepping has more proportionate activation than incline stepping in the dorsal horn and in the lateral intermediate laminae.

In all locomotor activities, there is a dorsal-ventral decline in the number of tdTomato neurons, which could indicate a sensory-motor filtering effect or feature extraction. Stepping tdTomato shows greater spatial counts than resting in almost all laminae besides VI and X. Resting tdTomato showed greater spatial counts than stepping in certain areas of lamina VI. Surprisingly, stepping showed higher spatial counts than incline stepping in all laminae besides parts of laminae VI and IX. This result could arise due to the effect of physical training on c-fos activation. Animals needed to be trained in order to complete 30 minutes of incline stepping as opposed to stepping without an incline in which no training was done. Previous studies have shown that physical training decreases the number of c-fos activation (Ichiyama, Courtine et al. 2008, Shah, Garcia-Alias et al. 2013, Duru, Tillakaratne et al. 2015, Chen, Marsh et al. 2017).

4) FosTRAP mice show more colabeling (positive for tdTomato and c-fos) when repeating the same task compared to performing different tasks.

Neurons colabeled with c-fos and tdTomato reveal unique insights in how neural networks execute repeated or different tasks. The total number and percentage of colabels

significantly differed in animals that repeated the same task as opposed to performing two

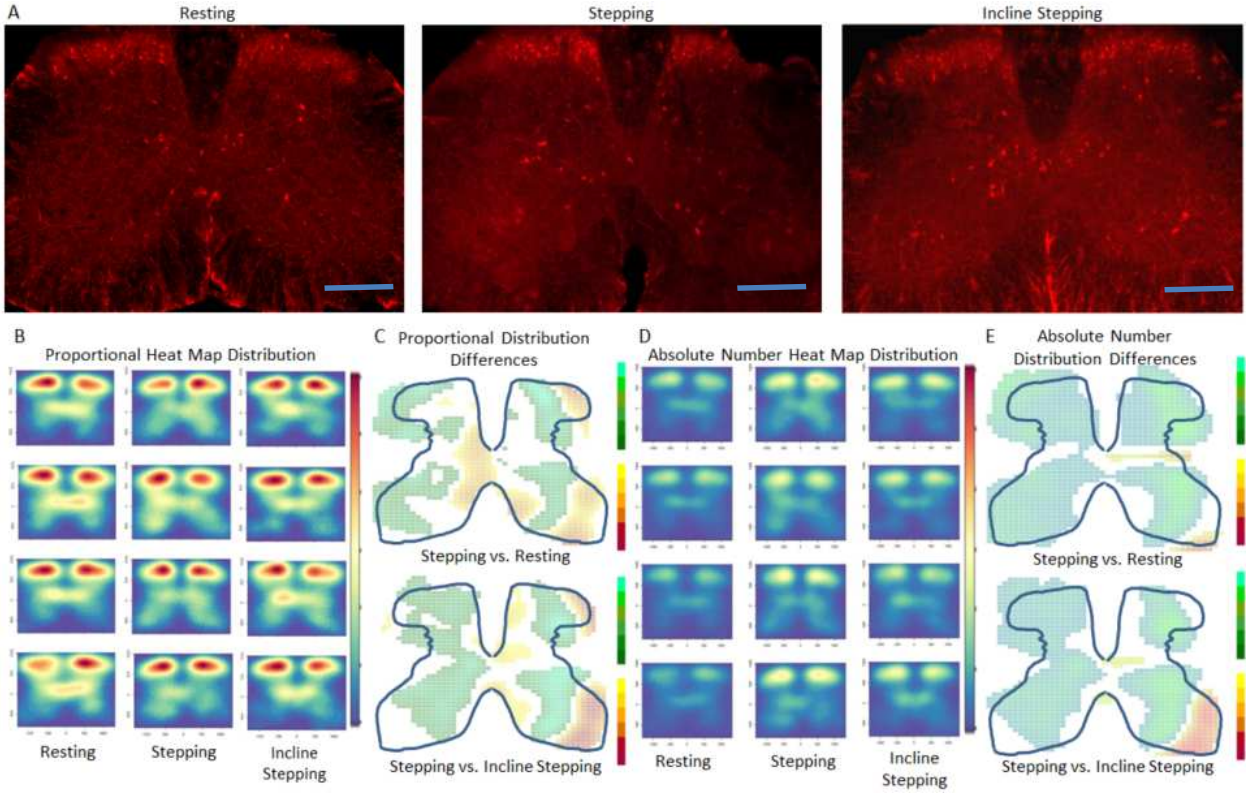

Figure 3-5: Spatial distribution and counts of tdTomato activated by different locomotor activities. A) Representative tdTomato stains for each locomotor activity. Blue scale bar is 500 µm. B) Each panel in a column is a KDE normalized with respect to itself of either tdTomato activated by resting, stepping, or incline stepping from a single animal. KDE's of all animals tested can be found in Figure S5. C) Map of the differences in proportional spatial distribution between resting, stepping, or incline stepping calculated from KDE's in Figure S5. The green end of the color bar represents areas where stepping is proportionately higher than resting (top panel) or incline stepping (bottom panel) and vice versa for yellow/red end of the color bar. D) KDE's from (B) normalized to the average KDE of stepping c-fos, allowing for a more direct comparison of location counts across animals and groups. More KDE's can be found in Figure S6 E) Map of the differences in spatial counts between resting, stepping, and incline stepping calculated from KDE's in Figure S6. The green end of the color bar represents areas where stepping outnumber resting (top panel) and incline stepping (bottom panel) and vice versa for the yellow/red end of the color bar.

different tasks (Figure 3-6). The S0 vs. S0 group had greater counts and percentages than the S0 vs. R and the R vs. S0 group. Repeated tasks (S0 vs. S0) and different tasks (R vs. S0) had different spatial distributions of colabeling. The R vs. S0 group has most of its colabeling in laminae I-V, whereas the S0 vs. S0 group shows a more even laminar distribution. Repeated tasks show the greatest difference in absolute number and proportionality in laminae VII-IX.

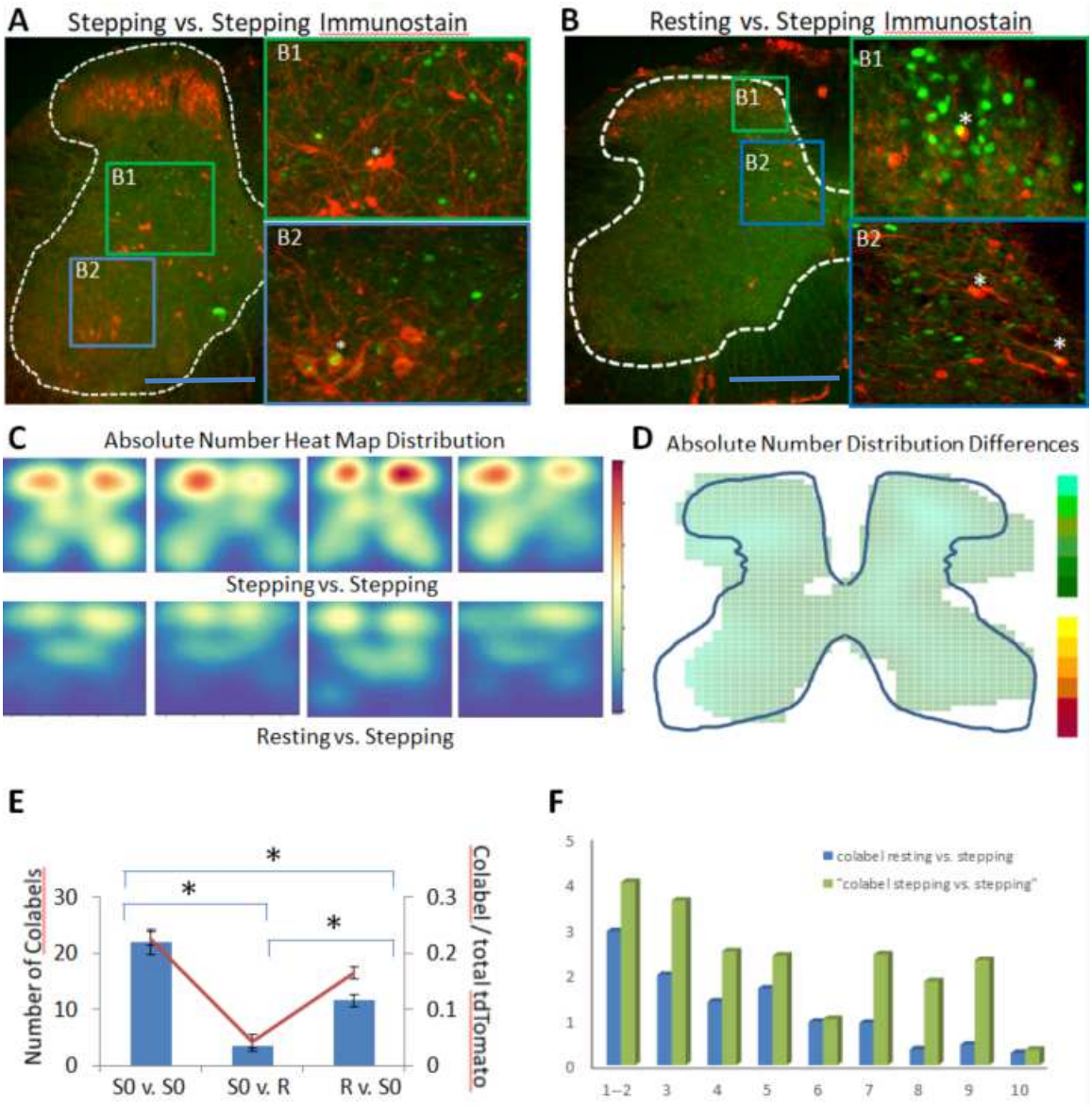

Figure 3-6: Counts and distribution of colabeling. A) Representative image of c-fos and tdTomato immunostain in a S0 vs. S0 animal. Asterisks indicate neurons that are considered colabeled. Blue scale bar is 500 µm. B) Representative image of c-fos and tdTomato immunostain in a R vs. S0 animal. C) KDE's of colabeled neurons in the S0 vs. S0 and R vs. S0 groups normalized to the average KDE of S0 vs. S0 to compare location counts between S0 vs. S0 and R vs. S0 animals. D) Map of the differences in location counts between colabeling in S0 vs. S0 and R vs. S0 groups calculated from KDE's seen in (C). The green end of the color bar represents areas where colabeling in S0 vs. S0 outnumber R vs. S0 and vice versa for the yellow/red end of the color bar. E) Comparing gross counts of colabeling between different groups. Blue bars indicate total number of colabels found in each group (left y-axis). Red line indicates the number of colabels as a percentage of total tdTomato (right y-axis). F) Shows the histogram of colabeling counts among spinal laminae between S0 vs. S0 and R vs. S0

5) Expression of Tdtomato and c-fos differs in spatial distribution and spatial counts when both are activated by the same locomotor task

Both tdTomato and c-fos counts significantly differed when activated by resting and stepping. However, there was no significant difference in tdTomato activation between incline stepping and resting or stepping without an incline (Figure 3-7). C-fos showed more activation in

A

Group	Task 1 (tdt)	Task 2 (cfos)	Tdt	C-fos	Colabel
S0 vs. S0 (n = 8)	Stepping	Stepping	98.7 ± 10.3	150.4 ± 34.4	21.9 ± 2.2
S0 vs. R (n=4)	Stepping	Resting	84.5 ± 8.7	38.1 ± 8.1	3.6 ± 1.0
R vs. S0 (n=4)	Resting	Stepping	68.9 ± 2.9	157.9 ± 14.1	11.6 ± 1.0
S15 vs. S0 (n= 8)	Incline Stepping	Stepping	76.8 ± 6.3	N/A	N/A

B

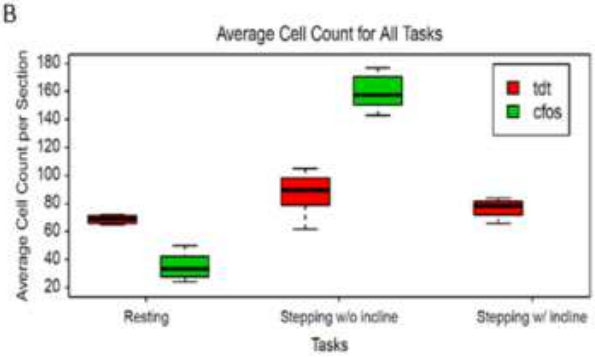

Figure 3-7: Gross counts of tdTomato (tdt), c-fos, and colabeling for different experimental groups and locomotor activities. A) Counts for the four experimental groups with different combinations of stepping, resting, and incline stepping. B) Counts of c-fos and tdTomato under different locomotor conditions derived from the experimental groups in (A).

response to stepping than tdTomato, and the opposite was true for the resting condition. C-fos shows a greater difference in expression between the resting and stepping condition than tdTomato. These results could arise due to the differences in how c-fos and tdTomato expression are activated.

Despite the Fos-Cre link, tdtomato has different spatial distribution and counts than c-fos when activated by stepping. C-fos shows increased activation in the medial dorsal horn and in the intermediate laminae, whereas tdtomato shows increased activation throughout the dorsal horn with the intermediate laminae showing less activation (Figure 3-8). TdTomato shows higher proportional activation in the dorsal and ventral horns compared to c-fos, and c-fos shows higher proportional activation in laminae V-VIII and X than tdTomato. C-fos and tdTomato also have different spatial counts. Tdtomato shows a decrease in the number of neurons activated when

going from dorsal to ventral while c-fos shows an increase in activation going from the dorsal horn to lamina V and then a decrease in activation ventral to lamina V. Overall, c-fos outnumbers tdTomato in medial laminae IV-VIII and lamina X. Tdtomato has small areas in lateral lamina III, IV, and IX where it outnumbers c-fos. The differences in expression between c-fos and tdTomato can also be seen during rest.

Tdtomato and c-fos also show differential laminar distribution when activated during rest. Resting tdtomato shows a similar expression profile to stepping tdtomato in which the dorsal horn has the most activation with the central canal and medial intermediate laminae having less activation (Figure 3-9). Resting c-fos has the most activation in medial laminae V-VII with the dorsal horn having less activation. Similar to stepping, c-fos shows a higher proportional activation in laminae V-VII and X, and tdTomato shows a higher proportional activation in the dorsal and ventral horn. Unlike stepping, the spatial count of tdtomato shows more activation than c-fos when activated by resting. Overall, tdTomato shows higher spatial counts than c-fos in all laminae except V and VI with the greatest discrepancy found in the dorsal horn. C-fos has greater counts in parts of laminae V and VI.

D. DISCUSSION

C-fos has been used as a biomarker for neuronal activity across a wide range of paradigms from somatosensory to locomotor experiments (Ruigrok, van der Burg et al. 1996, Dai, Noga et al. 2005, Ahn, Guu et al. 2006, Duru, Tillakaratne et al. 2015, Cazzulino, Martinez et al. 2016, Chen, Marsh et al. 2017, Groves, Kihara et al. 2018, Joshi and Panicker 2018). It allows scientists to probe whole network activity as opposed to more local activities seen in electrophysiology. C-fos has limitations, however, in its inability to directly compare neural network activity of two different or repeated tasks in the same animal. The FosTRAP animal

allows for permanent genetic access to neurons activated by a first task through tdTomato while also capturing neural activation in a future second task through immunohistochemistry to tag c-fos. Thus far, FosTRAP has been used to

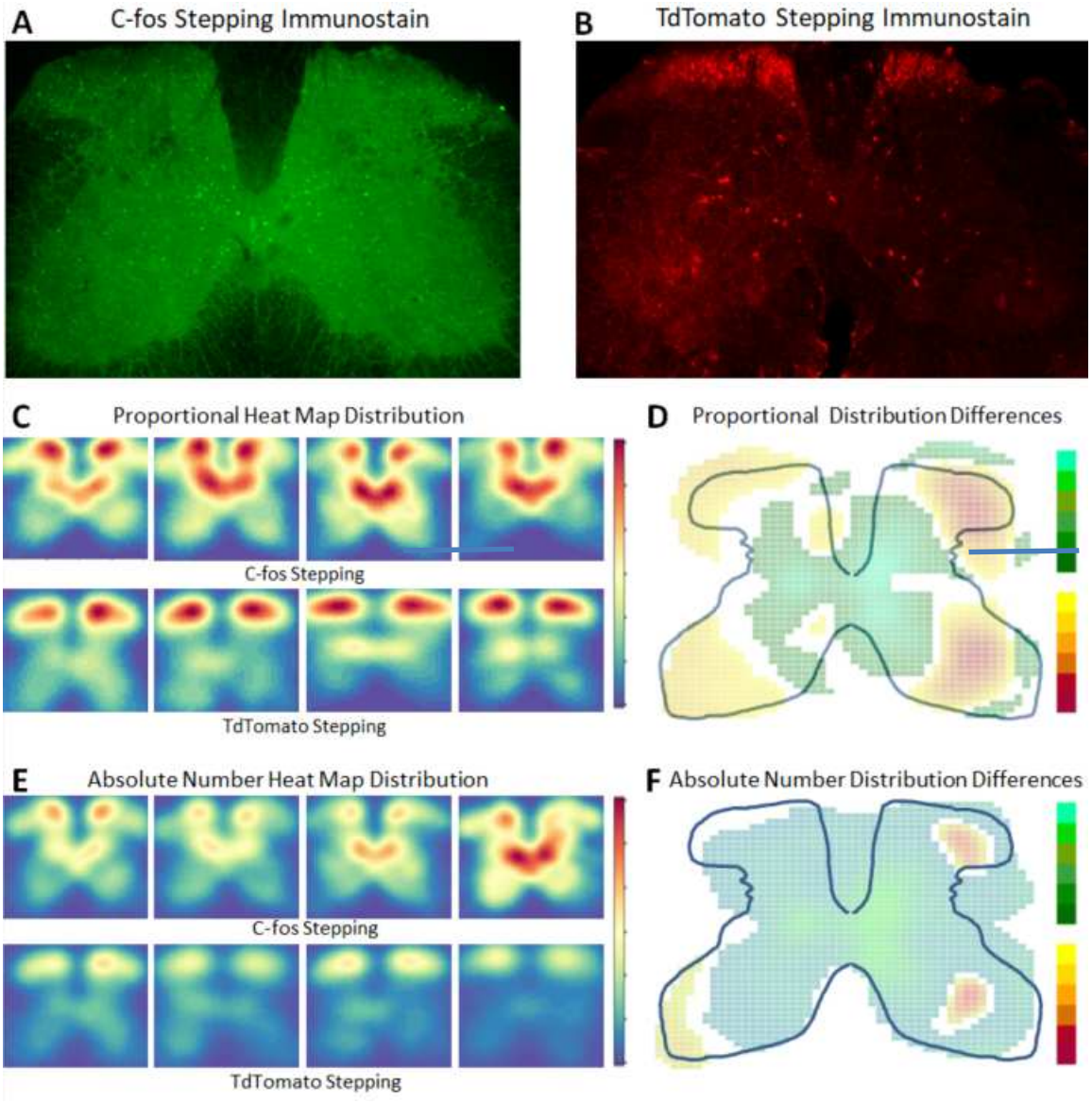

Figure 3-8: Differences in spatial distribution and counts of c-fos and tdTomato activated by stepping in the L4 spinal section. A) Representative image of c-fos stepping immunostain. Blue scale bar is 500 µm. B) Representative image of stepping tdTomato immunostain. C) Each panel is a KDE normalized with respect to itself of either c-fos or tdTomato activated by stepping from a single animal. KDE's from all animal in this experiment can be found in Figure S7 D) Map of the differences in proportional distribution between stepping c-fos and tdTomato calculated from KDE's seen in Figure S7. The green end of the color bar represents areas where c-fos is proportionately higher than tdTomato and vice versa for the yellow/red end of the color bar. E) The same KDE's from A, except all panels are normalized to the average KDE of stepping c-fos. The rest of these KDE's can be found in Figure S8. F) Map of the differences in spatial counts between stepping c-fos and tdTomato calculated from the KDE's in Figure S8. The green end of the color bar represents areas where c-fos outnumber tdTomato and vice versa for the yellow/red end of the color bar.

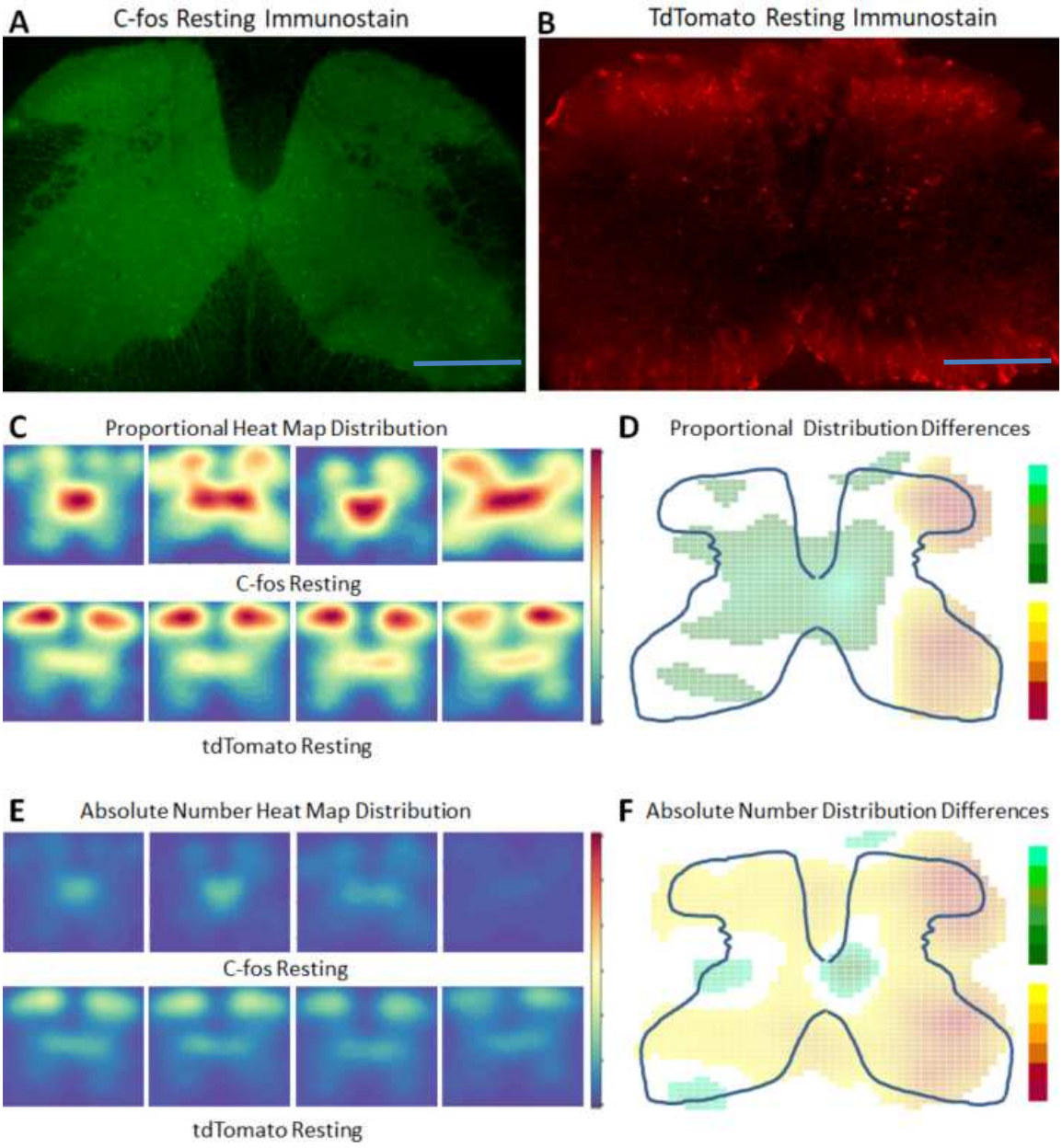

Figure 3-9: Differences in spatial distribution and counts of c-fos and tdTomato activated by resting in the L4 spinal section. A) Representative image of resting c-fos. Blue scale bar is 500 µm. B) Representative image of resting tdTomato. C) Each panel is a KDE normalized with respect to itself of either c-fos or tdTomato activated by resting from a single animal. D) Map of the differences in proportional distribution between resting c-fos and tdTomato calculated from KDE's seen in (C). The green end of the color bar represents areas where c-fos is proportionately higher than tdTomato and vice versa for the yellow/red end of the color bar. E) These are the same KDE's from (A), except all panels are normalized to the average KDE of stepping c-fos. F) Map of the differences in spatial counts between resting c-fos and tdTomato calculated from KDE's seen in (E). The green end of the color bar represents areas where c-fos outnumber tdTomato and vice versa for the yellow/red end of the color bar.

probe network activity from somatosensory and visual stimuli in the brain along with fear conditioning paradigms (Cazzulino, Martinez et al. 2016, Allen, DeNardo et al. 2017, Girasole, Lum et al. 2018, Tasaka, Guenthner et al. 2018, DeNardo, Liu et al. 2019). This paper explores the FosTRAP model for tracking spinal network activity that has occurred in two different motor tasks in the same animal.

1) Interpretations of network activity of different locomotor events based on c-fos, tdtomato, or both.

The patterns of tdTomato activation in fosTRAP animals reveal certain aspects of spinal network activation that c-fos does not, which arise from how these markers measure neural activity differently. The spatial counts of tdtomato shows a dorsal-ventral decrease in all locomotor tasks, indicating a spinal process that "filters" proprioceptive sensory input from the dorsal to ventral horn (Figure 3-5). In contrast, c-fos shows greater counts in laminae IV-VII than the dorsal horn during stepping, suggesting that supraspinal activity in the intermediate laminae could play a greater role than peripheral proprioception (Figure 3-4). TdTomato expression between stepping and incline stepping shows similarities and differences with a previous study done with c-fos. Both studies show an increased activation of neurons around the central canal for incline stepping versus stepping without an incline (Figure 3-5) (Tillakaratne, Duru et al. 2014). However, tdTomato shows no significant differences in the number of neurons activated between stepping and incline stepping, whereas a previous study (Tillakaratne, Duru et al. 2014) showed an increase in c-fos counts under similar conditions. This result seems inconsistent with the concept that an increase in power generation as required to step on an incline, arises primarily from an increase in the number of activated neurons. Increased power generation could arise from increased firing rates of the same neurons used for stepping which

might lead to more frequent firing of motor units rather than increased power generated from a from a larger population of interneurons compared to 0 degree stepping. It cannot be discounted, however, that differences in how c-fos and tdTomato labels activity could reflect unique features of neuronal activity being measured.

Understanding that tdtomato reveals the cumulative activation over six hours whereas c-fos reveals transiently active neurons in the shorter 1.5 hour time window gives a broader perspective of spinal network activity. During rest, the dorsal horn shows low levels of c-fos activation, but tdtomato reveals broad dorsal horn activation (Figure 3-9). Resting tdtomato expression highlights the importance of sensory activation over longer periods of "resting", though the dorsal horn activation may be sparse at any given moment in time as revealed by c-fos. Stepping c-fos had significantly greater counts in medial laminae IV-VII than did tdTomato (Figure 3-8). This area has been associated with the corticospinal tract, and c-fos highlights this importance whereas tdTomato does not capture this as clearly. One possibility is that the pattern of supraspinal activity may not be sufficiently continuous or sustained as in triggering tdTomato expression as during stepping. FosTRAP animals can give further insight into spinal locomotor networks by revealing shared c-fos and tdTomato activation (colabeling).

2) Colabeling in FosTRAP animals reveal insights into the physiology of spinal networks

The colabeling of FosTRAP reveals how spinal networks use spatial encoding for different motor tasks. This supports a previous study in which different locomotor activities have unique neurons associated with it at different spinal segments (Merkulyeva, Veshchitskii et al. 2018). Despite how c-fos and tdTomato measures activity differently, they both preserve spatial encoding differences between stepping and resting. C-fos and tdTomato show similar differences

in spatial counts and spatial distribution between stepping and resting (Figure 3-4, 3-5). They both show a broad increase in spatial counts throughout the gray matter when going from resting to stepping, and they both show a proportional increase in activation around the central canal when going from resting to stepping. Assuming that tdTomato and c-fos preserve changes in spatial distribution from activity to activity, the colabeling pattern of repeated and different tasks show distinct localization of neurons that are shared between stepping and resting and neurons that are unique to stepping (Figure 3-6).

The shared neurons mainly occupy the dorsal horn (laminae I-V), showing shared components of receiving and some processing of sensory input between the two locomotor events. This result gives further support of past research demonstrating the multi-functional nature of spinal interneurons 36-38. This multifunctionality could underlie the spinal cord's ability to learn a wide range of movement patterns more easily (ex. Cycling and swimming). The colabeling of repeated tasks show neurons unique to stepping, tend to occur more frequently in areas of the ventral horn (laminae VII-IX). This indicates a difference in the final phase of "decision making" among the pre-motor neuron levels between different locomotor events after the sensory information has been processed.

Using FosTRAP to compare neural populations activated by repeating the same motor behavior addresses a fundamental question that Edelmen has examined extensively. His hypothesis of "Neural Darwinism" proposes that the nervous system employs a "group selection" strategy of different populations of synapses to control different movements. This hypothesis contrasts with the more popular view of well-defined, unique and rigid neural pathways that perceive and execute each unique motor task. However, a range of different studies support "Neural Darwinism". While these issues are not likely to follow an all-or-none answer, there

have been relatively few challenges to the Neural Darwinistic perspective. The present data derived from spinal neuronal networks are consistent with Edelman's hypothesis, although it was originally thought to be uniquely associated with neural networks of the brain. Ironically, the neural strategies of spinal networks seem to provide more direct evidence of "Group Selection" of synapses than the brain.

While we observed some colabeling between two different events, the low colabeling rate of 22.6% for two similar bouts of stepping stands out (Figure 3-6). This compares to a colabeling rate of ~70% among sensory networks, for example, the response of the cochlear nuclei to identical audio stimuli (Guenthner, Miyamichi et al. 2013). This difference could be attributable to the fundamental differences between network complexity of sensory and motor systems. Sensory systems explored with FosTRAP have tonotopic or somatotopic organization that only receive sensory information, whereas the present experiments involve a dynamical sensorimotor system that adapts to complex and varying sensory inputs to create patterned movement. The 22.6% overlap supports the phenomena of probabilistic population activation of synapses to execute a task while also demonstrating a very high level of redundancies among neural networks to perform the same task. This is further supported by the differences in spatial distributions of c-fos and tdTomato activated by stepping, showing how multiple activation patterns can execute the same motor task (Figure 3-8). Numerous reports show that even the simplest repetitive movements are generated by varying pattern activities (Churchland, Yu et al. 2006).

These features allow the body to execute the same movement using different networks between the brain and spinal cord (cerebrospinal, intraspinal, etc.) which could be advantageous in avoiding fatigue as well as providing a virtually infinite number of options to complete the

same task. If the colabeling rate of this experiment was similar to previous sensory experiments in the cochlear nucleus (70% vs. 22.6%), this would indicate more limited number of pathways or neural networks available to execute stepping. If this were the case, experiments like unilateral deafferrentation (Lavrov, Courtine et al. 2008) may create a significant limitation in the execution of stepping. Furthermore, from this perspective, epidural and transcutaneous stimulation experiments combined with the extensive proprioceptive and cutaneous input tightly linked to repetitive step cycles could provide many options in facilitating reorganization of spinal networks that can form novel strategies to regain stepping following a spinal injury. The findings here and in previous studies highlight the enormous level of variation in the selection of population of synapses involved in a movement whose synaptic dynamics follow a probabilistic framework.

3) Locomotor neural network activities are measured differently with Tdtomato and c-fos

TdTomato and c-fos shows different features of cellular network activity when performing the same task. C-fos shows a higher cell count than tdTomato during stepping (Figure 3-7, 3-8), but a lower count during resting (Figure 3-7, 3-9). We hypothesize that tdTomato measures neural activity differently than c-fos are due to 1) the length of time that 4-OHT stays in the system and 2) its longer pathway to expression than c-fos. TdTomato captures network activity on a longer time scale than c-fos (6 hrs. vs. ~1.5 hrs) resulting from the amount of time 4-OHT stays in the system. This feature manifests itself in the timing optimization experiments where stepping tdTomato expression does not differ with time (Figure 3-2). It is also seen in the higher tdTomato counts than c-fos during resting where tdTomato records 6 hours of "resting" (Figure 3-9). Secondly, we hypothesize that tdTomato's longer reaction

pathway results in it having a different activity threshold in order to express. The expression of tdTomato requires the recombination of fos-linked CreER with 4-OHT and then subsequent targeting of a floxed tdTomato gene by the recombined product, resulting in two extra reaction steps to label Fos activity. Due to the probabilistic nature of biochemical reactions, in order to get more product (tdTomato) there needs to be a higher concentration of reactants (i.e. CreER), which requires an elevated activity-dependent production of CreER. Furthermore, CreER potentially has a longer half-life than c-fos (Chow, Tian et al. 2006, Reinert, Kantz et al. 2012). The longer half-life combined with the extended recording period of 4-OHT could signal that tdTomato could measure cumulative activation. These factors could lead to tdTomato measuring a more sustained increase in activity compared to c-fos.

TdTomato expression in laminae I-III shows the greatest increase between resting and stepping and also shows the greatest amount of expression during rest (Figure 3-5). These laminae continuously receive sensory input from the periphery. In contrast, the deeper laminae do not receive this same type of continuous input and only experience increased activity for 30 minutes in our stepping experiments, which may not be a long enough sustained activity to express tdTomato. This can explain the smaller difference in tdTomato counts between stepping and resting in laminae IV and VII compared to c-fos (Figure 3-4, 3-5). Even though tdTomato and c-fos appear to measure neural activity differently, they can provide insight into locomotor network activity.

4) Limitations

Guenthner et al have outlined some of the limitations of FosTRAP. Most of the limitations derive from the use of c-fos as an activity marker. C-fos and TRAP-derived tdTomato have been found to be underrepresented in certain areas and neuronal phenotypes. Furthermore, this study

did not validate TRAP activity through electrophysiology or stimulation. However, other studies have validated TRAP elicited by complex experiences such as fear-conditioning and maternal auditory processing using electrophysiology and optogenetic activation (Tasaka, Guenthner et al. 2018). Despite these limitations, the present data demonstrate new potential in using the FosTRAP experimental strategy to gain a more behaviorally relevant awareness of how spinal networks can so finely control highly complex motor tasks such as posture and locomotion under *in vivo* conditions.

E. CONCLUSION

These sets of experiments have allowed us to view neural activity through three different lenses of c-fos, tdTomato, and colabeling. The present data using FosTRAP for locomotor experiments reinforce the notion of marked redundancy of networks that perform the same motor tasks in spinal networks and the multi-functional nature of populations of spinal interneurons having different combinations of distinct genetic linkages. In future experiments FosTRAP can be combined with other tools like neural tracers and biomarkers for interneurons with distinct genetic lineages (i.e. v2a interneurons etc.) to systematically elucidate the multifunctionality and connections of these neurons. We have already shown preliminary evidence for this by combining CLARITY with pseudorabies virus tracing, with staining for Chx10, a V2A interneuron marker, and with FosTRAP animals (Figure 3-3). Further development in image recognition algorithms will give us a comprehensive network level view of spinal networks using tissue clearing techniques (Chung and Deisseroth 2013, Yang, Treweek et al. 2014, Treweek, Chan et al. 2015). Perhaps, more readily, creating circuit tracing algorithms that can uncover the connectivity of activated neural networks can potentially inspire future deep learning

architectures. Combining FosTRAP, neural tracers, genetic markers for interneurons, and tissue clearing researchers can begin a systematic effort to define the degree to which there is spatial and cellular identity and connectivity of spinal interneurons linked to a given behavior.

IV. APPLICATION OF MACHINE LEARNING TO IMMUNOHISTOLOGICAL IMAGES

ABBREVIATIONS USED:

IHC: immunohistochemistry; DSI: dice score; ML: machine learning; DL: deep learning; HoG: histogram of gradients; SVM: support vector machine; RF: random forest; CNN: convolutional neural network; FCN: fully convolutional network;

ABSTRACT:

Estimation of cell nuclei in images stained for the c-fos protein using immunohistochemistry (IHC) is infeasible in large image sets. Use of multiple human raters to increase throughput often creates variance in the data analysis. Machine learning techniques for biomedical image analysis have been explored for cell-counting in pathology, but their performance on IHC staining, especially to label activated cells in the spinal cord is unknown. In this study, we evaluate different machine learning techniques to segment and count spinal cord neurons that have been active during stepping. We present a qualitative as well as quantitative comparison of algorithmic performance versus two human raters. Quantitative ratings are presented with cell-count statistics and Dice (DSI) scores. We also show the degree of variability between multiple human raters' segmentations and observe that there is a higher degree of variability in segmentations produced by classic machine learning techniques (SVM and Random forest) as compared to the newer deep learning techniques. The work presented here, represents the first steps towards addressing the analysis time bottleneck of large image data sets generated by c-fos IHC staining techniques, a task that would be impossible to do manually.

A. INTRODUCTION

Identifying the location and functionality of neurons in the biological neural networks responsible for behavioral tasks provide insight into how to treat neurological diseases that affect them. An example would be enhancing the efficacy of spinal epidural stimulation to facilitate stepping and standing in spinal cord injured patients. The ability to spatially map the spinal cord's locomotor circuit would provide new targets and strategies for electrical stimulation (Harkema, Gerasimenko et al.). Neuroscientists can use tissue processing techniques like immunohistochemistry (IHC) to understand the anatomy and function of biological neural networks.

IHC is a tissue processing technique done on thin sections of tissue (<50 μm) that stains cellular proteins using specialized antibodies. IHC can reveal anatomical, functional, and connectivity properties of spinal cord neurons depending on the target protein and its location in the neuron. In this study we look at the c-fos protein, a biomarker for neural activation located in the cell nucleus. The images in this paper show c-fos expression in mouse spinal cord neurons activated during quadrupedal stepping on a treadmill for 30 minutes. Typically, analysis of IHC images requires manual segmentation, which provides accurate analysis that is robust to image and IHC staining quality, but it consumes a lot of time. Multiple raters can decrease analysis time, but adds variance to the data analysis because different raters have different criteria for what constitutes a positive stain (Lacroix-Triki, Mathoulin-Pelissier et al.). Recently, researchers have explored the use of machine learning tools to analyze IHC images, however, these tools have not been applied to cell counting in the spinal cord.

Automatic cell-counting in pathological images first started by using algorithms based on intensity thresholding, edge detection, template matching, and active shape models (Ginneken,

Frangi et al. , Di Cataldo, Ficarra et al. , Dong, Li et al. , Chen, Wang et al. , Yang, Peng et al.). Machine learning techniques like support vector machines (SVM), random forests (RF), k-means clustering, and fuzzy c-means algorithms were explored later (Di Cataldo, Ficarra et al. , Arteta, Lempitsky et al. , Mualla, Scholl et al. , Oscanoa, Doimi et al. , Shi, Zhong et al.). The next generation of automatic segmentation algorithms utilizes deep learning techniques for a variety of biomedical image analysis such as mitosis detection, epithelial tumor nuclei identification, brain tumor classification, glioma grading, and segmentation of a variety of tissue including neurons, colon glands, nuclei, and epithelium (Janowczyk and Madabhushi). Recently, analysis of IHC images have explored the use deep learning methods like convolutional neural networks (CNN) for segmentation (Xie, Noble et al.).

Previous uses of machine learning and deep learning for IHC analysis has focused on immune cells and retinal cells, but have neither been used to segment neurons expressing c-fos, nor have they been used to analyze the spinal cord. We compare the performance of several different machine learning techniques like multi-scale fully convolutional networks (FCN), U-net, SVM, and RF's with DSI scores of .784, .621, .825, and .821 respectively. This work shows that machine learning algorithms trained by a particular rater, are highly biased to agree with that rater; even more so than a second human rater agrees with the first one. The high variability of human rater generated cell counts is a particularly challenging aspect of IHC cell nuclei segmentation.

The work presented in this paper lays the groundwork for solving the data analysis bottleneck of next-generation tissue processing techniques. This will be especially important, once newer techniques like CLARITY, which generate large data sets containing hundreds or thousands of

images get mainstreamed. The extension of the algorithms presented here to large CLARITY data is reviewed in the discussion.

B. METHODS

1) Dataset

We train and test the machine learning algorithms on images from the lumbar region of the mouse spinal cord, specifically the L4 segment. The tissues were cut into 30 μm thick cross sections and stained for c-fos by immunohistochemistry (IHC). Positive c-fos immunostains mark activated neurons during a 30-minute session of quadrupedal stepping on a treadmill. Images taken had a 1200 x 1600 pixel resolution. The training set composed of 20 images from 4 different mice with varying degrees of brightness and image quality. These variations arise from different IHC trials, varied microscope settings, and different qualities of stepping behavior. The training set was intentionally designed this way to best capture the variable nature of behavioral and histological data sets. The testing set composed of 15 images from 3 different animals independent of the training set. A second testing set, created by a second human rater, included 6 images from the same 3 animals as the first testing set. This second testing was used to demonstrate variability between human raters and to test the generalizability of the automated techniques when compared to multiple human raters.

In our analysis, we compare four different machine learning techniques: Support vector machine (SVM), Random forest (RF), U-net, and Multi-scale fully convolutional network (FCN).

2) Classic Machine Learning Techniques

We use two classic machine learning techniques, SVM and RF. For both approaches, histogram equalization followed by a convolution with a Ricker wavelet was used to enhance the signal to noise ratio. The resulting image underwent intensity thresholding followed by a size filter to find candidate patches (40x40 pixels) for classification. This was done to decrease the number of patches to be analyzed compared to the total number of 40x40 patches that could be extracted from a 1200 x 1600 image. This patch size was chosen so that only one c-fos positive stain could fit in one patch. Shape, MR8 texture, and histogram of oriented gradients (HoG) features were extracted from the patches.

Shape features included solidity, orientation, diameter, area, eccentricity, convex area, major axis length, minor axis length, and extent. Textures features were based on the MR8 filter banks which include 36 bar and edge filters, a Gaussian filter, and a Laplacian of Gaussian filter. The eight highest responses are extracted to maintain rotation invariance. Histogram of Oriented Gradients (HoG) (Dalal and Triggs 2005) features were also extracted. Combined, these features were input to SVM and RF for binary classification. We trained a linear SVM model using the default settings in LibSVM (Chang) and the RF algorithm using 200 bagged classification trees.

3) U-nets

We include a deep learning architecture known as the U-net in our analysis. U-nets have been successfully used in segmentation of biomedical images. Our U-Net implementation closely follows the original one from (Ronneberger, Fischer et al.).

4) D. Multi-scale network

We employ the use of a multi-scale cascade of fully convolutional neural networks (FCN). Each network in the cascade operates at a different scale and its results are fed as input, in addition to the original image, to the subsequent network in the cascade. The first network, or

stage, delineates anatomy on a $1/8^{th}$ scale version of the image. When the image is scaled down, large contextual features in the image shrink in dimension, allowing the neural networks to interpret large image features without having to process more pixels. The first stage's segmentation result is scaled up by a factor of two, and is added alongside the original image to become part of the input to the next stage. The second stage segments the image at 1/4th scale and the pattern continues. The second stage adds its output to the input for the third stage (1/2 scale), which then passes its output to a full-scale segmentation network that makes the final fine-scaled prediction. This method of chaining networks together is inspired by work presented by Eigen (Eigen and Fergus) for scene segmentation challenges.

Each stage is a FCN consisting of an initial pooling layer, six 3x3 convolutional layers, and a final 1x1 convolutional layer for output. Inspired by the Inception architecture (Szegedy, Wei et al. 2015), each of the main 3x3 convolutional layers consists of 1x1 and 3x3 convolutions in parallel. These two convolutions have an equal number of features, operate on the entire input feature space, and output half of the total output features. When results from the two convolutions are concatenated, the output dimensions are the same as the input dimensions. It is also important to understand each stage as a pixel-wise segmentation network (Long, Shelhamer et al. 2015). Unlike SVM and RF, we used raw images as input to the multi-scale network and U-net with minimal to no preprocessing (e.g. histogram equalization)

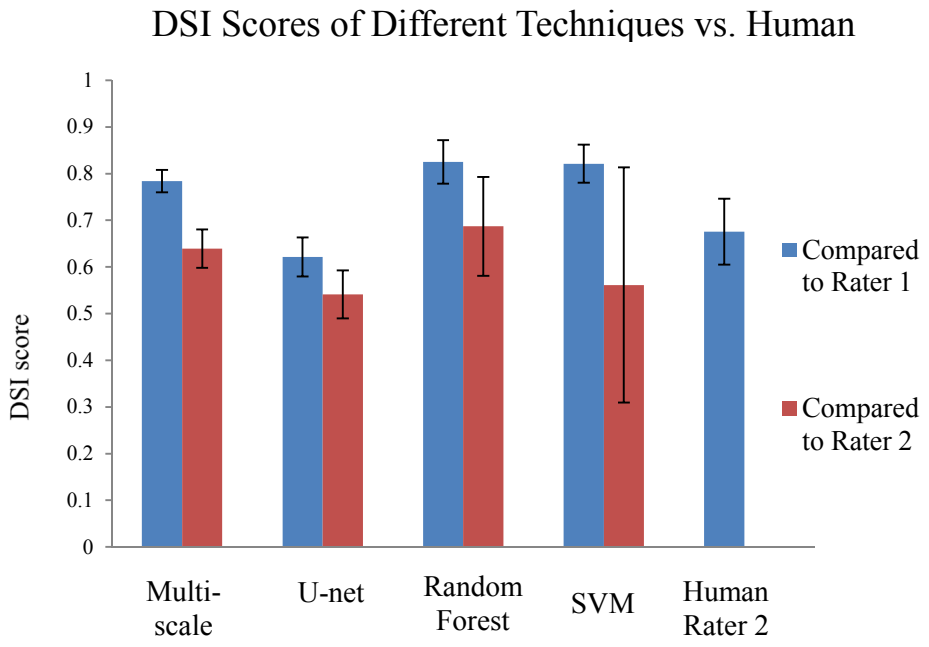

Figure 4-1. Performance of different segmenting techniques compared to human rater 1(blue bar) and human rater 2 (red bar). Last blue bar on the right denotes inter-rater variability

C. RESULTS

Multi-scale FCN, U-net, RF, and SVM all show similar segmentation performances with Dice scores of .785, .621, .825, and .821 respectively. The results are summarized in (Figure 4-1). The mean value of both Dice scores and cell counts is generally higher for the Deep Learning techniques.

Machine Learning Method	Compared to Rater 1		Compared to rater 2	
	Recall	Precision	Recall	Precision
SVM	0.795	0.860	0.429	0.822
Random Forest	0.835	0.825	0.540	0.973
Multi-scale FCN	0.836	0.835	0.635	0.927
U-net	0.811	0.598	0.672	0.700

Table 4-1: Precision and recall for machine learning techniques when compared to human rater 1 or human rater 2 as the ground truth

However, the differences between either techniques is not statistically significant. The variance in performance when compared to human rater 2 is more in classical techniques (RF and SVM) as compared to multi-scale FCN and U-net (Figure 4-1). The similarity of all the automated techniques vs. human rater 2 shows that the machine learning techniques have acquired human rater 1's biases when it comes to the criteria for what constitutes a positive c-fos stain; even though a cross validation based paradigm was employed during evaluation. Precision and recall for cell count values have been presented in Table 4-1.

Qualitatively, deep learning techniques are able to recognize cells in distorted c-fos; where RF and SVM can sometimes miss the identification of nuclei (Figure 4-2).

D. DISCUSSION AND FUTURE WORK

The results shown here has compared the performance of multi-scale fully convolutional networks (FCN), U-net, random forests (RF), and support vector machines (SVM) to segment images of 30 μm thick tissue slices stained for c-fos by immunohistochemistry (IHC). The variability of manual segmentation between human raters highlights the trade-off between

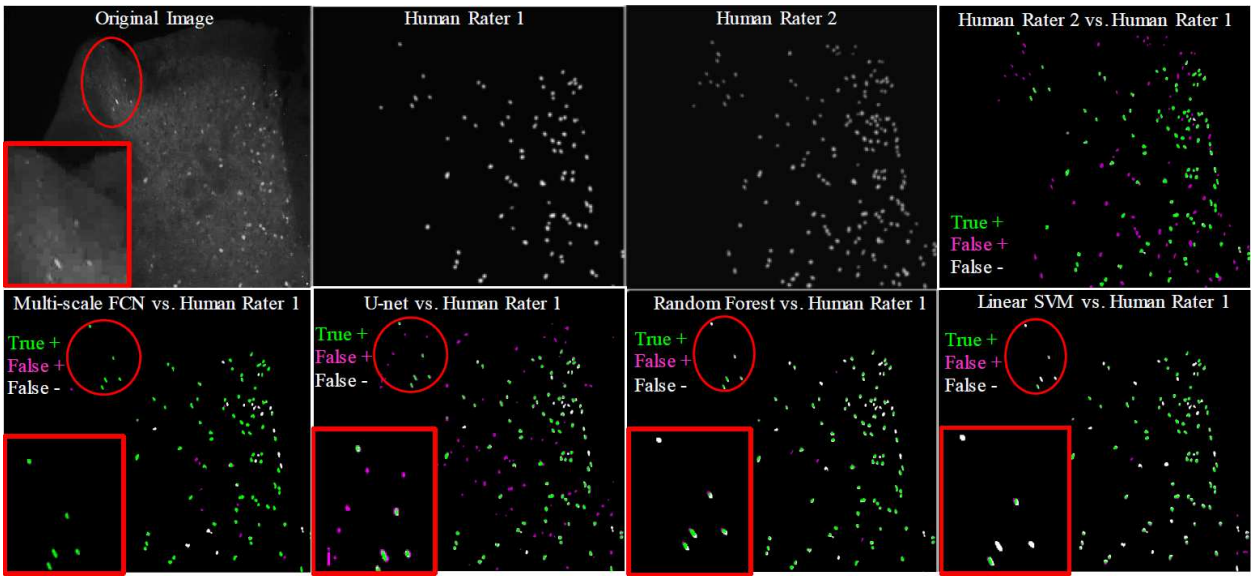

Figure 4-2: Qualitative results of machine learning techniques and human raters. Notice the variability between the segmentation of human rater 1 and 2. Red circled area represents where c-fos has been distorted due to a mounting error and is enlarged in the red box. These red boxes highlight that deep learning techniques are able to detect this distortion without prior training while the classic machine learning techniques only properly identify a few of them

decreasing analysis time and increasing the variability of the analyzed data when using multiple human raters. Using trained machine learning (ML) techniques for image segmentation guarantees that the criteria for what constitutes a positive signal stays the same for all images analyzed, while also decreasing the segmentation time by orders of magnitude compared to using multiple human raters. These automated analyses also do not suffer from fatigue or attention deficits that affect human raters.

The decrease in recall (Table 4-1) and DSI scores (Figure 4-1) when going from rater 1 to rater 2 demonstrates that trained algorithms have acquired the bias of human rater 1 for which it has been trained on. This discrepancy highlights the possibility of needing to train machine learning algorithms on multiple raters to compensate for the differences in criteria for multiple raters. The increased variance in DSI scores when going from rater 1 to rater 2 of RF and SVM versus deep learning (DL) techniques shows that the deep learning techniques may be capturing a more

effective underlying representation. This is further highlighted by the better precision of DL methods when going from rater 1 to rater 2. Future work will focus on refining and developing DL methods. DL methods simplify image segmentation by using the raw image. Secondly, there is an intense focus on deep learning, within the broader community, leading to the availability of several open source nature DL packages.

The use of automated segmentation greatly facilitates the analysis of c-fos IHC staining in the spinal cord. However, the automated analysis compared here can extend to other proteins stained by IHC as long as there is sufficient training data. Segmentation of c-fos alone reveals the spatial distribution of neurons in the biological neural networks responsible for particular tasks (i.e. walking) and thus reveal potential target locations for treatments of disorders that affect them (i.e. electrical stimulation for spinal cord injury). C-fos staining combined with other IHC stains can further reveal how and where the biological network as a whole delegates subsets of functionality to accomplish a behavior. For example, combining c-fos staining with staining for inhibitory or excitatory neural markers can reveal how and where the neural network uses excitation and suppression to accomplish the goal of stepping. This provides a richer understanding of biological neural networks that combines physical architecture with functionality. This deeper understanding has the potential to allow us to manipulate or artificially recreate these networks.

The current study uses automated machine learning techniques on thinly sliced tissue sections, but this has the potential to quickly analyze images generated from next-generation tissue processing techniques like CLARITY. CLARITY renders thick sections of tissue (>500 μm) optically transparent. The transparency of the tissue allows a confocal or light sheet microscope to create 3-D reconstructions by take hundreds to thousands of images through the whole

thickness of the tissue at sub-micron steps. CLARITY-cleared tissue sections can also undergo IHC staining despite the increased thickness of tissue sections. Though this processing technique provides a distinct advantage in imaging biological neural networks, there is no way to analyze the large amount of data generated in a timely manner, which limits the potential that this processing technique can offer. Automated DL techniques can analyze these image sets in a timely manner, and will aid in future work on tract tracing to identify the connectivity of biological neural networks that would be impossible to analyze manually. This would allow us to accomplish the goals outlined in the previous paragraph, except on a more global scale.

V. CONCLUSION AND FUTURE DIRECTIONS

ABBREVIATIONS USED:

CPG: central pattern generation; IHC: immunohistochemistry; ES: epidural stimulation; SCI: spinal cord injury; TS: transcutaneous stimulation

A. CONCLUSIONS

Understanding the anatomy and physiology of spinal locomotor circuits that enables us to execute movement in a seemingly infinite number of ways has occupied neuroscientists since the discovery of the mammalian central pattern generation (CPG) circuit over 100 years ago (Brown 1911). Over the past hundred years, how scientists have attacked evolved through the use of different animal models and experimental techniques. The first studies looked at lower vertebrates like lamprey and Xenopus tadpoles (Roberts, Soffe et al. 1998, McLean, Merrywest et al. 2000, Buchanan 2001, Roberts, Li et al. 2010) which then progressed to the use of cats (Grillner and Zangger 1979) and rodents. Current studies now employ the use of mice, due to the ability to manipulate its genetics. Experimental techniques have evolved from the use of single-cell electrophysiological recordings (Jankowska 2008) to isolated spinal cord preparations (Iizuka, Nishimaru et al. 1998, Bertrand and Cazalets 2002) to genetic ablation studies *in vivo* (Crone, Zhong et al. 2009, Zhong, Droho et al. 2010). However, all of these techniques have their drawbacks and this thesis sought to develop a new strategy in how to understand the *in vivo* dynamics of spinal locomotor networks.

To understand the dynamics of a 3D neural network that spans the entire length of the spinal cord, this thesis aimed to adapt an engineering approach that used big data techniques to gather

and analyze immunohistological (IHC) data. IHC techniques have the advantage of providing system wide activation and characterization with cellular resolution that other neural activity recording techniques do not quite have. This thesis applies this approach by using tissue clearing to gather large amounts of IHC data, adapting the FosTRAP animal model to capture two different c-fos activation patterns in the same animal, and applying machine learning techniques to quickly and efficiently analyze the large amounts of IHC data gathered. Laying down the foundation of this type of workflow for IHC data has implications for many fields besides investigating spinal locomotor networks.

The workflow established in this thesis can answer questions about neural networks like characterizing the distribution of neurons in 3D space, identifying and tracing neural networks, and understanding how network activation changes with different events (traumatic or transformative) or the execution of different tasks. It can analyze a whole neural network while also doing this in a manner that decreases the time and labor intensiveness through the use of automated analysis techniques. Furthermore, with the advent of proprietary machines that can clear and stain tissue, the rate at which applying this workflow has increased. Most importantly, the developments outlined in this thesis can be applied to a broad range of neuroscience problems that involve many different neural networks. The FosTRAP model has been used to understand complicated circuits like the primary auditory cortex and how it changes with motherhood (Tasaka, Guenthner et al. 2018) or the effects of exercise on hippocampal circuits (Chatzi, Zhang et al. 2019), and the workflow established here can be applied in these situations to gather more comprehensive data and analyzing them quickly. It was one of my goals to create a broad spectrum solution to show how you can potentially answer many questions as opposed to being specific to the problem my laboratory sought to understand. I hope that the results of this

thesis can show the neuroscience community "how to fish" as opposed to catching one and giving it to them.

B. FUTURE DIRECTIONS

This thesis laid the foundation to answer many prominent questions in the field of spinal cord research along with furthering and advancing the use of epidural stimulation (ES) and physical training as a solution for spinal cord injury (SCI). In order to establish this workflow, we performed many pilot studies that did not directly address the questions related to ES, physical training, and the effect of SCI on spinal locomotor networks. With the completion of these pilot experiments, future experiments can answer some of these fundamental questions.

1) Learning how spinal networks differentially activate to execute different types of movement

FosTRAP can better enable researchers understand how spinal locomotor networks activate to execute different movements. Setting up this experiment involves TRAPing one movement while using c-fos to capture a second movement. This experiment can potentially show us the differences in the 3D distribution of activated spinal networks to execute different tasks, which has been shown previously in cats for forward stepping vs. backward stepping (Merkulyeva, Veshchitskii et al. 2018). The nature of FosTRAP can allow us many different permutation and combination of different activities like forward stepping, sideward stepping, backward stepping, or even capturing the transition from forward to sideward or forward to backward stepping. Finding the differences the 3D distribution of neural activation between these different events can teach us which spatial or stimulation parameters that should be used to best facilitate different types of movements using ES or transcutaneous stimulation (TS). Furthermore, these

types of studies can show us overlaps between the networks used for these types of movements and can potentially reveal what combinations of physical training can lead to robust outcomes for the different types of movement. Using quadrupedal step training has shown a robust effect on bipedal stepping in SCI injured rats (Shah, Garcia-Alias et al. 2013). Additionally, these types of studies can provide insight in ES or TS electrode design by showing us the fineness or coarseness of electrical stimulation needed to facilitate these activities.

2) Understanding the effects of acute and chronic spinal cord injury

The emergence of FosTRAP allows for the study of the before and after effects of SCI on spinal networks with a built-in control. These animals allow for a true one to one neuronal mapping of the effects of SCI. In this experiment, several groups can be constructed. The first TRAPed task can capture either 30 minutes to an hour of treadmill stepping or resting. Capturing stepping can tell us what happens to the stepping locomotor circuit after SCI while capturing the resting state can serve as a comparison of the noted hyperactivation after an acute injury. The second task can capture the resting state after an acute injury or capture an attempt at bipedal stepping after injury. Together this experiment would have 4 different combinations of animals. Looking at the patterns of tdTomato and c-fos activation can indicate parts of the spinal networks involved in this hyperactivity immediately post SCI and their effects on the circuits involved in locomotion. Furthermore, another group can be added to study the effects of different treatments like anti-NOGO to ameliorate this hyperactivation after SCI. This set of experiments can be repeated for chronic spinal cord injuries. Insights potentially revealed by this experiment can help inform treatments and regimens to be given to patients in the wake of spinal cord injury, like treatments that can minimize the formation of scar tissue, treatments that can decrease the

occurrence of demyelination or apoptosis surrounding the scar tissue. Furthermore, these types of experiments can highlight the importance of physical therapy or fitness in the transition from acute SCI to chronic SCI.

3) How do spinal networks change with ES, physical training, and pharmacological intervention

Having a built-in control with FosTRAP better enables us to understand the effects that ES, physical training, and pharmacology have on the spinal locomotor networks. Furthermore, this can be used to test different theories that we have on how these interventions work in SCI. The simplest experiments involve understanding how each of these treatments individually affects spinal locomotor networks. In the case of ES, we can use FosTRAP to capture intact resting, intact stepping, or resting in the chronic SCI case before or after step training with Task 1 while Task 2 captures either ES facilitated stepping or the resting state with ES. This experimental setup can answer many questions in regards to the mechanisms of ES. Comparing intact resting with SCI resting plus ES can elucidate whether ES raises the excitability of spinal networks and transforms them into a functional state in a similar manner in which how supraspinal input provides constant and tonic excitability to the spinal neurons in the intact state. Furthermore, it can indicate whether ES primarily works through the action of stimulating I-a afferents in the dorsal root ganglion. On another level it can also show which parts of the ES facilitated network has reawakened circuitry that was active before the injury and circuitry that is *de novo* or new that has been created with ES. This type of experiment can also be repeated to test the mechanisms of pharmacological intervention like quipazine and strychnine and how they affect spinal locomotor circuitry or the entire spinal circuitry.

These types of experiments can also be performed to understand how different combinations of ES with physical training and pharmacology can affect spinal networks. The previous experiments outlined mainly touch on the effects of these three treatments individually. The combination experiments can answer whether their effects in combinations arises through an additive or multiplicative effect. Furthermore these experiments can test combinations of therapies that will achieve the best outcome and then look at their effects on the spinal locomotor networks. These types of experiments will TRAP the first training session after chronic SCI and Task 2 will capture the final training session after different combinations of therapies.

4) Shedding light on modeling spinal epidural stimulation and recordings

Mathematical modeling has simulated the spread of electrical current through the spinal cord using ES (Danner, Hofstoetter et al. 2011, Capogrosso, Wenger et al. 2013). However, these types of models cannot exactly predict which neurons will fire based solely upon the strength of current at a particular location. Some factors that predict neuronal firing that these models do not take into account include morphology, orientation, and size (Merrill, Bikson et al. 2005). Current mathematical models of electrical spread make assumptions about biological tissue using permittivity constants or modeling extracellular tissue as a combination of resistors and capacitances in order to predict current spread. Furthermore these models do not take individually model neurons so that it can predict neuronal firing as current passes through the tissue. The use of tissue clearing techniques along with an animal model that allows for fluorescent labeling of neurons or a certain set of neurons can provide a detailed map of neural networks that can give provide these additional parameters that predict neuronal firing. Combining physical models of current spread along with detailed maps of neuronal arrangement

can provide a basis in which we can make further inferences of how electrical stimulation can influence networks. Furthermore, it can provide details in the stimulation parameters needed to stimulate certain types of neurons at particular locations.

Providing a detailed map of activated neuronal networks using FosTRAP and tissue clearing can provide some insight when it comes to electrical recordings taken from the epidural surface of the spinal cord. The FosTRAP animal model can provide detailed maps of neurons activated during an *in vivo* activity. A detailed map like this combined with neural spiking simulation software can model the forward problem in which the current spread from an active neuron to the epidural surface can be simulated based upon the location and orientation of the TRAPed active neuron. However, this is under the assumption that we know the spiking properties of TRAPed neurons or that we make assumptions of their firing properties. This is due to the very poor time resolution of TRAPing neurons compared to electrical recordings. However, understanding the 3D distribution of activated neurons relative to a recording electrode during an *in vivo* can give a rough estimate of the source localization behind the electrical recordings taken from the epidural surface. The ability of understanding the physiological meaning behind epidural recordings have many implications in regards to ES as a treatment for SCI such as the ability to create a bidirectional prosthesis that can mix and match recording with precise stimulation to facilitate plasticity based upon the physiological state of the spinal cord. Furthermore this ability allows us to create a closed loop device to deliver ES. Additionally, understanding the physiological state of the spinal cord through recordings can help specialize ES and physical training regimens in patients based upon knowledge of how their spinal networks are responding to treatment.

5) Towards reverse engineering activated neural networks and creating bio-inspired architectures for artificial intelligence or artificial general intelligence

Mammalian nervous systems have inspired a branch of machine learning known as deep learning, and in some cases, like convolutional neural networks adapting concepts from the visual cortex, have drawn direct inspiration from their biological counterparts. Tissue clearing, neural tracing, and FosTRAP present an interesting combination that can, piece by piece, map out the neural network associated with a certain task. Neural tracers over the years have become increasingly complex, and perhaps future designs of neural tracers will have the ability to travel a programmed number of synapses. These tools hold the potential of reverse engineering biological networks and translating this information to artificial neural networks. Having a tracer that can travel a specified number of synapses and combining it with FosTRAP can answer questions like: 1) How many "hidden layers" are there in the spinal locomotor network? 2) How many neurons are in each of these layers? 3) Do neurons connect to multiple and different hidden layers as opposed to artificial neural networks that only connect to the next layer in a feed-forward way? 4) Can molecular phenotyping show that these hidden layers in biological networks contain populations of neurons that are functionally heterogeneous compared to artificial neural networks whose layers are functionally homogenous? Perhaps answering these types of questions can inspire future design of artificial neural networks specifically for locomotion. There are programming language packages like TensorFlow that are built to implement specialized graph structures and network connectivity. Furthermore, new types of processors known as neuromorphic chips can implement neural networks on hardware. Neuromorphic chips like the TrueNorth chip from IBM have 1 million neurons that form 256 million synapses. The ability to reverse engineer the locomotor network has implications in

robotics and in neural prostheses. However, this is under the assumption that biological neural networks can successfully translate to artificial neural networks. Not all biological neural networks can successfully translate to artificial neural networks like the visual system to convolutional neural networks.

Another intriguing question that neural tracing and tissue clearing can potentially answer is how do different neural circuits interface with each other. How does the locomotor network integrate supraspinal and sensory input to produce locomotion? The neural circuits of sensory and motor systems have different architectures. Biological networks can seamlessly integrate these different architectures to execute a goal, a feature that is lacking in artificial neural networks. Combinations of anterograde and retrograde neural tracing from different neural circuits (e.g. sensory anterograde tracers and retrograde motor racers) can provide how these circuits interface with each and in which processing steps do they integrate. However, the infrastructure and tools to answer these types of problem do not currently exist, but I believe that the combination of tissue clearing, neural tracing, and automated analysis can potentially shed light on these questions once the proper neural tracing tools become available in the future.

REFERENCES

Ahn, S. N., J. J. Guu, A. J. Tobin, V. R. Edgerton and N. J. Tillakaratne (2006). "Use of c-fos to identify activity-dependent spinal neurons after stepping in intact adult rats." Spinal Cord **44**(9): 547-559.

Alam, M., W. Rodrigues, B. N. Pham and N. V. Thakor (2016). "Brain-machine interface facilitated neurorehabilitation via spinal stimulation after spinal cord injury: Recent progress and future perspectives." Brain Res **1646**: 25-33.

Allen, W. E., L. A. DeNardo, M. Z. Chen, C. D. Liu, K. M. Loh, L. E. Fenno, C. Ramakrishnan, K. Deisseroth and L. Luo (2017). "Thirst-associated preoptic neurons encode an aversive motivational drive." Science **357**(6356): 1149-1155.

Andersson, O., H. Forssberg, S. Grillner and P. Wallen (1981). "Peripheral feedback mechanisms acting on the central pattern generators for locomotion in fish and cat." Can J Physiol Pharmacol **59**(7): 713-726.

Angeli, C. A., V. R. Edgerton, Y. P. Gerasimenko and S. J. Harkema (2014). "Altering spinal cord excitability enables voluntary movements after chronic complete paralysis in humans." Brain **137**(Pt 5): 1394-1409.

Arteta, C., V. Lempitsky, J. A. Noble and A. Zisserman (2012). Learning to Detect Cells Using Non-overlapping Extremal Regions, Berlin, Heidelberg, Springer Berlin Heidelberg.

Azim, E., J. Jiang, B. Alstermark and T. M. Jessell (2014). "Skilled reaching relies on a V2a propriospinal internal copy circuit." Nature **508**(7496): 357-363.

Barbeau, H. and S. Rossignol (1987). "Recovery of locomotion after chronic spinalization in the adult cat." Brain Res **412**(1): 84-95.

Barbeau, H. and S. Rossignol (1994). "Enhancement of locomotor recovery following spinal cord injury." Curr Opin Neurol **7**(6): 517-524.

Berkowitz, M. (1998). Spinal cord injury : an analysis of medical and social costs. New York, N.Y., Demos.

Bertrand, S. and J. R. Cazalets (2002). "The respective contribution of lumbar segments to the generation of locomotion in the isolated spinal cord of newborn rat." Eur J Neurosci **16**(9): 1741-1750.

Borowska, J., C. T. Jones, H. Zhang, J. Blacklaws, M. Goulding and Y. Zhang (2013). "Functional subpopulations of V3 interneurons in the mature mouse spinal cord." J Neurosci **33**(47): 18553-18565.

Bretzner, F. and R. M. Brownstone (2013). "Lhx3-Chx10 reticulospinal neurons in locomotor circuits." J Neurosci **33**(37): 14681-14692.

Briscoe, J., L. Sussel, P. Serup, D. Hartigan-O'Connor, T. M. Jessell, J. L. Rubenstein and J. Ericson (1999). "Homeobox gene Nkx2.2 and specification of neuronal identity by graded Sonic hedgehog signalling." Nature **398**(6728): 622-627.

Britz, O., J. Zhang, K. S. Grossmann, J. Dyck, J. C. Kim, S. Dymecki, S. Gosgnach and M. Goulding (2015). "A genetically defined asymmetry underlies the inhibitory control of flexor-extensor locomotor movements." Elife **4**.

Brown, T. (1911). "The intrinsic factors in the act of progression in the mammal." Proc. R. Soc. Lond. B **84**.

Brownstone, R. M. and J. M. Wilson (2008). "Strategies for delineating spinal locomotor rhythm-generating networks and the possible role of Hb9 interneurones in rhythmogenesis." Brain research reviews **57**(1): 64-76.

Buchanan, J. T. (2001). "Contributions of identifiable neurons and neuron classes to lamprey vertebrate neurobiology." Prog Neurobiol **63**(4): 441-466.

Capogrosso, M., N. Wenger, S. Raspopovic, P. Musienko, J. Beauparlant, L. Bassi Luciani, G. Courtine and S. Micera (2013). "A computational model for epidural electrical stimulation of spinal sensorimotor circuits." J Neurosci **33**(49): 19326-19340.

Cazzulino, A. S., R. Martinez, N. K. Tomm and C. A. Denny (2016). "Improved specificity of hippocampal memory trace labeling." Hippocampus **26**(6): 752-762.

Chang, C.-C. a. L., C.-J. (2011.). " LIBSVM: A library for support vector machines. ." ACM Trans. Intell. Syst. Technol. **2, 3,**(Article 27): 27 pages.

Charles Watson, G. P., Gulgun Kayalioglu, Claire Heise (2009). The Spinal Cord, Academic Press.

Chatzi, C., Y. Zhang, W. D. Hendricks, Y. Chen, E. Schnell, R. H. Goodman and G. L. Westbrook (2019). "Exercise-induced enhancement of synaptic function triggered by the inverse BAR protein, Mtss1L." Elife **8**.

Chen, C., W. Wang, J. A. Ozolek and G. K. Rohde (2013). "A flexible and robust approach for segmenting cell nuclei from 2D microscopy images using supervised learning and template matching." Cytometry A **83**(5): 495-507.

Chen, K., B. C. Marsh, M. Cowan, Y. D. Al'Joboori, S. Gigout, C. C. Smith, N. Messenger, N. Gamper, M. E. Schwab and R. M. Ichiyama (2017). "Sequential therapy of anti-Nogo-A antibody treatment and treadmill training leads to cumulative improvements after spinal cord injury in rats." Exp Neurol **292**: 135-144.

Chevalier, C., J. F. Nicolas and A. C. Petit (2014). "Preparation and delivery of 4-hydroxy-tamoxifen for clonal and polyclonal labeling of cells of the surface ectoderm, skin, and hair follicle." Methods Mol Biol **1195**: 239-245.

Chow, L. M., Y. Tian, T. Weber, M. Corbett, J. Zuo and S. J. Baker (2006). "Inducible Cre recombinase activity in mouse cerebellar granule cell precursors and inner ear hair cells." Dev Dyn **235**(11): 2991-2998.

Chung, K. and K. Deisseroth (2013). "CLARITY for mapping the nervous system." Nat Methods **10**(6): 508-513.

Churchland, M. M., B. M. Yu, S. I. Ryu, G. Santhanam and K. V. Shenoy (2006). "Neural variability in premotor cortex provides a signature of motor preparation." J Neurosci **26**(14): 3697-3712.

Clarac, F., E. Pearlstein, J. F. Pflieger and L. Vinay (2004). "The in vitro neonatal rat spinal cord preparation: a new insight into mammalian locomotor mechanisms." Journal of comparative physiology. A neuroethology, sensory, neural, and behavioral physiology **190**(5): 343-357.

Courtine, G., Y. Gerasimenko, R. van den Brand, A. Yew, P. Musienko, H. Zhong, B. Song, Y. Ao, R. M. Ichiyama, I. Lavrov, R. R. Roy, M. V. Sofroniew and V. R. Edgerton (2009). "Transformation of nonfunctional spinal circuits into functional states after the loss of brain input." Nat Neurosci **12**(10): 1333-1342.

Courtine, G., B. Song, R. R. Roy, H. Zhong, J. E. Herrmann, Y. Ao, J. Qi, V. R. Edgerton and M. V. Sofroniew (2008). "Recovery of supraspinal control of stepping via indirect propriospinal relay connections after spinal cord injury." Nature medicine **14**(1): 69-74.

Courtine, G., B. Song, R. R. Roy, H. Zhong, J. E. Herrmann, Y. Ao, J. Qi, V. R. Edgerton and M. V. Sofroniew (2008). "Recovery of supraspinal control of stepping via indirect propriospinal relay connections after spinal cord injury." Nat Med **14**(1): 69-74.

Cowley, K. C. and B. J. Schmidt (1994). "A comparison of motor patterns induced by N-methyl-D-aspartate, acetylcholine and serotonin in the in vitro neonatal rat spinal cord." Neurosci Lett **171**(1-2): 147-150.

Crone, S. A., K. A. Quinlan, L. Zagoraiou, S. Droho, C. E. Restrepo, L. Lundfald, T. Endo, J. Setlak, T. M. Jessell, O. Kiehn and K. Sharma (2008). "Genetic ablation of V2a ipsilateral interneurons disrupts left-right locomotor coordination in mammalian spinal cord." Neuron **60**(1): 70-83.

Crone, S. A., G. Zhong, R. Harris-Warrick and K. Sharma (2009). "In mice lacking V2a interneurons, gait depends on speed of locomotion." J Neurosci **29**(21): 7098-7109.

Csobonyeiova, M., S. Polak, R. Zamborsky and L. Danisovic (2019). "Recent Progress in the Regeneration of Spinal Cord Injuries by Induced Pluripotent Stem Cells." Int J Mol Sci **20**(15).

Dai, X., B. R. Noga, J. R. Douglas and L. M. Jordan (2005). "Localization of spinal neurons activated during locomotion using the c-fos immunohistochemical method." J Neurophysiol **93**(6): 3442-3452.

Dai, Y. and L. M. Jordan (2010). "Multiple effects of serotonin and acetylcholine on hyperpolarization-activated inward current in locomotor activity-related neurons in Cfos-EGFP mice." J Neurophysiol **104**(1): 366-381.

Dalal, N. and B. Triggs (2005). Histograms of oriented gradients for human detection. 2005 IEEE Computer Society Conference on Computer Vision and Pattern Recognition (CVPR'05).

Dale, E. A., M. Ng, H. Zhong, R. R. Roy, N. J. K. Tillakaratne, V. R. Edgerton and J. A. Kim (2014). "Characterization of spinal interneurons responsible for stepping in spinally transected mice." 2014 Neuroscience Meeting Planner. Washington, DC Society for Neuroscience.

Danner, S. M., U. S. Hofstoetter, J. Ladenbauer, F. Rattay and K. Minassian (2011). "Can the human lumbar posterior columns be stimulated by transcutaneous spinal cord stimulation? A modeling study." Artif Organs **35**(3): 257-262.

de Leon, R. D., J. A. Hodgson, R. R. Roy and V. R. Edgerton (1998). "Full weight-bearing hindlimb standing following stand training in the adult spinal cat." J Neurophysiol **80**(1): 83-91.

DeNardo, L. A., C. D. Liu, W. E. Allen, E. L. Adams, D. Friedmann, L. Fu, C. J. Guenthner, M. Tessier-Lavigne and L. Luo (2019). "Temporal evolution of cortical ensembles promoting remote memory retrieval." Nat Neurosci **22**(3): 460-469.

Denk, W. and H. Horstmann (2004). "Serial block-face scanning electron microscopy to reconstruct three-dimensional tissue nanostructure." PLoS Biol **2**(11): e329.

DeVivo, M. J. and Y. Chen (2011). "Trends in new injuries, prevalent cases, and aging with spinal cord injury." Arch Phys Med Rehabil **92**(3): 332-338.

Di Cataldo, S., E. Ficarra, A. Acquaviva and E. Macii (2010). "Automated segmentation of tissue images for computerized IHC analysis." Computer Methods and Programs in Biomedicine **100**(1): 1-15.

Dong, J., J. Li, A. Fu and H. Lv (2010). Automatic Segmentation for Ovarian Cancer Immunohistochemical Image Based on YUV Color Space. 2010 International Conference on Biomedical Engineering and Computer Science.

Dougherty, K. J. and O. Kiehn (2010). "Firing and cellular properties of V2a interneurons in the rodent spinal cord." J Neurosci **30**(1): 24-37.

Dougherty, K. J. and O. Kiehn (2010). "Functional organization of V2a-related locomotor circuits in the rodent spinal cord." Annals of New York Academy of Science **1198**: 85-93.

Dougherty, K. J. and O. Kiehn (2010). "Functional organization of V2a-related locomotor circuits in the rodent spinal cord." Ann N Y Acad Sci **1198**: 85-93.

Duru, P. O., N. J. Tillakaratne, J. A. Kim, H. Zhong, S. M. Stauber, T. T. Pham, M. S. Xiao, V. R. Edgerton and R. R. Roy (2015). "Spinal neuronal activation during locomotor-like activity enabled by epidural stimulation and 5-hydroxytryptamine agonists in spinal rats." J Neurosci Res **93**(8): 1229-1239.

Duru, P. O., N. J. Tillakaratne, J. A. Kim, H. Zhong, S. M. Stauber, T. T. Pham, M. S. Xiao, V. R. Edgerton and R. R. Roy (2015). "Spinal neuronal activation during locomotor-like activity enabled by epidural stimulation and 5-hydroxytryptamine agonists in spinal rats." J Neurosci Res.

Edgerton, V. R., G. Courtine, Y. P. Gerasimenko, I. Lavrov, R. M. Ichiyama, A. J. Fong, L. L. Cai, C. K. Otoshi, N. J. Tillakaratne, J. W. Burdick and R. R. Roy (2008). "Training locomotor networks." Brain Res Rev **57**(1): 241-254.

Edgerton, V. R., S. Grillner, A. Sjöström and P. Zangger (1976). Central Generation of Locomotion in Vertebrates. Neural Control of Locomotion. R. M. Herman, S. Grillner, P. S. G. Stein and D. G. Stuart. Boston, MA, Springer US**:** 439-464.

Edgley, S. A. and E. Jankowska (1987). "An interneuronal relay for group I and II muscle afferents in the midlumbar segments of the cat spinal cord." J Physiol **389**: 647-674.

Eigen, D. and R. Fergus (2015). Predicting Depth, Surface Normals and Semantic Labels with a Common Multi-scale Convolutional Architecture. 2015 IEEE International Conference on Computer Vision (ICCV).

Esposito, M. S., P. Capelli and S. Arber (2014). "Brainstem nucleus MdV mediates skilled forelimb motor tasks." Nature **508**(7496): 351-356.

Ewald, A. J., H. McBride, M. Reddington, S. E. Fraser and R. Kerschmann (2002). "Surface imaging microscopy, an automated method for visualizing whole embryo samples in three dimensions at high resolution." Dev Dyn **225**(3): 369-375.

Fong, A. J., L. L. Cai, C. K. Otoshi, D. J. Reinkensmeyer, J. W. Burdick, R. R. Roy and V. R. Edgerton (2005). "Spinal cord-transected mice learn to step in response to quipazine treatment and robotic training." J Neurosci **25**(50): 11738-11747.

Furlan, J. C., B. M. Sakakibara, W. C. Miller and A. V. Krassioukov (2013). "Global incidence and prevalence of traumatic spinal cord injury." Can J Neurol Sci **40**(4): 456-464.

Gad, P., Y. Gerasimenko, S. Zdunowski, A. Turner, D. Sayenko, D. C. Lu and V. R. Edgerton (2017). "Weight Bearing Over-ground Stepping in an Exoskeleton with Non-invasive Spinal Cord Neuromodulation after Motor Complete Paraplegia." Front Neurosci **11**: 333.

Gazdic, M., V. Volarevic, C. R. Harrell, C. Fellabaum, N. Jovicic, N. Arsenijevic and M. Stojkovic (2018). "Stem Cells Therapy for Spinal Cord Injury." Int J Mol Sci **19**(4).

Gerasimenko, Y., D. Sayenko, P. Gad, C. T. Liu, N. J. K. Tillakaratne, R. R. Roy, I. Kozlovskaya and V. R. Edgerton (2017). "Feed-Forwardness of Spinal Networks in Posture and Locomotion." Neuroscientist **23**(5): 441-453.

Gerasimenko, Y. P., R. M. Ichiyama, I. A. Lavrov, G. Courtine, L. Cai, H. Zhong, R. R. Roy and V. R. Edgerton (2007). "Epidural spinal cord stimulation plus quipazine administration enable stepping in complete spinal adult rats." J Neurophysiol **98**(5): 2525-2536.

Gerasimenko, Y. P., I. A. Lavrov, G. Courtine, R. M. Ichiyama, C. J. Dy, H. Zhong, R. R. Roy and V. R. Edgerton (2006). "Spinal cord reflexes induced by epidural spinal cord stimulation in normal awake rats." J Neurosci Methods **157**(2): 253-263.

Gill, M. L., P. J. Grahn, J. S. Calvert, M. B. Linde, I. A. Lavrov, J. A. Strommen, L. A. Beck, D. G. Sayenko, M. G. Van Straaten, D. I. Drubach, D. D. Veith, A. R. Thoreson, C. Lopez, Y. P. Gerasimenko, V. R. Edgerton, K. H. Lee and K. D. Zhao (2018). "Neuromodulation of lumbosacral spinal networks enables independent stepping after complete paraplegia." Nat Med **24**(11): 1677-1682.

Ginneken, B. v., A. F. Frangi, J. J. Staal, B. M. t. H. Romeny and M. A. Viergever (2002). "Active shape model segmentation with optimal features." IEEE Transactions on Medical Imaging **21**(8): 924-933.

Girasole, A. E., M. Y. Lum, D. Nathaniel, C. J. Bair-Marshall, C. J. Guenthner, L. Luo, A. C. Kreitzer and A. B. Nelson (2018). "A Subpopulation of Striatal Neurons Mediates Levodopa-Induced Dyskinesia." Neuron **97**(4): 787-795 e786.

Gosgnach, S., G. M. Lanuza, S. J. Butt, H. Saueressig, Y. Zhang, T. Velasquez, D. Riethmacher, E. M. Callaway, O. Kiehn and M. Goulding (2006). "V1 spinal neurons regulate the speed of vertebrate locomotor outputs." Nature **440**(7081): 215-219.

Griener, A., W. Zhang, H. Kao, C. Wagner and S. Gosgnach (2015). "Probing diversity within subpopulations of locomotor-related V0 interneurons." Dev Neurobiol **75**(11): 1189-1203.

Grillner, S. (2003). "The motor infrastructure: from ion channels to neuronal networks." Nat Rev Neurosci **4**(7): 573-586.

Grillner, S. and P. Zangger (1979). "On the central generation of locomotion in the low spinal cat." Exp Brain Res **34**(2): 241-261.

Grillner, S. and P. Zangger (1984). "The effect of dorsal root transection on the efferent motor pattern in the cat's hindlimb during locomotion." Acta Physiol Scand **120**(3): 393-405.

Groves, A., Y. Kihara, D. Jonnalagadda, R. Rivera, G. Kennedy, M. Mayford and J. Chun (2018). "A Functionally Defined In Vivo Astrocyte Population Identified by c-Fos Activation in a Mouse Model of Multiple Sclerosis Modulated by S1P Signaling: Immediate-Early Astrocytes (ieAstrocytes)." eNeuro **5**(5).

Guenthner, C. J., K. Miyamichi, H. H. Yang, H. C. Heller and L. Luo (2013). "Permanent genetic access to transiently active neurons via TRAP: targeted recombination in active populations." Neuron **78**(5): 773-784.

Guenthner, C. J., K. Miyamichi, H. H. Yang, H. C. Heller and L. Luo (2013). "Permanent genetic access to transiently active neurons via TRAP: targeted recombination in active populations." Neuron **78**(5): 773-784.

Harkema, S., Y. Gerasimenko, J. Hodes, J. Burdick, C. Angeli, Y. Chen, C. Ferreira, A. Willhite, E. Rejc, R. G. Grossman and V. R. Edgerton (2011). "Effect of epidural stimulation of the lumbosacral spinal cord on voluntary movement, standing, and assisted stepping after motor complete paraplegia: a case study." Lancet **377**(9781): 1938-1947.

Helmchen, F. and W. Denk (2005). "Deep tissue two-photon microscopy." Nat Methods **2**(12): 932-940.

Huang, A., B. R. Noga, P. A. Carr, B. Fedirchuk and L. M. Jordan (2000). "Spinal cholinergic neurons activated during locomotion: localization and electrophysiological characterization." J Neurophysiol **83**(6): 3537-3547.

Huang, A., B. R. Noga, P. A. Carr, B. Fedirchuk and L. M. Jordan (2000). "Spinal cholinergic neurons activated during locomotion: localization and electrophysiological characterization." Journal of neurophysiology **83**(6): 3537-3547.

Ichiyama, R. M., J. Broman, R. R. Roy, H. Zhong, V. R. Edgerton and L. A. Havton (2011). "Locomotor training maintains normal inhibitory influence on both alpha- and gamma-motoneurons after neonatal spinal cord transection." J Neurosci **31**(1): 26-33.

Ichiyama, R. M., G. Courtine, Y. P. Gerasimenko, G. J. Yang, R. van den Brand, I. A. Lavrov, H. Zhong, R. R. Roy and V. R. Edgerton (2008). "Step training reinforces specific spinal locomotor circuitry in adult spinal rats." J Neurosci **28**(29): 7370-7375.

Ichiyama, R. M., Y. P. Gerasimenko, H. Zhong, R. R. Roy and V. R. Edgerton (2005). "Hindlimb stepping movements in complete spinal rats induced by epidural spinal cord stimulation." Neurosci Lett **383**(3): 339-344.

Iizuka, M., H. Nishimaru and N. Kudo (1998). "Development of the spatial pattern of 5-HT-induced locomotor rhythm in the lumbar spinal cord of rat fetuses in vitro." Neurosci Res **31**(2): 107-111.

Jankowska, E. (2008). "Spinal interneuronal networks in the cat: elementary components." Brain Res Rev **57**(1): 46-55.

Jankowska, E., M. G. Jukes, S. Lund and A. Lundberg (1967). "The effect of DOPA on the spinal cord. 5. Reciprocal organization of pathways transmitting excitatory action to alpha motoneurones of flexors and extensors." Acta Physiol Scand **70**(3): 369-388.

Janowczyk, A. and A. Madabhushi (2016). "Deep learning for digital pathology image analysis: A comprehensive tutorial with selected use cases." Journal of Pathology Informatics **7**(1): 29-29.

Jazayeri, S. B., S. Beygi, F. Shokraneh, E. M. Hagen and V. Rahimi-Movaghar (2015). "Incidence of traumatic spinal cord injury worldwide: a systematic review." European Spine Journal **24**(5): 905-918.

Jin, M. C., Z. A. Medress, T. D. Azad, V. M. Doulames and A. Veeravagu (2019). "Stem cell therapies for acute spinal cord injury in humans: a review." Neurosurg Focus **46**(3): E10.

Joshi, R. S. and M. M. Panicker (2018). "Identifying the In Vivo Cellular Correlates of Antipsychotic Drugs." eNeuro **5**(5).

Ke, M. T., S. Fujimoto and T. Imai (2013). "SeeDB: a simple and morphology-preserving optical clearing agent for neuronal circuit reconstruction." Nat Neurosci **16**(8): 1154-1161.

Ke, M. T. and T. Imai (2014). "Optical clearing of fixed brain samples using SeeDB." Curr Protoc Neurosci **66**: Unit 2 22.

Kiehn, O. (2006). "Locomotor circuits in the mammalian spinal cord." Annual reviews in neuroscience **29**: 279-306.

Kiehn, O. (2006). "Locomotor circuits in the mammalian spinal cord." Annu Rev Neurosci **29**: 279-306.

Kiehn, O. and S. J. Butt (2003). "Physiological, anatomical and genetic identification of CPG neurons in the developing mammalian spinal cord." Progress in neurobiology **70**(4): 347-361.

Kim, J. A., M. S. Xiao, A. J. Hornak, M. Mikhaeil, V. Esquivel, E. J. Gonzalez, P. Duru, M. S. Joseph, H. Zhong, R. R. Roy, V. R. Edgerton and N. J. K. Tillakaratne (2013). "Activated spinal neurons during quadrupedal stepping in adult intact mice injected with pseudorabies virus into the tibialis anterior." 2013 Neuroscience Meeting Planner. San Diego: Society for Neuroscience **832.04**.

Kjaerulff, O. and O. Kiehn (1996). "Distribution of networks generating and coordinating locomotor activity in the neonatal rat spinal cord in vitro: a lesion study." J Neurosci **16**(18): 5777-5794.

Kleinfeld, D., A. Bharioke, P. Blinder, D. D. Bock, K. L. Briggman, D. B. Chklovskii, W. Denk, M. Helmstaedter, J. P. Kaufhold, W. C. Lee, H. S. Meyer, K. D. Micheva, M. Oberlaender, S. Prohaska, R. C. Reid, S. J. Smith, S. Takemura, P. S. Tsai and B. Sakmann (2011). "Large-scale automated histology in the pursuit of connectomes." J Neurosci **31**(45): 16125-16138.

Kudo, N. and T. Yamada (1987). "N-methyl-D,L-aspartate-induced locomotor activity in a spinal cord-hindlimb muscles preparation of the newborn rat studied in vitro." Neurosci Lett **75**(1): 43-48.

Kullander, K., S. J. Butt, J. M. Lebret, L. Lundfald, C. E. Restrepo, A. Rydstrom, R. Klein and O. Kiehn (2003). "Role of EphA4 and EphrinB3 in local neuronal circuits that control walking." Science **299**(5614): 1889-1892.

Lacroix-Triki, M., S. Mathoulin-Pelissier, J. P. Ghnassia, G. Macgrogan, A. Vincent-Salomon, V. Brouste, M. C. Mathieu, P. Roger, F. Bibeau, J. Jacquemier, F. Penault-Llorca and L. Arnould (2006). "High inter-observer agreement in immunohistochemical evaluation of HER-2/neu expression in breast cancer: a multicentre GEFPICS study." Eur J Cancer **42**(17): 2946-2953.

Lanuza, G. M., S. Gosgnach, A. Pierani, T. M. Jessell and M. Goulding (2004). "Genetic identification of spinal interneurons that coordinate left-right locomotor activity necessary for walking movements." Neuron **42**(3): 375-386.

Lavrov, I., G. Courtine, C. J. Dy, R. van den Brand, A. J. Fong, Y. Gerasimenko, H. Zhong, R. R. Roy and V. R. Edgerton (2008). "Facilitation of stepping with epidural stimulation in spinal rats: role of sensory input." J Neurosci **28**(31): 7774-7780.

Levine, A. J., C. A. Hinckley, K. L. Hilde, S. P. Driscoll, T. H. Poon, J. M. Montgomery and S. L. Pfaff (2014). "Identification of a cellular node for motor control pathways." Nature neuroscience **15**: 586-593.

Li, A., H. Gong, B. Zhang, Q. Wang, C. Yan, J. Wu, Q. Liu, S. Zeng and Q. Luo (2010). "Micro-optical sectioning tomography to obtain a high-resolution atlas of the mouse brain." Science **330**(6009): 1404-1408.

Liu, C.-t. (2007). Short-term and long-term spinal learning in rats : swing phase force field paradigm Ph D, UCLA.

Livet, J., T. A. Weissman, H. Kang, R. W. Draft, J. Lu, R. A. Bennis, J. R. Sanes and J. W. Lichtman (2007). "Transgenic strategies for combinatorial expression of fluorescent proteins in the nervous system." Nature **450**(7166): 56-62.

Long, J., E. Shelhamer and T. Darrell (2015). Fully convolutional networks for semantic segmentation. 2015 IEEE Conference on Computer Vision and Pattern Recognition (CVPR).

Lovely, R. G., R. J. Gregor, R. R. Roy and V. R. Edgerton (1986). "Effects of training on the recovery of full-weight-bearing stepping in the adult spinal cat." Exp Neurol **92**(2): 421-435.

Lovely, R. G., R. J. Gregor, R. R. Roy and V. R. Edgerton (1990). "Weight-bearing hindlimb stepping in treadmill-exercised adult spinal cats." Brain Res **514**: 206-218.

Maitan, P., S. Frigerio, A. Conti, M. Clari, E. Vellone and R. Alvaro (2018). "The effect of the burden of caregiving for people with spinal cord injury (SCI): a cross-sectional study." Ann Ist Super Sanita **54**(3): 185-193.

McLean, D. L., S. D. Merrywest and K. T. Sillar (2000). "The development of neuromodulatory systems and the maturation of motor patterns in amphibian tadpoles." Brain Res Bull **53**(5): 595-603.

Merkulyeva, N., A. Veshchitskii, O. Gorsky, N. Pavlova, P. V. Zelenin, Y. Gerasimenko, T. G. Deliagina and P. Musienko (2018). "Distribution of Spinal Neuronal Networks Controlling Forward and Backward Locomotion." J Neurosci **38**(20): 4695-4707.

Merrill, D. R., M. Bikson and J. G. Jefferys (2005). "Electrical stimulation of excitable tissue: design of efficacious and safe protocols." J Neurosci Methods **141**(2): 171-198.

Micheva, K. D. and S. J. Smith (2007). "Array tomography: a new tool for imaging the molecular architecture and ultrastructure of neural circuits." Neuron **55**(1): 25-36.

Miller, J. E., A. T. Hilliard and S. A. White (2010). "Song practice promotes acute vocal variability at a key stage of sensorimotor learning." PLoS One **5**(1): e8592.

Moran-Rivard, L., T. Kagawa, H. Saueressig, M. K. Gross, J. Burrill and M. Goulding (2001). "Evx1 is a postmitotic determinant of v0 interneuron identity in the spinal cord." Neuron **29**(2): 385-399.

Mualla, F., S. Scholl, B. Sommerfeldt, A. Maier and J. Hornegger (2013). "Automatic Cell Detection in Bright-Field Microscope Images Using SIFT, Random Forests, and Hierarchical Clustering." IEEE Trans Med Imaging **32**(12): 2274-2286.

Muir, D. A. and D. A. Compston (1996). "Growth factor stimulation triggers apoptotic cell death in mature oligodendrocytes." J Neurosci Res **44**(1): 1-11.

Murray, E., J. H. Cho, D. Goodwin, T. Ku, J. Swaney, S. Y. Kim, H. Choi, Y. G. Park, J. Y. Park, A. Hubbert, M. McCue, S. Vassallo, N. Bakh, M. P. Frosch, V. J. Wedeen, H. S. Seung and K. Chung (2015). "Simple, Scalable Proteomic Imaging for High-Dimensional Profiling of Intact Systems." Cell **163**(6): 1500-1514.

Myers, C. P., J. W. Lewcock, M. G. Hanson, S. Gosgnach, J. B. Aimone, F. H. Gage, K. F. Lee, L. T. Landmesser and S. L. Pfaff (2005). "Cholinergic input is required during embryonic development to mediate proper assembly of spinal locomotor circuits." Neuron **46**(1): 37-49.

Oscanoa, J., F. Doimi, R. Dyer, J. Araujo, J. Pinto and B. Castaneda (2016). Automated segmentation and classification of cell nuclei in immunohistochemical breast cancer images with estrogen receptor marker. 2016 38th Annual International Conference of the IEEE Engineering in Medicine and Biology Society (EMBC).

Osten, P. and T. W. Margrie (2013). "Mapping brain circuitry with a light microscope." Nat Methods **10**(6): 515-523.

Oteir, A. O., K. Smith, P. A. Jennings and J. U. Stoelwinder (2014). "The prehospital management of suspected spinal cord injury: an update." Prehosp Disaster Med **29**(4): 399-402.

Otsuka, M. and S. Konishi (1974). "Electrophysiology of mammalian spinal cord in vitro." Nature **252**(5485): 733-734.

Pierani, A., L. Moran-Rivard, M. J. Sunshine, D. R. Littman, M. Goulding and T. M. Jessell (2001). "Control of interneuron fate in the developing spinal cord by the progenitor homeodomain protein Dbx1." Neuron **29**(2): 367-384.

Ragan, T., L. R. Kadiri, K. U. Venkataraju, K. Bahlmann, J. Sutin, J. Taranda, I. Arganda-Carreras, Y. Kim, H. S. Seung and P. Osten (2012). "Serial two-photon tomography for automated ex vivo mouse brain imaging." Nat Methods **9**(3): 255-258.

Rauschning, W. (1986). "Surface cryoplaning. A technique for clinical anatomical correlations." Ups J Med Sci **91**(3): 251-255.

Reinert, R. B., J. Kantz, A. A. Misfeldt, G. Poffenberger, M. Gannon, M. Brissova and A. C. Powers (2012). "Tamoxifen-Induced Cre-loxP Recombination Is Prolonged in Pancreatic Islets of Adult Mice." PLoS One **7**(3): e33529.

Rejc, E., C. Angeli and S. Harkema (2015). "Effects of Lumbosacral Spinal Cord Epidural Stimulation for Standing after Chronic Complete Paralysis in Humans." PLoS One **10**(7): e0133998.

Roberts, A., W. C. Li and S. R. Soffe (2010). "How neurons generate behavior in a hatchling amphibian tadpole: an outline." Front Behav Neurosci **4**: 16.

Roberts, A., S. R. Soffe, E. S. Wolf, M. Yoshida and F. Y. Zhao (1998). "Central circuits controlling locomotion in young frog tadpoles." Ann N Y Acad Sci **860**: 19-34.

Ronneberger, O., P. Fischer and T. Brox (2015). U-Net: Convolutional Networks for Biomedical Image Segmentation, Cham, Springer International Publishing.

Roy, R. R., S. J. Harkema and V. R. Edgerton (2012). "Basic concepts of activity-based interventions for improved recovery of motor function after spinal cord injury." Arch Phys Med Rehabil **93**(9): 1487-1497.

Ruigrok, T. J., H. van der Burg and E. Sabel-Goedknegt (1996). "Locomotion coincides with c-Fos expression in related areas of inferior olive and cerebellar nuclei in the rat." Neurosci Lett **214**(2-3): 119-122.

Sayenko, D. G., M. Rath, A. R. Ferguson, J. W. Burdick, L. A. Havton, V. R. Edgerton and Y. P. Gerasimenko (2019). "Self-Assisted Standing Enabled by Non-Invasive Spinal Stimulation after Spinal Cord Injury." J Neurotrauma **36**(9): 1435-1450.

Selvarajah, S., E. R. Hammond, A. H. Haider, C. J. Abularrage, D. Becker, N. Dhiman, O. Hyder, D. Gupta, J. H. Black, 3rd and E. B. Schneider (2014). "The burden of acute traumatic spinal cord injury among adults in the united states: an update." J Neurotrauma **31**(3): 228-238.

Shah, P. K., G. Garcia-Alias, J. Choe, P. Gad, Y. Gerasimenko, N. Tillakaratne, H. Zhong, R. R. Roy and V. R. Edgerton (2013). "Use of quadrupedal step training to re-engage spinal interneuronal networks and improve locomotor function after spinal cord injury." Brain **136**(Pt 11): 3362-3377.

Shefchyk, S., D. McCrea, D. Kriellaars, P. Fortier and L. Jordan (1990). "Activity of interneurons within the L4 spinal segment of the cat during brainstem-evoked fictive locomotion." Exp Brain Res **80**(2): 290-295.

Shi, P., J. Zhong, J. Hong, R. Huang, K. Wang and Y. Chen (2016). "Automated Ki-67 Quantification of Immunohistochemical Staining Image of Human Nasopharyngeal Carcinoma Xenografts." Sci Rep **6**: 32127.

Shik, M. L. and G. N. Orlovsky (1976). "Neurophysiology of locomotor automatism." Physiol Rev **56**(3): 465-501.

Sillar, K. T., D. Combes, S. Ramanathan, M. Molinari and J. Simmers (2008). "Neuromodulation and developmental plasticity in the locomotor system of anuran amphibians during metamorphosis." Brain Res Rev **57**(1): 94-102.

Smith, J. C. and J. L. Feldman (1987). "In vitro brainstem-spinal cord preparations for study of motor systems for mammalian respiration and locomotion." J Neurosci Methods **21**(2-4): 321-333.

Soderblom, C., D. H. Lee, A. Dawood, M. Carballosa, A. Jimena Santamaria, F. D. Benavides, S. Jergova, R. M. Grumbles, C. K. Thomas, K. K. Park, J. D. Guest, V. P. Lemmon, J. K. Lee and P.

Tsoulfas (2015). "3D Imaging of Axons in Transparent Spinal Cords from Rodents and Nonhuman Primates." eNeuro **2**(2).

Stepien, A. E. and S. Arber (2008). "Probing the locomotor conundrum: descending the 'V' interneuron ladder." Neuron **60**(1): 1-4.

Szegedy, C., L. Wei, J. Yangqing, P. Sermanet, S. Reed, D. Anguelov, D. Erhan, V. Vanhoucke and A. Rabinovich (2015). Going deeper with convolutions. 2015 IEEE Conference on Computer Vision and Pattern Recognition (CVPR).

Talpalar, A. E., J. Bouvier, L. Borgius, G. Fortin, A. Pierani and O. Kiehn (2013). "Dual-mode operation of neuronal networks involved in left-right alternation." Nature **500**(7460): 85-88.

Tasaka, G. I., C. J. Guenthner, A. Shalev, O. Gilday, L. Luo and A. Mizrahi (2018). "Genetic tagging of active neurons in auditory cortex reveals maternal plasticity of coding ultrasonic vocalizations." Nat Commun **9**(1): 871.

Tillakaratne, N. J., P. Duru, H. Fujino, H. Zhong, M. S. Xiao, V. R. Edgerton and R. R. Roy (2014). "Identification of interneurons activated at different inclines during treadmill locomotion in adult rats." J Neurosci Res **92**(12): 1714-1722.

Toga, A. W., K. Ambach, B. Quinn, M. Hutchin and J. S. Burton (1994). "Postmortem anatomy from cryosectioned whole human brain." J Neurosci Methods **54**(2): 239-252.

Treweek, J. B., K. Y. Chan, N. C. Flytzanis, B. Yang, B. E. Deverman, A. Greenbaum, A. Lignell, C. Xiao, L. Cai, M. S. Ladinsky, P. J. Bjorkman, C. C. Fowlkes and V. Gradinaru (2015). "Whole-body tissue stabilization and selective extractions via tissue-hydrogel hybrids for high-resolution intact circuit mapping and phenotyping." Nat Protoc **10**(11): 1860-1896.

Tsai, P. S., B. Friedman, A. I. Ifarraguerri, B. D. Thompson, V. Lev-Ram, C. B. Schaffer, Q. Xiong, R. Y. Tsien, J. A. Squier and D. Kleinfeld (2003). "All-optical histology using ultrashort laser pulses." Neuron **39**(1): 27-41.

Tsai, P. S., J. P. Kaufhold, P. Blinder, B. Friedman, P. J. Drew, H. J. Karten, P. D. Lyden and D. Kleinfeld (2009). "Correlations of neuronal and microvascular densities in murine cortex revealed by direct counting and colocalization of nuclei and vessels." J Neurosci **29**(46): 14553-14570.

Vartak, M., S. Rahman, S. Madden, A. Parameswaran and N. Polyzotis (2015). "SeeDB: Efficient Data-Driven Visualization Recommendations to Support Visual Analytics." Proceedings VLDB Endowment **8**(13): 2182-2193.

Whelan, P. J. (2003). "Developmental aspects of spinal locomotor function: insights from using the in vitro mouse spinal cord preparation." J Physiol **553**(Pt 3): 695-706.

Williams, T. L., K. A. Sigvardt, N. Kopell, G. B. Ermentrout and M. P. Remler (1990). "Forcing of coupled nonlinear oscillators: studies of intersegmental coordination in the lamprey locomotor central pattern generator." J Neurophysiol **64**(3): 862-871.

Wilson, J. M., E. Blagovechtchenski and R. M. Brownstone (2010). "Genetically defined inhibitory neurons in the mouse spinal cord dorsal horn: a possible source of rhythmic inhibition of motoneurons during fictive locomotion." J Neurosci **30**(3): 1137-1148.

Xie, W., J. A. Noble and A. Zisserman (2016). "Microscopy cell counting and detection with fully convolutional regression networks." Computer Methods in Biomechanics and Biomedical Engineering: Imaging & Visualization: 1-10.

Yang, B., J. B. Treweek, R. P. Kulkarni, B. E. Deverman, C. K. Chen, E. Lubeck, S. Shah, L. Cai and V. Gradinaru (2014). "Single-cell phenotyping within transparent intact tissue through whole-body clearing." Cell **158**(4): 945-958.

Yang, T., W. Peng, X. Li and Y. Wang (2014). A Robust IHC Color Image Automatic Segmentation Algorithm, Berlin, Heidelberg, Springer Berlin Heidelberg.

Ye, L., W. E. Allen, K. R. Thompson, Q. Tian, B. Hsueh, C. Ramakrishnan, A. C. Wang, J. H. Jennings, A. Adhikari, C. H. Halpern, I. B. Witten, A. L. Barth, L. Luo, J. A. McNab and K. Deisseroth (2016). "Wiring and Molecular Features of Prefrontal Ensembles Representing Distinct Experiences." Cell **165**(7): 1776-1788.

Zhang, J., G. M. Lanuza, O. Britz, Z. Wang, V. C. Siembab, Y. Zhang, T. Velasquez, F. J. Alvarez, E. Frank and M. Goulding (2014). "V1 and v2b interneurons secure the alternating flexor-extensor motor activity mice require for limbed locomotion." Neuron **82**(1): 138-150.

Zhang, Y., S. Narayan, E. Geiman, G. M. Lanuza, T. Velasquez, B. Shanks, T. Akay, J. Dyck, K. Pearson, S. Gosgnach, C. M. Fan and M. Goulding (2008). "V3 spinal neurons establish a robust and balanced locomotor rhythm during walking." Neuron **60**(1): 84-96.

Zhong, G., S. Droho, S. A. Crone, S. Dietz, A. C. Kwan, W. W. Webb, K. Sharma and R. M. Harris-Warrick (2010). "Electrophysiological characterization of V2a interneurons and their locomotor-related activity in the neonatal mouse spinal cord." J Neurosci **30**(1): 170-182.

Zhong, G., K. Sharma and R. M. Harris-Warrick (2011). "Frequency-dependent recruitment of V2a interneurons during fictive locomotion in the mouse spinal cord." Nat Commun **2**: 274.

Zhong, H., R. R. Roy, K. K. Nakada, S. Zdunowski, N. Khalili, R. D. de Leon and V. R. Edgerton (2012). "Accommodation of the spinal cat to a tripping perturbation." Front Physiol **3**: 112.